



## 저작자표시-비영리 2.0 대한민국

이용자는 아래의 조건을 따르는 경우에 한하여 자유롭게

- 이 저작물을 복제, 배포, 전송, 전시, 공연 및 방송할 수 있습니다.
- 이차적 저작물을 작성할 수 있습니다.

다음과 같은 조건을 따라야 합니다:



저작자표시. 귀하는 원저작자를 표시하여야 합니다.



비영리. 귀하는 이 저작물을 영리 목적으로 이용할 수 없습니다.

- 귀하는, 이 저작물의 재이용이나 배포의 경우, 이 저작물에 적용된 이용허락조건을 명확하게 나타내어야 합니다.
- 저작권자로부터 별도의 허가를 받으면 이러한 조건들은 적용되지 않습니다.

저작권법에 따른 이용자의 권리는 위의 내용에 의하여 영향을 받지 않습니다.

이것은 [이용허락규약\(Legal Code\)](#)을 이해하기 쉽게 요약한 것입니다.

[Disclaimer](#) 

공학박사학위논문

Synthesis and characterization of phthalocyanine  
dyes for liquid crystal display black matrix and  
phenoxazine dyes for dye-sensitized solar cells

액정 디스플레이 블랙 매트릭스 용 프탈로시아닌 염료 및  
염료감응 태양전지용 페녹사진 염료의  
합성과 특성에 대한 연구

2014년 2월

서울대학교 대학원

재료공학부

이 우 성

## **Abstract**

# **Synthesis and characterization of phthalocyanine dyes for liquid crystal display black matrix and phenoxazine dyes for dye-sensitized solar cells**

**Lee Woosung**

Department of Material Science and Engineering

The Graduated School

Seoul National University

The most frequently used material for black matrix is carbon black, which has advantages of high thermal stability and high light absorption. However, black matrices fabricated with carbon black have high dielectric constants, causing electrical signal transduction errors on thin film transistors. To avoid this problem, organic pigment BMs with a low dielectric constant can be used, but their low spectral properties due to the lower molar extinction coefficient of

organic pigments have limited their applications.

In general, dyes have much lower dielectric constants compared with carbon black, and show much higher light absorption properties than organic pigments. Thus, if dyes are used for the manufacture of the black matrix, the high dielectric constant and low light absorption of conventional black matrices can be overcome. On the other hand, dyes generally have low thermal stability compared to carbon black and organic pigments. Therefore, the dyes for black matrix need to be structurally stable. They also should have good solubility in industrial solvents, such as propylene glycol methyl ether acetate and cyclohexanone. In addition, as dyes generally have sharp absorption ranges, dye-based black matrices need to be fabricated by mixing red, green and blue dyes, or cyan, magenta and yellow dyes, as well as by mixing dyes and carbon black..

In this study, green metal-free phthalocyanine dyes with high thermal stability and high solubility were designed. Three phthalocyanine dyes were synthesized by introducing substituents including alkyl or alkoxy groups to the peripheral position of the phthalocyanine rings, and their spectral properties, solubilities and thermal stabilities were measured. In addition, dye-based black matrices were fabricated and their optical and dielectric properties were examined.

The metal-free phthalocyanine dyes showed the increase in solubility due to bulky functional substituents at the peripheral positions of them. In addition, the dyes including terminal alkoxy groups showed suitable thermal stability for commercial use due to terminal alkoxy groups are stable at postbaking temperature. Since all dyes had high molar extinction coefficients, dye-based black matrices absorbed light in the visible region with the small amounts of the dyes. The dielectric constants of the black matrices containing more than 30wt% of dyes were significantly lower than that of the black matrix prepared with carbon black only.

Furthermore, greenish zinc phthalocyanine dyes and reddish perylene dyes were synthesized and employed to fabricate black matrices with low dielectric constant and light absorption in the whole visible region. The spectral and thermal properties and solubility of the prepared dyes were investigated, and optical, thermal and dielectric properties of the dye-based black matrices were examined. For further investigation of surface morphology of the black matrix films, dye-based black matrices were probed by field emission scanning electron microscopy and atomic force microscopy.

The dye-based black matrix showed the high thermal stability due to the rigid molecular structures of the dyes. In addition, due to the low dielectric

characteristics of the dye, the dielectric constants of the dye-based black matrices were significantly lower than that of the black matrix prepared with carbon black only. However, the low solubility of the dyes in industrial solvents and dye aggregations in the baking process limited the input of the dye in the black matrix resist, resulting in low light absorption of the dye-based black matrix.

Dye-sensitized solar cells have attracted considerable attention as promising solar devices and the Ru complex dyes typical used as sensitizers in dye-sensitized solar cells have shown high electronic conversion efficiencies of over 11% with good stability. However, high production cost and difficulties in purification of Ru complex dyes have limited their development for large-scale applications. Recently, more attention has been paid to sensitizers without Ru (metal-free organic dyes and organometallic dyes) due to their lower cost, easier modification and purification, high molar extinction coefficient, and environmental friendliness.

Phenoxazine-based sensitizers have exhibited higher conversion efficiencies than triphenylamine and phenothiazine-based sensitizers, which are structurally similar. This is because phenoxazine-based sensitizers, with electron-rich nitrogen and oxygen heteroatoms, have stronger electron-donating ability than

triphenylamine and phenothiazine-based sensitizers. phenoxazine-based sensitizers also show sufficient electrochemical properties for use in dye-sensitized solar cells. However, despite their potential for application to dye-sensitized solar cells, phenoxazine-based sensitizers have not been studied extensively.

In this research, to study effects of conjugated bridges with a phenoxazine moiety on photovoltaic performance, five-membered heterocyclic rings were introduced as a conjugated bridge unit to phenoxazine molecules. Furthermore, to improve the donating power and molar extinction coefficient, an ethoxy phenyl ring was substituted in the 7 position of the phenoxazine -furan dye as an additional donor. Based on these strategies, three organic dyes were synthesized and the photophysical, electrochemical, and photovoltaic properties of the solar cells based on these dyes were investigated.

The introduced heterocyclic bridge units furan and thiophene improved the short-circuit current due to the red-shifted absorption spectra of the dyes. The ethoxyphenyl ring introduced to the phenoxazine moiety as an additional donor broadened the spectrum of the dye, while the reduced adsorption of the dye caused by its non-planar structure limited the enhancement of the short-circuit

current. As a result, among the synthesized dyes, the one with furan as a bridge unit showed the best overall conversion efficiency of 5.26%.

In addition, to study the effects of the number of anchoring groups and *N*-substitution on the performance of phenoxazine dyes in dye-sensitized solar cells, cyanoacrylic acid as an additional anchoring group was introduced to the phenoxazine for efficient electron extraction from the donor part, and an *N*-methoxyphenyl unit was added to suppress dye aggregation. Based on these strategies, four phenoxazine derivatives were synthesized and the photophysical, electrochemical and photovoltaic properties of the solar cells based on these dyes were investigated.

The additional cyanoacrylic acid acceptor improved the short-circuit current because it widened the absorption ranges of the dyes, although it also increased the recombination rate. The *N*-methoxyphenyl unit decrease charge recombinations, resulting in higher open-circuit voltage. However, the bulky substituent decreased the amount of dye absorbed on the TiO<sub>2</sub>. As a result, the fabricated cells with the four dyes exhibited similar overall conversion efficiencies and, of these cells, the solar cell based on the *N*-4-methoxyphenyl mono-cyanoacrylate substituted dye showed the highest conversion efficiency of 5.09%.



**KEYWORDS:** Liquid crystal display, Black Matrix, dyes, Phthalocyanine, Dielectric constant, Light absorption, Solubility, Thermal stability, Light Absorption, Dye-sensitized solar cells, Phenoxazine dyes, Five-membered heterocyclic bridges, Ethoxyphenyl substitution, Dihedral angle, Dye adsorption, Di-anchor, N-substituent, Dihedral angle, Dye adsorption

**Student Number: 2007-20735**

# **Contents**

**Abstract**

**Contents**

**List of Tables**

**List of Schemes**

**List of Figures**

## **Chapter 1. Introduction**

1.1 An overview of LCDs (Liquid Crystal Displays)

1.2 Structures and requirements of LCD black matrix

1.3 Fabrication of black matrix pattern using black matrix photo-resist

1.4 An overview of DSSCs (Dye-sensitized Solar Cells)

1.5 Operating principle and fabrication of DSSCs

1.6 Requirements of organic sensitizers

1.7 References

## **Chapter 2. Synthesis and characterization of solubility enhanced metal-free phthalocyanines for liquid crystal display black matrix of low dielectric constant**

2.1 Introduction

2.2 Experimental

2.2.1 General

2.2.2 Synthesis

2.2.3 Preparation of dye-based black matrix

2.2.4 Measurement of spectral and chromatic properties

2.2.5 Measurement of solubility

2.2.6 Measurement of thermal stability

2.2.7 Geometry optimization of the synthesized dyes

2.3 Results and Discussion

2.3.1 Synthesis of dyes

2.3.2 Solubility

2.3.3 UV-vis absorption spectra

2.3.4 Thermal properties

2.3.5 Dielectric properties

2.4 Conclusions

2.5 References

## **Chapter 3. Analysis and characterization of dye-based black matrix film of low dielectric constant containing phthalocyanine and perylene dyes**

3.1 Introduction

3.2 Experimental

3.2.1 General

3.2.2 Synthesis

3.2.3 Preparation of dye-based black matrix

3.2.4. Measurement of spectral and optical properties

3.2.5 Investigation of solubility

- 3.2.6 Measurement of thermal stability
- 3.2.7 Field emission scanning electron microscopy and Atomic force microscopy
- 3.3 Results and Discussion
  - 3.3.1 Properties of dyes
  - 3.3.2 Spectral and optical properties of dye-based black matrix
  - 3.3.3 Thermal properties of dye-based black matrix
  - 3.3.4 Dielectric properties of dye-based black matrix
  - 3.3.5 Surface investigation of BM film by FE-SEM and AFM
- 3.4 Conclusion
- 3.5 References

**Chapter 4. The effect of five-membered heterocyclic bridges and ethoxyphenyl substitution on the performance of phenoxazine-based dye-sensitized solar cells**

4.1 Introduction

4.2 Experimental

4.2.1 Materials and reagents

4.2.2 Analytical instruments and measurements

4.2.3 Fabrication of dye-sensitized solar cells and measurements

4.2.4 Synthesis of dyes

4.3 Results and Discussion

4.3.1. Synthesis

4.3.2 Photophysical properties

4.3.3 Electrochemical properties

4.3.4 Photovoltaic properties

4.4 Conclusion

4.5 Reference

**Chapter 5. The effects of the number of anchoring groups and  
*N*-substitution on the performance of phenoxazine dyes in dye-  
sensitized solar cells**

- 5.1 Introduction
- 5.2 Experimental
  - 5.2.1 Materials and reagents
  - 5.2.2 Analytical instruments and measurements
  - 5.2.3 Fabrication of dye-sensitized solar cells and measurements
  - 5.2.4 Synthesis of dyes
- 5.3 Results and Discussion
  - 5.3.1 Synthesis of dyes
  - 5.3.2 Density functional theory (DFT) calculations
  - 5.3.3 Photophysical properties of the dyes in solution and on TiO<sub>2</sub> film
  - 5.3.4 Electrochemical properties
  - 5.3.5 Photovoltaic properties
  - 5.3.6 Electrochemical impedance spectroscopy
- 5.4 Conclusion
- 5.5 References

**Summary**

**Korean Abstract**

**List of Publications**

**List of Presentations**



## List of Tables

**Table 2.1** Solubility of the dyes at 20 °C.

**Table 2.2** Absorption maxima and extinction coefficients of the prepared dyes in CH<sub>2</sub>Cl<sub>2</sub> and PB 16 in sulfuric acid.

**Table 2.3** Electronic energies of the prepared dyes.

**Table 2.4** The coordinate values corresponding to the CIE 1931 chromaticity diagram of the dye-based black matrix.

**Table 2.5** Dielectric constants and constitutions of the dye-based black matrix.

**Table 3.1** Absorption maxima and molar extinction coefficients of the prepared dyes in cyclohexanone.

**Table 3.2** Solubility of the dyes in cyclohexanone at 20 °C.

**Table 3.3** Optical density <sup>a</sup> of the prepared films.

**Table 3.4** Retention rates of film without dye and film C.

**Table 3.5** Dielectric constants the dye-based black matrix at 10kHz.

**Table 3.6** Rq of the prepared films.

**Table 4.1** Photophysical and electrochemical properties of WS1, WS2 and WS3 dyes.

**Table 4.2** Optimized structures, dihedral angles and electronic distributions in HOMO and LUMO levels of the prepared dyes.

**Table 4.3** DSSC performance parameters of POX, WS1, WS2, and WS3.

**Table 5.1** Optimized structures, dihedral angles and electronic distributions in HOMO and LUMO levels of the prepared dyes.

**Table 5.2** Photophysical and electrochemical properties of POX, WB, WH1 and WH2.

**Table 5.3** DSSC performance parameters of POX, WB, WH1, and WH2.

**Table 5.4** Lifetime calculations of POX, WB, WH1 and WH2.

## List of Schemes

**Scheme 2.1** Synthesis of the prepared dyes.

**Scheme 3.1** Conventional and BOT structures of LCD.

**Scheme 4.1** Synthesis of POX, WS1, WS2, and WS3: (a) 1-iodobutane, NaOH, DMSO (b) NBS, CHCl<sub>3</sub> (c) POCl<sub>3</sub>, DMF, CHCl<sub>3</sub> (d) 2M aqueous of K<sub>2</sub>CO<sub>3</sub>, Pd(pph<sub>3</sub>)<sub>4</sub>, THF (e) cyanoacetic acid, piperidine, acetonitrile.

**Scheme 5.1** Synthesis of POX, WB, WH1 and WH2.

## List of Figures

**Figure 1.1** Basic structure of liquid crystal display.

**Figure 1.2** Fundamental structure of liquid crystal display color filter..

**Figure 1.3** a) Fundamental processes in a dye-sensitized solar cell b) Energy-level diagram of a DSSC.

**Figure 1.4.** Fabrication of the dye sensitized solar cells.

**Figure 2.1** Structure of Pigment Blue 16.

**Figure 2.2** Geometry-optimized structures of the prepared dyes.

**Figure 2.3** Absorption spectra of the synthesized dyes in  $\text{CH}_2\text{Cl}_2(10^{-5}\text{mol litre}^{-1})$  and PB 16 in sulfuric acid( $10^{-5}\text{mol}$ ).

**Figure 2.4** Transmittance spectra of the spin-coated black matrix with dye 1b.

**Figure 2.5** Thermogravimetric analysis (TGA) of the prepared dyes.

**Figure 3.1** Structure of Zn-PC and PER.

**Figure 3.2** Absorbtion spectra of Zn-PC and PER in cyclohexanone( $10^{-5}\text{molL}^{-1}$ ).

**Figure 3.3** Differential scanning calorimetry(DSC) measurements of the prepared dyes.

**Figure 3.4** Thermogravimetric analysis (TGA) of the prepared dyes.

**Figure 3.5** Transmittance spectrum of film A.

**Figure 3.6** Transmittance spectrum of film B ( Zn-PC : PER = 2 mol:1 mol) , film C ( Zn-PC : PER = 3 mol:1 mol) and solution (Zn-PC : PER = 1 mol:1 mol).

**Figure 3.7** SEM images of film B and film C.

**Figure 3.8** AFM images of film B and film C.

**Figure 4.1** Structure of POX, WS1, WS2, and WS3.

**Figure 4.2** Absorbtion spectra of WS1, WS2, and WS3 in (a) EtOH/CH<sub>2</sub>Cl<sub>2</sub> (7 : 2; v/v) (10<sup>-5</sup>molL<sup>-1</sup>) and (b) on TiO<sub>2</sub>.

**Figure 4.3** Dyes' HOMO and LUMO energy levels.

**Figure 4.4** CV curves of Fc/Fc<sup>+</sup>, POX, WS1, WS2, and WS3 in CH<sub>2</sub>Cl<sub>2</sub>.

**Figure 4.5** (a) IPCE spectra DSSCs based on POX, WS1, WS2, WS3, and N719 and (b) the DSSCs' *J-V* curves under AM 1.5G simulated sunlight (100

mWcm<sup>-2</sup>).

**Figure 4.6** DSSCs'  $J-V$  curves based on POX, WS1, WS2, and WS3 in the dark.

**Figure 4.7** Impedance spectra of DSSCs based on POX, WS1, WS2, and WS3;

Nyquist plots measured at 0.60 V forward bias in the dark.

**Figure 4.8** Electron lifetime of N719, POX, WS1, WS2, and WS3 as a function of bias voltage.

**Figure 5.1** Structure of POX, WB, WH1 and WH2.

**Figure 5.2** Absorbtion spectra of POX, WB, WH1 and WH2 in (a) THF ( $10^{-5}$  molL<sup>-1</sup>) and (b) on TiO<sub>2</sub>.

**Figure 5.3** Dyes' HOMO and LUMO energy levels.

**Figure 5.4** CV curves of Fc/Fc<sup>+</sup>, POX, WB, WH1 and WH2 in DMF.

**Figure 5.5** Emission spectra of POX, WB, WH1 and WH2 in THF.

**Figure 5.6** Normalized absorption and emission spectra of POX, WB, WH1 and WH2 in THF.

**Figure 5.7** (a) IPCE spectra DSSCs based on POX, WB, WH1 and WH2 and (b) the DSSCs'  $J-V$  curves under AM 1.5G simulated sunlight (100 mWcm<sup>-2</sup>).

**Figure 5.8** FT-IR spectra of (a) WB absorbed on TiO<sub>2</sub> and (b) WH2 absorbed on TiO<sub>2</sub>.

**Figure 5.9.** DSSCs'  $J-V$  curves based on POX, WB, WH1 and WH2 in the dark.

**Figure 5.10** Impedance spectra of DSSCs based on POX, WB, WH1, and WH2. (a) Nyquist plots measured at 0.55 V forward bias in the dark, (b) Bode phase plots measured under illuminations (AM 1.5G).

**Figure 5.11** Electron lifetime of POX, WB, WH1, and WH2 as a function of bias voltage.

**Figure 5.12** (a) Resistance and (b) capacitance of POX, WB, WH1 and WH2 as a function of bias voltage.

## **Chapter 1**

### **Introduction**

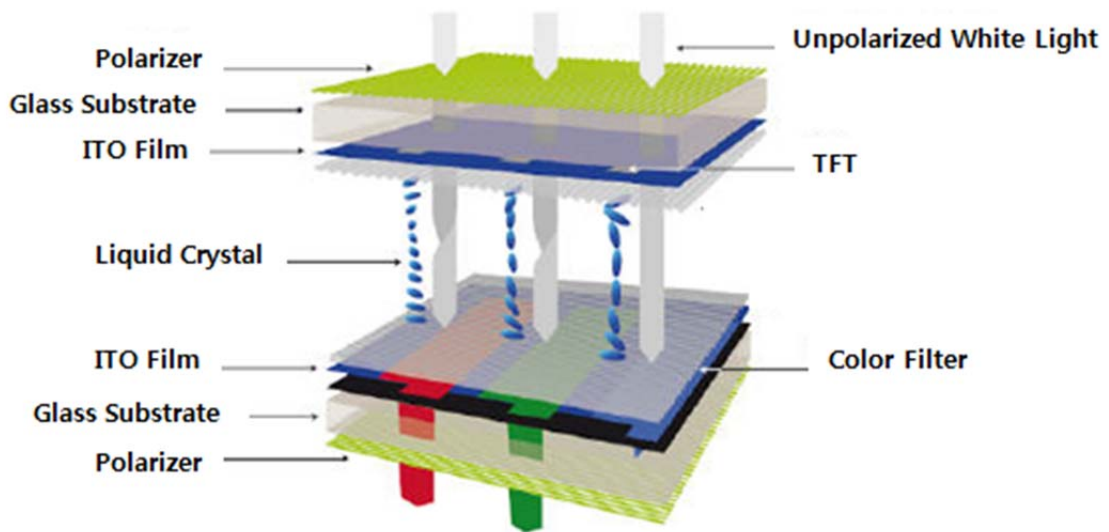
#### 1.1 An overview of LCDs (Liquid Crystal Displays)

There exist several types of display system to visualize information such as cathode ray tubes (CRTs), electroluminescence (EL) devices, field emission devices (FEDs), plasma display panels (PDPs) and liquid crystal displays (LCDs). Each of the displays has its own special characteristics and the proper choice of display for a particular use depends on many factors such as cost, size, brightness, definition, life, power consumption, temperature range, operating voltage and device circuit, etc. [1, 2].

Among these display systems, the LCDs have emerged as the most promising displays during last decade. The extremely low power consumption, low voltage operation, high definition, compactness and flexibility of size are the distinctive features which make LCDs preferable over other types of displays [3,4]. Figure 1.1 shows a basic structure of LCD panel. The LCD is basically consisted of a thin layer of liquid crystal sandwiched between a pair of polarizers. To control the optical transmission of the display element



electronically, the liquid crystal layer is placed between transparent electrodes [e.g., indium tin oxide (ITO)]. The thickness of the liquid crystal layer is kept uniform by using spacers that are made of photosensitive polymers. The polarizer and the electrodes are cemented on the surfaces of the glass plates. By applying a voltage across the electrodes, an electric field inside the liquid crystal can be obtained to control the light transmission through the liquid crystal cell.



**Figure 1.1** Basic structure of liquid crystal display

## 1.2 Structures and requirements of LCD black matrix

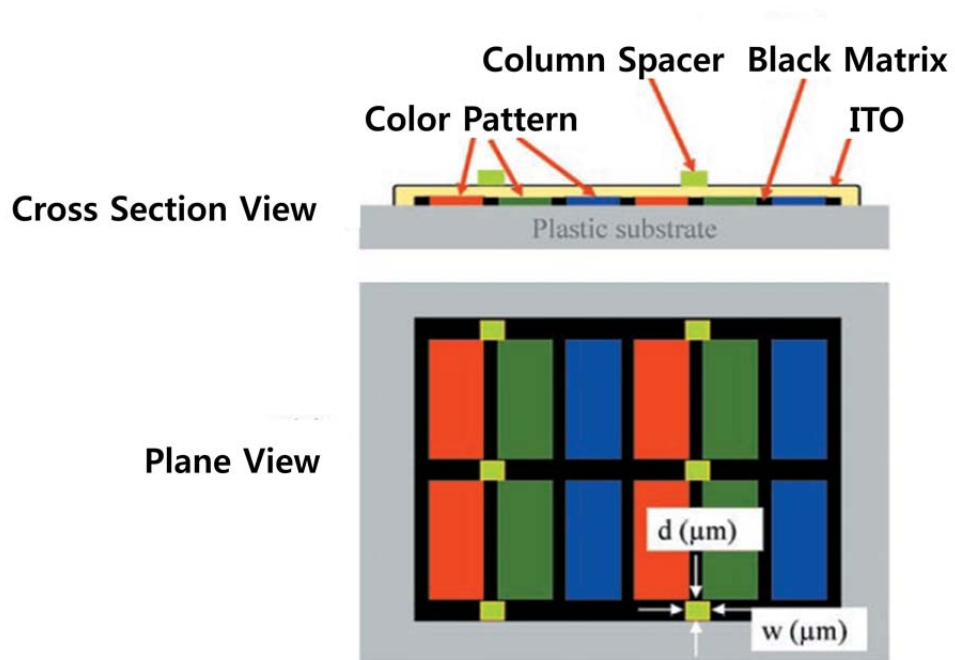
Generally, a color filter consists of clear substrate, black matrix (BM), RGB color layers, overcoat layer, and column spacer. The BM material is coated on clear substrate in the optically inactive areas to prevent light leakage and provide a light shield for the amorphous silicon transistors. BM material can be organic or inorganic and carbon black is the most popular organic choice. The RGB color layers are fabricated with either dyes or pigments and protection overcoat layer is deposited over the color layers. A column spacer is a material used to maintain a uniform cell gap between the TFT and the color filter glass. The structural configuration of BM films on color filters is shown in Figure 1.2 [3,4].

The BM film plays vital role in blocking the light to TFT and defending the contrast ratio reduction by photo leak from a non-display area. Therefore, for a practical use, the BM with a high opacity property or optical density (OD) over  $4/\mu\text{m}$  and a good resolution of  $10\text{-}30\mu\text{m}$  is desired. In addition, low reflectance is also preferred property of BM for LCD applications.

It is also important to increase the aperture ratio of BM for high transmittance. Fabrication of BM with high aperture ratio can reduce the power consumption

of TFT-LCDs by lowering backlight power. Besides, in case of LCDs with a black matrix-on-thin film transistor (BOT) structure, the dielectric constant of BMs needs to be  $<7$  for satisfactory industrial application. The high dielectric constant of BM can cause malfunctions of LCD TFTs due to interference of the TFT electric signal with BM materials.

In addition, BM must exhibit high heat resistance without thermal flow and small chromatic changes during the alignment layer formation step. The chromatic changes ( $\Delta E_{ab}$ ) should be less than 3 after heating at  $250^{\circ}\text{C}$  for 1 h and the retention rate of BM (the ratio between the thickness of the film after prebaking and post-baking) needs to be  $>80\%$  for satisfactory thermal stability [4,5]. The light stability of the pixels is important because BMs are exposed to a lamp with ultraviolet (UV) filter for more than two million lux. The chemical stability is also important since BMs are exposed to solvents, acids and bases during the LCD fabrication process. In detail, the cured film must be stable when exposed to solvents such as NMP and  $\gamma$ -butyrolactone, and to acids used in etching process or bases used in the development system [4,5].



**Figure 1.2** Fundamental structure of Liquid crystal display color filter

### 1.3 Fabrication of black matrix pattern using black matrix photo-resist

BM pattern is fabricated using a BM photo-resist. The BM photo-resist is a light-sensitive material used in several industrial processes, such as photolithography and photo-engraving to form a patterned coating on a surface. Photo-resists are classified into two groups: positive and negative-tone resists.

> A *positive-tone photo-resist* is a type of photo-resist in which the portion of the photo-resist that is exposed to light becomes soluble to the photo-resist developer. The portion of the photo-resist that is unexposed remains insoluble to the photo-resist developer.

> A *negative-tone photo-resist* is a type of photo-resist in which the portion of the photo-resist that is exposed to light becomes insoluble to the photo-resist developer. The unexposed portion of the photo-resist is dissolved by the photo-resist developer.

The BM photo-resist is negative-tone photo-resist which is made up of BM material, dispersant, photo-sensitive binder, multi-functional monomer, photo-

initiator and additives such as leveling agent and coupling agent. Conventional fabrication process of BM is following complicated photolithographic method using BM photo-resist [4,5] as shown below.

1. Spin coating process;

BM photo-resist is dropped onto a glass substrate to prepare a black film by a spin coating process.

2. Prebaking process;

The black film is prebaked on a hot plate.

3. Exposure;

To make the pattern insoluble, it is UV cured by exposure through a photo-mask.

4. Development & postbaking;

After the removal of unnecessary portions of the color resist by the developing solution, the pattern is cured through postbaking.

## 1.4 An overview of DSSCs (Dye-sensitized Solar Cells)

The generation speed of fossil fuels is much slower than the depletion rate, leading to human society getting close to an energy and environmental crisis. Solar energy is regarded as one of the perfect energy resources owing to its huge reserves, inexhaustibility and pollution-free character. Direct conversion of solar light to electric energy based on photovoltaics is the optimal way for electrified modern society.

Different technologies in photovoltaics, such as crystalline Si, semiconductor(e.g., GaAs)-based cells, thin-film (e.g., CdTe) solar cells, organic bulk heterojunction (BHJ) solar cells and dye-sensitized solar cells (DSSCs), co-exist to compete in the future market. Among them, the DSSCs have been considered as a highly promising and cost-effective alternative for the photovoltaic energy sector and attracted considerable attention in recent years.[6]

Dye-sensitized solar cells generate electricity by converting energy from light absorbed by the dye. Since these solar cells can be produced from low-cost materials using simple manufacturing processes, overall manufacturing expenditures are expected to be comparatively low. Other advantages over

silicon-based solar cells include the ability to use a variety of designs and colors and, achieve high performance under indoor and low light settings. In addition, changes in the angle at which light hits the surface of the cells have minimal effect on the performance. Such advantages are expected to expand the range of use for solar cells, which are ideal for a variety of consumer-related applications in which conventional solar cells are unsuitable.

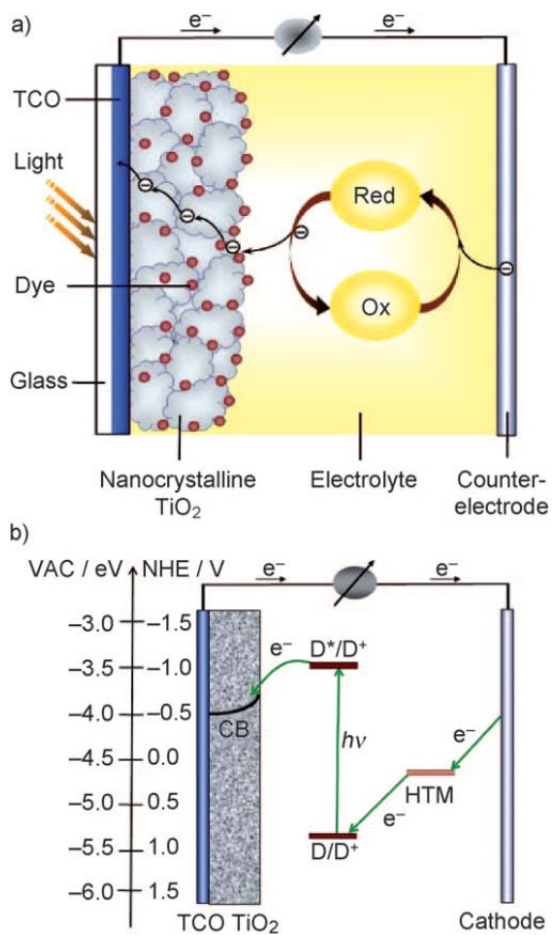
Presently, organic sensitizers for DSSCs fall into two broad categories: metal-polypyridyl complexes and pure metal-free organic dyes. DSSCs based on ruthenium (Ru)-polypyridyl dyes usually show high efficiency (10–11%) due to their wide absorption range from the visible to the near-infrared (NIR) regime. However, high production cost and difficulties in purification have limited their development for large-scale applications. Recently, with focus on the cost and limited Ru resource, a metal-free organic sensitizer could become very promising once the efficiency and stability were improved to a viable level. Compared to Ru dyes, metal-free sensitizers have advantages of low cost and structural design flexibility. Moreover, the molar extinction coefficients of metal-free dyes are normally much higher than that of Ru dyes. Undoubtedly, molecular engineering is the most effective method to improve the performance from the viewpoint of sensitizers[7]. For these reasons, sensitizers without Ru



such as triphenylamine, indoline, cyanine, coumarin, perylene, porphyrin, phthalocyanine, and phenothiazine have been extensively studied. Among these, porphyrin derivatives have shown high electronic conversion efficiency (12.3%).

## 1.5 Operating principle and fabrication of DSSCs

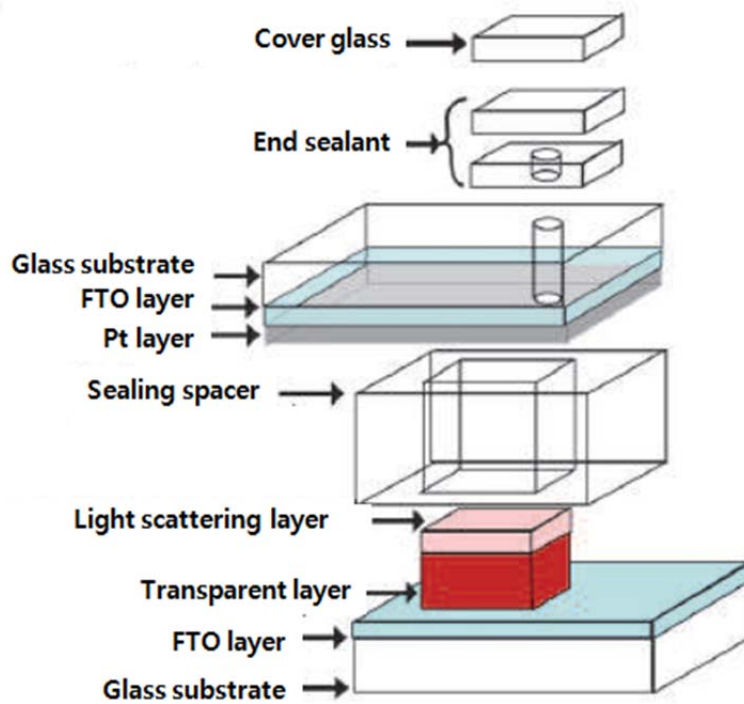
Conventional DSSCs typically contain five components: 1) a photoanode, 2) a mesoporous semiconductor metal oxide film, 3) a sensitizer (dye), 4) an electrolyte/hole transporter, and 5) a counterelectrode. In DSSCs, the photosensitizer dye can absorb sunlight and create a high energy state, from which a photo-excited electron is injected into the conduction band of the  $\text{TiO}_2$  semiconductor. After percolation through the thin mesoscopic semiconductor film, the injected electrons are collected by the conducting substrate and flow into the external circuit. Simultaneously, the oxidized sensitizers generated after electron injection are reduced to their neutral state by the reducing species (generally iodide ions) in the electrolyte solution. The oxidized species in the electrolyte diffuse into the counter electrode and receive the external circuit electrons to complete the whole circuit. Such a cycle is kept repeating without any material being consumed but energy being transformed from light to electricity. The general operating principle of a dye-sensitized solar cell is depicted in Figure 1.3. [8]



**Figure 1.3** a) Fundamental processes in a dye-sensitized solar cell b) Energy-level diagram of a DSSC.

Figure 1.4 depicts fabrication of the dye sensitized solar cells. First, one prepares glass substrate with a transparent conducting layer. Then, the DSSC

working electrodes are prepared. For the paste used in the light-scattering layers, 10nm TiO<sub>2</sub> particles which were obtained after the peptization step were mixed with 400 nm TiO<sub>2</sub> colloidal solution. Pastes are coated on FTO, forming the TiO<sub>2</sub> film. It is treated with TiCl<sub>4</sub> before sintering. After cooling, the electrode is immersed in dye solutions. Finishing fabrication of all parts, the dye-covered TiO<sub>2</sub> electrode and Pt-counter electrode are assembled into a sandwich type cell and sealed with a hot-melt gasket. For the counter electrode, a hole (1-mm diameter) is drilled in the FTO glass. The hole is made to let the electrolyte in via vacuum backfilling. After the injection of electrolyte, the hole is sealed using a hot-melt film and a cover glass.



**Figure 1.4** Fabrication of the dye sensitized solar cells.

## 1.6 Requirements of organic sensitizers

Dyes employed in highly efficient DSSC have to meet several requirements; the absorption spectrum on the nanoporous TiO<sub>2</sub> layer, the energy level of the ground/exited state, the charge injection/recombination and the stability. [9]

### 1) Absorption spectrum

The dye concentration within the nanoporous TiO<sub>2</sub> electrode and the absorption coefficient determine the amount of light that is absorbed. Therefore, the dye should have a high absorption coefficient in the visible region and a high affinity to the TiO<sub>2</sub> to ensure a high efficiency. With increasing absorbance of the TiO<sub>2</sub>-electrode, the layer thickness can be decreased, which is advantageous for two reasons:

- The recombination probability decreases with decreasing electrode thickness.
- More viscous electrolytes with low vapor pressure can be applied.

In addition, the dye also should have a broad absorption range. If it is possible to synthesize novel dyes with an absorption that extends into the near infrared (NIR), the short circuit current can be significantly improved.

## 2) Energy level

The energy level of the excited dye molecule should be about 0.2 - 0.3 eV above the conduction band of the TiO<sub>2</sub> to ensure efficient charge injection. In this case, the activation energy for the back reaction is also high and the corresponding rate is too slow to compete with the dye regeneration by the electrolyte. In addition, the highest occupied molecular orbital of the dye should lie below the energy level of the hole transporter, so that the oxidized dyes formed after electron injection into the conduction band of TiO<sub>2</sub> can be effectively regenerated by accepting electrons from the hole transport material.

## 3) Charge injection and charge recombination

Charge injection occurs from the  $\pi^*$ -orbitals of the anchoring group (carboxylic or phosphonic acid) to the titanium 3d-orbitals. Thus, a good overlap of these orbitals is mandatory for efficient charge injection. Injection of electrons from the dye into the TiO<sub>2</sub> typically happens on a femto- to picosecond time scale whereas charge recombination in the micro to millisecond time scale.

For an efficient charge injection, the regeneration of the sensitizer by a hole

transporter should be much faster than the recombination of the conduction band electrons with the oxidized sensitizer. For example, one finds a recombination rate of  $k_{\text{rec}} = 1.4 \times 10^3 \text{ s}^{-1}$  and a regeneration rate of  $k_{\text{reg}} = 1.1 \times 10^5 \text{ s}^{-1}$  for the prepared dye. Thus the regeneration is a hundred times faster, which ensures an injection yield of 99 %.

#### 4) Stability

Any sensitizer in DSSC has to sustain at least twenty years of operation without significant degradation. Ideally, the electron injection and regeneration is completely reversibly. However, in any real device, some degradation of the dye occurs. The standard accelerated aging test lasts typically for 1000 hours, which corresponds to one year of outdoor application.



## 1.7 References

- [1] Yeh P, Gu C. Optics of liquid crystal displays. John Wiley & Sons, Inc; 1999. P. 1-5.
- [2] Yang DK, Wu ST. Fundamentals of liquid crystal devices. New Jersey: Wiley-SID; 2006: 278–281.
- [3] Choi J, Kim SH, Lee WS, Yoon C, Kim JP. Synthesis and characterization of thermally stable dyes with improved optical properties for dye-based LCD color filters. *New J. Chem.* 2012; 36:812–818.
- [4] Sabnis RW. Color filter technology for liquid crystal displays. *Displays* 1999; 20:119–29.
- [5] Tsuda K. Color filters for LCDs. *Displays* 1993;14:115–124.
- [6] (a) Hagberg DP, Yum J-H, Lee H, De Angelis F, Marinado T, Karlsson KM. Molecular engineering of organic sensitizers for dye-sensitized solar cell applications. *Journal of the American Chemical Society* 2008; 130: 6259-66
- (b) Zhang G, Bala H, Cheng Y, Shi D, Lv X, Yu Q, et al. High efficiency and stable dye-sensitized solar cells with an organic chromophore featuring a binary  $\pi$ -conjugated spacer. *Chemical Communications* 2009; 16: 2198-200
- [7] (a) O'Regan B, Grätzel M. A low-cost, high-efficiency solar cell based on

- dye-sensitized colloidal TiO<sub>2</sub> films. *Nature* 1991; 353: 737-40
- (b) Grätzel M. Dye-sensitized solar cells. *Journal of Photochemistry and Photobiology C* 2003; 4: 145-53
- (c) Grätzel M. Conversion of sunlight to electric power by nanocrystalline dye-sensitized solar cells. *Journal of Photochemistry and Photobiology A* 2004; 164(3): 3-14
- (d) Park N-G, Kim K. Transparent solar cells based on dye-sensitized nanocrystalline semiconductors. *Physica Status Solidi (a)* 2008; 205(8): 1895-904
- [8] (a) Yongzhen W and Weihong Zhu, Organic sensitizers from D–p–A to D–A–p–A: effect of the internal electron-withdrawing units on molecular absorption, energy levels and photovoltaic performances. *Chem Soc Rev* 2013; 42: 2039-58
- (b) Mishra A, Fischer MKR, and Bäuerle P, Metal-Free Organic Dyes for Dye-Sensitized Solar Cells: From Structure: Property Relationships to Design Rules. 2009: 48: 2474-99
- [9] (a) Kim S, Lee JK, Kang SO, Ko J, Yum J-H, Fantacci S, et al. Molecular engineering of organic sensitizers for solar cell applications. *Journal of the American Chemical Society* 2006; 128(51): 16701-7

(b) Koumura N, Wang Z-S, Miyashita M, Uemura Y, Sekiguchi H, Cui Y, et al. Substituted carbazole dyes for efficient molecular photovoltaics: long electron lifetime and high open circuit voltage performance. *Journal of Materials Chemistry* 2009; 19: 4829-36

(c) Yella A, Lee H-W, Tsao HN, Yi C, Chandiran AK, Nazeeruddin MK, et al. Porphyrin-sensitized solar cells with cobalt (II/III)-Based redox electrolyte exceed 12 percent efficiency. *Science* 2011; 334: 629-34

## **Chapter 2**

### **Synthesis and characterization of solubility enhanced metal-free phthalocyanines for liquid crystal display black matrix of low dielectric constant**

#### 2.1 Introduction

The black matrix (BM), a component of LCD color filters, divides the red, green and blue (RGB) pixels of the color filter and blocks light leaking from the areas between the RGB color patterns enhancing contrast ratio of color filters.[1] According to the component materials, BM can be divided into metal oxide, carbon black, titanium black and organic pigment types.[2] Among the various types of BMs, a carbon black BM manufactured by spin-coating is generally employed in industry. The advantage of using carbon black as a BM component arises from its high light absorption property, high thermal stability and low cost.[2, 3] On the other hand, malfunctions of the thin film transistor (TFT) of a LCD can occur due to the high dielectric constant of carbon black. To avoid this problem, an organic pigment BM with a low dielectric constant can be used despite its low spectral property due to the lower molar extinction coefficient of

organic pigments.[4]

If dyes are used for the manufacture of the BM, the high dielectric constant and low light absorption of conventional BMs can be overcome. On the other hand, dyes generally have low thermal stability compared to carbon black and organic pigments. Therefore, the dyes for BM need to be structurally stable.[5, 6] They also should have good solubility in industrial solvents, such as propylene glycol methyl ether acetate (PGMEA) and cyclohexanone.[6]

In this study, green phthalocyanine (PC) dyes with high thermal stability and high solubility were designed. Three metal-free PC dyes were synthesized by introducing substituents including alkyl or alkoxy groups to the peripheral position of the PC rings, and their spectral properties, solubilities and thermal stabilities were measured. Dye-based BMs were fabricated and their optical and dielectric properties were examined.

## 2.2 Experimental

### 2.2.1 General

2,5-bis-(1,1-dimethylbutyl)-methoxyphenol, 4-hydroxy-3-tert-butylanisole, 2,4-bis(1,1-dimethylpropyl)phenol were purchased from TCI and, dimethyl sulfoxide (DMSO), potassium carbonate anhydrous, dichloromethane, m-xylene anhydrous, ethanol anhydrous and lithium granule purchased from Sigma Aldrich were used as received. All reagents and solvents were of reagent-grade quality and obtained from commercial suppliers. Transparent glass substrates were provided by Paul Marienfeld GmbH & Co. KG and acrylic binder LC20160 were supplied by SAMSUNG Cheil industries Inc.

<sup>1</sup>H NMR spectra were recorded on a Bruker Avance 500 spectrometer at 500MHz using chloroform-d and tetramethylsilane (TMS), as the solvent and internal standard, respectively. Matrix Assisted Laser Desorption/Ionization Time Of Flight (MALDI-TOF) mass spectra were collected on a Voyager-DE STR Biospectrometry Workstation with  $\alpha$ -cyano-4-hydroxy-cynamic acid (CHCA) as the matrix. Fourier transform infrared (FT-IR) spectra were recorded in the form of solid on a Thermo Scientific Nicolet 6700 FT-IR

spectrometer. Elemental analysis was done on CE Instrument EA1112. Absorption spectra were measured using a HP 8452A spectrophotometer. Thermogravimetric analysis (TGA) was conducted under nitrogen at a heating rate of  $10\text{ }^{\circ}\text{C min}^{-1}$  using a TA Instruments Thermogravimetric Analyzer 2050. Dielectric constants were measured using Edward E306 thermal evaporator and HP 4294A precision impedance analyzer.

### 2.2.2 Synthesis

Preparation of 4-(2,5-Bis(1,1-dimethylbutyl)-4-methoxyphenoxy) phthalonitrile (1a) 4-nitrophthalonitrile(1g, 5.77mmol) and 2,5-bis-(1,1-dimethylbutyl)-methoxyphenol(1.68g, 5.77mmol) were dissolved in dry DMSO(30ml) and anhydrous  $\text{K}_2\text{CO}_3$ (1.06g, 7.66mmol) was added in portions during 4h. The mixture was stirred at  $40\text{ }^{\circ}\text{C}$  for 24h under nitrogen atmosphere. After filtering the reaction mixture, the residue was extracted with  $\text{CH}_2\text{Cl}_2$  and dried by rotary evaporation. Pure product in 91%(2.19g, 5.23mmol) yield was collected by column chromatography on silica gel using EA/hexane (10:1)mixture as an eluent.  $^1\text{H NMR}$  ( 500MHz;  $\text{CDCl}_3$ ; Me $_4\text{Si}$ ):  $\delta\text{H}$ , ppm 7.69 (1H, d), 7.22 (1H, s), 7.14 (1H, d), 6.82 (1H, s), 6.63(1H, s), 3.08 (3H, s, -O-CH $_3$ ), 1.71 (2H, m),

1.56 (2H, m), 1.26(12H, d), 1.04 (2H, m), 0.96 (2H, m), 0.81 (3H, t), 0.71 (3H, t).

Preparation of 4-(3-tert-butyl-4-methoxyphenoxy)phthalonitrile (2a) 2a (yield 85%) was synthesized following the same procedure for 1a using 2 (1g, 5.54mmol), 4-nitrophthalonitrile(0.96g, 5.54mmol), DMSO(30ml), and anhydrous K<sub>2</sub>CO<sub>3</sub>(1.06g, 7.66mmol). <sup>1</sup>H NMR ( 500MHz; CDCl<sub>3</sub>; Me<sub>4</sub>Si): δH, ppm 7.71 (1H, d), 7.26 (1H, s), 7.22 (1H, d), 7.01 (1H, s), 6.77(2H, m), 3.83 (3H, s, -O-CH<sub>3</sub>), 1.30 (9H, m).

Preparation of 4-(2,4-Bis(1,1-dimethyl-propyl)phenoxy)phthalonitrile (3a) 3a (yield 82%) was synthesized following the same procedure for 1a using 3 (1.2g, 5.12mmol), 4-nitrophthalonitrile(0.89g, 5.12mmol), DMSO(30ml), and anhydrous K<sub>2</sub>CO<sub>3</sub>(1.06g, 7.66mmol). ). <sup>1</sup>H NMR ( 500MHz; CDCl<sub>3</sub>; Me<sub>4</sub>Si): δH, ppm 7.71 (1H, d), 7.35 (1H, s), 7.27 (1H, s), 7.22 (1H, d), 7.18 (1H, d), 6.75 (1H, d), 1.66 (4H, m), 1.30 (12H, d), 0.70 (3H, t), 0.63 (3H, t).

Preparation of 1(4)-Tetrakis(2,5-Bis(1,1-dimethylbutyl)-4-methoxyphenoxy)-phthalocyaninatozinc(II) (1a).

Preparation of tetrakis(2,5-Bis(1,1-dimethylbutyl)-4-methoxyphenoxy)-phthalocyanine (1b) 1a(0.9g, 2.38mmol) was dissolved in anhydrous xylene(50ml) and ethanol(10ml) under nitrogen atmosphere and Li(0.13g,



18.7mmol) was added in the solution. The reaction mixture was stirred at 150 °C for 5h. After cooling the solution, the resulting slurry was extracted with CH<sub>2</sub>Cl<sub>2</sub>(100ml) and washed with saturated NaCl solution. The pure product in 54%(0.53g, 0.31mmol) yield was obtained by column chromatography on silica gel using CH<sub>2</sub>Cl<sub>2</sub> as an eluent. Anal. calcd.(%) for C<sub>108</sub>H<sub>138</sub>N<sub>8</sub>O<sub>8</sub>: C, 77.38; H, 8.30; N, 6.68; O, 7.64. Found(%): C, 77.36; H, 8.27; N, 6.66; O, 7.69. MALDI-TOF MS: m/z 1675.9 (100%, [M+2K]<sup>+</sup>). IR: ν, cm<sup>-1</sup> 3289 (NH).

Preparation of tetrakis(3-tert-butyl-4-methoxyphenoxy)-phthalocyanine (2b) 2b (yield 41%) was synthesized following the same procedure for 1b using 2a (1g, 3.26mmol), Li, ethanol(10ml), and anhydrous xylene(50ml). Anal. calcd.(%) for C<sub>76</sub>H<sub>74</sub>N<sub>8</sub>O<sub>8</sub>: C, 74.37; H, 6.08; N, 9.13; O, 10.43. Found(%): C, 74.37; H, 6.08; N, 9.12; O, 10.45. MALDI-TOF MS: m/z 1227.1 (100%, [M+2K]<sup>+</sup>). IR: ν, cm<sup>-1</sup> 3289 (NH).

Preparation of tetrakis(2,4-Bis(1,1-dimethyl-propyl)phenoxy)-phthalocyanine(3b) 3b(yield 49%) was synthesized following the same procedure for 1b using 3a (1.1g, 3.05mmol), Li, ethanol(10ml), and anhydrous xylene(50ml). Anal. calcd.(%) for C<sub>96</sub>H<sub>114</sub>N<sub>8</sub>O<sub>4</sub>: C, 79.85; H, 7.96; N, 7.76; O, 4.43. Found(%): C, 79.88; H, 8.75; N, 6.33; O, 4.25. MALDI-TOF MS: m/z 1443.7 (100%, [M+2K]<sup>+</sup>). IR: ν, cm<sup>-1</sup> 3293 (NH).

### *2.2.3 Preparation of dye-based black matrix*

The ink for a black matrix was composed of the dye (0.01g), cyclohexanone (4.0g), and LC20160 (14g) as a binder based on acrylate. The prepared dye-based inks were coated on a transparent glass substrate using a MIDAS System SPIN-1200D spin coater. The coating speed was initially 100 rpm for 5s, which was then increased to 200 rpm and kept constant for 20s. The wet dye-coated black matrix was then dried at 80 °C for 20 min, prebaked at 150 °C for 10 min, and postbaked at 230 °C for 1h. After each step, the coordinate values of the black matrix were measured.

### *2.2.4 Measurement of spectral and chromatic properties*

The absorption spectra of the synthesized dyes and the transmittance spectra of the dye-based BM were measured using a UV-vis spectrophotometer. The chromatic values were recorded on a color spectrophotometer (Scinco colormate).

### *2.2.5 Measurement of solubility*

Small amounts of the dyes (0.05g) were added to the solvents (0.5g). The solutions were stirred for 20 min and left to stand for 24 h at room temperature. Precipitations were visually checked and additional solvents (0.25g) were added into the solutions to until it made clear solutions. The solubility of the dye was recorded as weight percentage of dyes in the clear solutions.

### *2.2.6 Measurement of thermal stability*

The thermal stability of the synthesized dyes was evaluated by thermogravimetry (TGA). The prepared dyes were heated to 110°C and held at that temperature for 10 min to remove the residual water and solvents. The dye was then heated to 230°C and held at that temperature for 60 min to simulate the processing thermal conditions of color filter manufacturing. The dyes were finally heated to 500°C to determine their degradation temperature. The heating was carried out at the rate of 10°C min<sup>-1</sup> under nitrogen atmosphere. To check the thermal stability of the dyes in black matrix, the fabricated black matrix were heated to 230°C for 1 h in a forced convection oven (OF-02GW Jeitech

Co., Ltd.). The color difference values ( $\Delta E_{ab}$ ) before and after heating were measured on a color spectrophotometer (Scinco colormate) in CIE L'a'b' mode.

#### *2.2.7 Geometry optimization of the synthesized dyes*

The geometry and electric structure of the studied dyes are optimized by the hybrid density functional theory (DFT) method at the PBE/DNP theory level performed on Materials Studio 5.0 DMol3 program package.

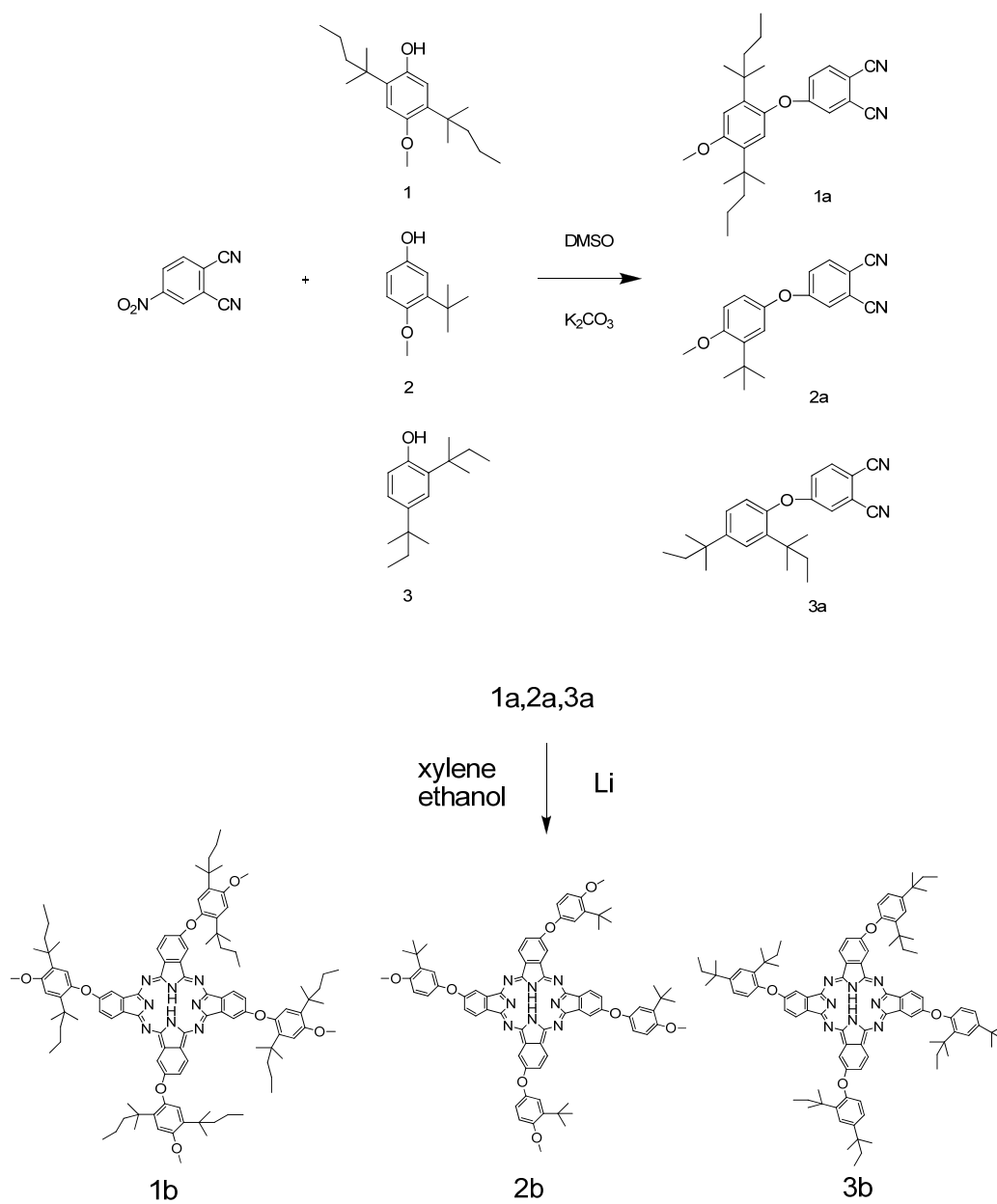
## 2.3 Results and Discussion

### *2.3.1. Synthesis of dyes*

Three metal-free PCs with enhanced solubility were designed and synthesized, as shown in Scheme 2.1. Precursors (1a,2a,3a) were synthesized through a nucleophilic aromatic substitution reaction between nitro phthalonitriles and phenols including functional groups (1,2,3).[7] Each reaction was conducted under similar conditions and all products were obtained

in high yield over 80%. The structures of the synthesized precursors were confirmed by  $^1\text{H}$  NMR.

The metal-free PCs (1b,2b,3b) were synthesized by a cyclotetramerization reaction of the precursors and purified by column chromatography.[8] Theoretically, metal-free PCs synthesized by monosubstituted phthalonitriles can have 4 constitutional isomers:  $\text{C}_{4h}, \text{C}_{2v}, \text{C}_s, \text{D}_{2h}$ . Assuming a statistical distribution, The 4 isomers are expected to be mixed in the ratio of 1:2:4:1.[9] No attempts to separate these isomers were made and all metal-free PCs were obtained in relatively high yield. The structures of synthesized PCs were confirmed by MALDI-TOF spectroscopy, FT-IR spectroscopy, and elemental analysis.



Scheme 2.1. Synthesis of the prepared dyes.

### 2.3.2 Solubility

The dyes need to be dissolved in industrial solvents, such as PGMEA and cyclohexanone, to a concentration of at least 4~5 wt% to be applied for BM.[6] Generally, non-substituted PCs tend to form various crystal structures due to molecular interactions caused by their planar structures. Therefore, non-substituted PCs have low solubility in most organic solvents, which has limited their applications.[9]

Substituents including bulky alkyl groups or alkoxy groups were introduced at their peripheral positions to enhance the solubility of PCs. As a result, the solubility of metal-free PCs increased significantly compared to that of non-substituted metal-free PC (PB 16). This is due to the steric hindrance between the planes of the PC molecules caused by the bulky aromatic substituents rotated out of the plane of the molecule. In addition, as previously mentioned, the synthesized dyes would exist in a mixture of 4 isomers, which would increase their solubility due to the unsymmetrical isomers  $C_s$  and  $C_{2v}$  among them.[10] Table 2.1 lists the solubility of the PC dyes and PB 16, and Figure 2.1 shows the structure of PB 16.

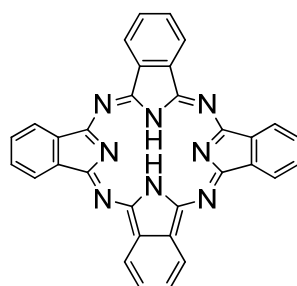
Dyes 1b and 2b, which included alkyl and alkoxy groups at their terminal positions, showed higher solubility than dye 3b, which contained only alkyl groups as substituents. In particular, the solubility of dye 1b in cyclohexanone reached 10wt% due to the anti-aggregation effects between the PC molecules as well as the affinity between the ether linkages of the dyes and solvent molecules.[6] The solubility of dye 2b was relatively lower than that of dye 1b because of its less bulky alkyl substituents. Dye 3b was barely soluble in industrial solvents due to little affinity between the dyes and solvent molecules.

The solubility of the dyes corresponded to the simulation data optimized by the Materials Studio 5.0 DMol3 program. Figure 2.2 shows the optimized structures of the dyes with bulky substituents out of the planar core. The bulky substituents of dyes 1b and 2b were twisted perpendicular to upward and downward directions of the molecular plane, whereas those of dye 3b were twisted toward one side of the molecular plane. Therefore, dyes 1b and 2b were more soluble in industrial solvents than dye 3b.



Table 2.1. Solubility of the dyes at 20 °C.

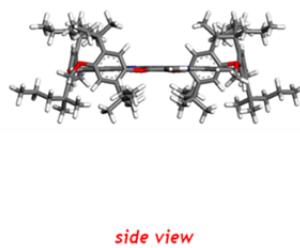
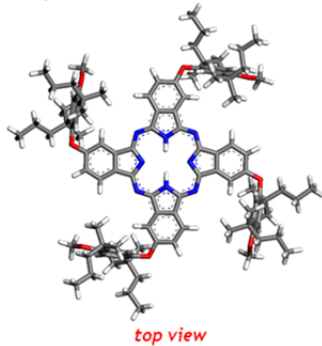
Dye	PGMEA	Cyclohexanone
1b	4wt%	10wt%
2b	2.2wt%	2.8wt%
3b	less than 1.0%	less than 1.0%
PB 16	insoluble	insoluble



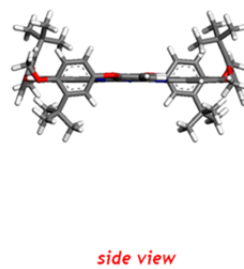
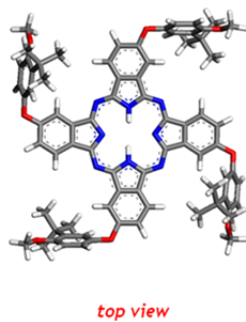
PB 16

Fig. 2.1. Structure of Pigment Blue 16.

□ Optimized structure (1b)



□ Optimized structure (2b)



□ Optimized structure (3b)

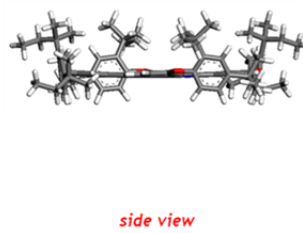
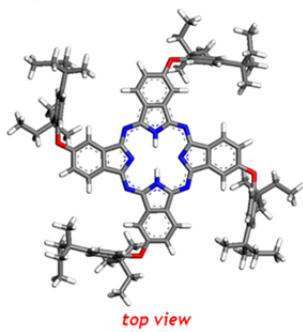


Fig. 2.2. Geometry-optimized structures of the prepared dyes.

### 2.3.3 UV-vis absorption spectra

Figure 2.3 and Table 2.2 show the absorption spectra of dye 1b~3b in  $\text{CH}_2\text{Cl}_2$  and PB 16 in sulfuric acid, respectively. To apply a dye to a BM, it should have strong and broad absorptions in the visible region. The greenish dyes exhibited absorption maxima in the 706~708nm range, displaying typical Q-band absorptions in the 600~750nm range as well as B-band absorptions in the 300~450nm range.[11] The characteristic Q and B bands were due to  $\pi$ - $\pi^*$  transitions in the heteroaromatic 18- $\pi$  electron system.[12] The dyes showed similar spectral properties, indicating that the conjugations of the dyes were not much affected by the change in introduced substituents.[11] The molar extinction coefficients of the dyes were approximately 140000~150000, which significantly exceeded those of the pigments. Therefore, the amounts of the dyes needed for BM can be reduced.

These results corresponded to the simulation data optimized by the Materials Studio 5.0 DMol3 program. As shown in Table 2.3, the orbital lobes and HOMO-LUMO energy gaps of the dyes were almost identical. Accordingly, the changes in substituents did not affect the absorption maxima of the dyes. Figure 2.4 shows the transmittance spectra of the dye-based BM fabricated with the

dye 1b. The fabricated BM absorbed light broadly in the 400~450nm and 600~700nm ranges. Therefore, compensatory dyes absorbing light in the 450~600nm range will be needed for complete absorption of light in the visible range.

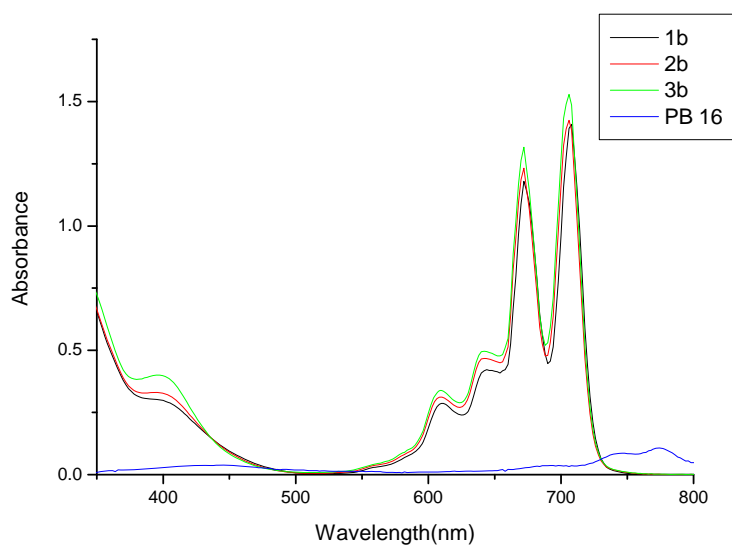


Fig. 2.3. Absorption spectra of the synthesized dyes in  $\text{CH}_2\text{Cl}_2(10^{-5}\text{mol litre}^{-1})$  and PB 16 in sulfuric acid( $10^{-5}\text{mol}$ ).

Table 2.2. Absorption maxima and extinction coefficients of the prepared dyes in CH<sub>2</sub>Cl<sub>2</sub> and PB 16 in sulfuric acid.

Dye	$\lambda_{\text{max}}$ (nm)	$\epsilon_{\text{max}}$ (L mol <sup>-1</sup> cm <sup>-1</sup> )
1b	708	140875
2b	706	142473
3b	706	152855
PB 16	774	10756

Table 2.3. Electronic energies of the prepared dyes.

	1b	2b	3b
HOMO+3	-5.061	-5.086	-5.506
HOMO+2	-4.972	-5.002	-5.258
HOMO+1	-4.958	-4.934	-5.233
HOMO	-4.432	-4.445	-4.501
$\Delta E$	1.316	1.318	1.326
LUMO	-3.116	-3.127	-3.175
LUMO-1	-3.076	-3.093	-3.133
LUMO-2	-1.722	-1.733	-1.783
LUMO-3	-1.515	-1.531	-1.573

$\Delta E$  means the energy gap difference between HOMO and LUMO

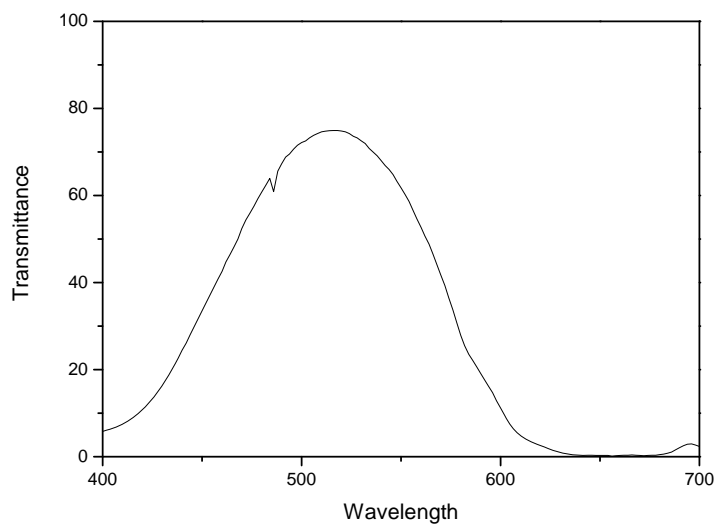


Fig. 2.4. Transmittance spectra of the spin-coated black matrix with dye 1b.

#### 2.3.4 Thermal properties

Phthalocyanines are highly stable dyes due to the strong  $\pi$ - $\pi$  stacking interactions from their planar structures.[13] In addition, their high molecular weight is favorable for intermolecular interactions, such as Van der Waals forces. On the other hand, phthalocyanines including substituents show reduced stability due to anti-aggregation effects.

For the current LCD manufacturing process, dye molecules need to be stable up to 230°C.[6] As shown in Figure 2.5, dyes 1b and 2b showed < 1% weight loss after 1 hour at 230°C, whereas dye 3b showed approximately 10% weight loss and degraded gradually with increasing temperature. This was attributed to the initial decomposition of phthalocyanines from the terminal groups at 230~250°C. As PC dyes containing alkoxy groups as substituents were reported to be more stable than those containing terminal alkyl groups, dye 1b and 2b showed higher stability than dye 3b.[14]

To measure the thermal stability of BM film, dye 1b was spin coated on a glass and the  $\Delta E_{ab}$  value of the film was measured. As shown in Table 2.4, the  $\Delta E_{ab}$  value of the film was 3.434 after heating for 90 minutes at 230°C. This suggests that the original color of the BM was well maintained due to little



degradation of the dye.[15] The thermal stability of dye-based BMs would be improved further if a commercial binder, adjusted for the pigments, can be optimized to the dye.[16]

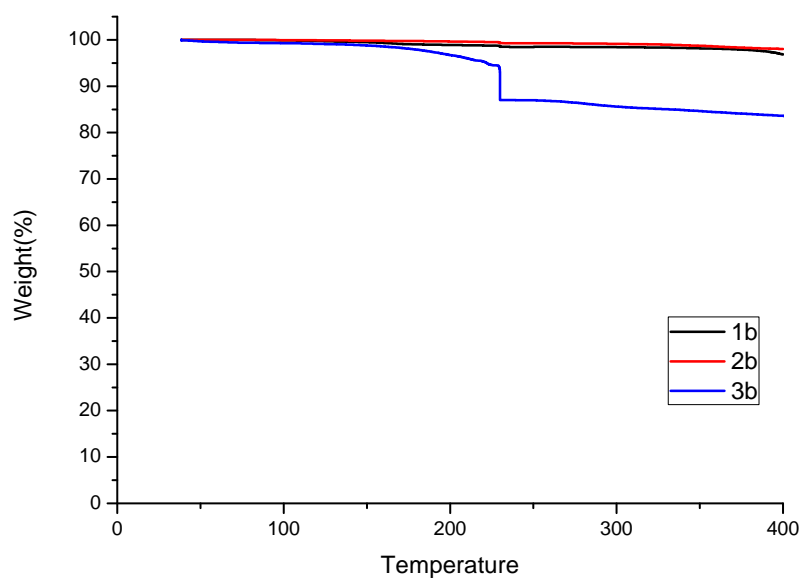


Fig. 2.5. Thermogravimetric analysis (TGA) of the prepared dyes.

Table 2.4. The coordinate values corresponding to the CIE 1931 chromaticity diagram of the dye-based black matrix.

Black Matrix		L	a	b	$\Delta E_{ab}$
1b	prebake	74.6417	-65.6547	6.851	3.434
	postbake	77.3913	-66.2442	8.824	

### 2.3.5 Dielectric properties

The dielectric constant of BM needs to be  $< 7$  for satisfactory industrial applications with a current thickness of BM (1-1.5 $\mu\text{m}$ ). On the other hand, carbon black BM has a high dielectric constant  $> 20$ , which can cause malfunctions of LCD TFTs due to interference of the TFT electric signal with carbon black.[4] Therefore, to reduce the dielectric constant of BM, dye-based BM and carbon black-dye hybrid type BMs were fabricated and their dielectric properties were tested.

Table 2.5 lists the dielectric constants and constitutions of the prepared BMs. The 6 hybrid type BMs were fabricated with varied compositions of dye 1b and

carbon black. The BM 1b-00 prepared with carbon black only had the highest dielectric constant. The dielectric constant of BM decreased significantly with decreasing carbon black and increasing dye concentration due to the low dielectric character of the dye. In particular, BM 1b-100 prepared with the dye only had the lowest dielectric constant of 3.99 at a frequency of 1000kHz. In addition, the dielectric constants of the samples were a function of the applied electric field frequency. The dielectric constant of BM decreased gradually with increasing frequency from 0.1kHz to 1000kHz. This was attributed to the lag in charge transfer inside the dye molecule caused by the rapid change in the external electronic field.[17] Among the 6 BMs prepared, those containing more than 30wt% of dye had a dielectric constant  $< 7$  at the working frequency range (100~300Hz).

Table 2.5. Dielectric constants and constitutions of the dye-based black matrix.

Frequency(kHz)	Dielectric constant( $\epsilon_r$ , average)					
	1b-00	1b-20	1b-40	1b-60	1b-80	1b-100
0.1	26.39	20.07	13.94	6.90	6.92	4.96
1	25.47	19.44	13.56	6.78	6.81	4.84
10	20.65	16.10	11.60	6.16	6.25	4.23
100	18.72	14.78	10.89	5.95	6.04	4.12
200	18.22	14.41	12.61	5.87	5.96	4.08
500	17.57	13.94	10.44	5.78	5.86	4.02
700	17.34	13.77	10.35	5.74	5.83	3.99
1,000	17.11	13.61	10.25	5.70	5.79	3.99
Thickness	1.2013 $\mu\text{m}$					
Electrode radius	280, 285, 280 $\mu\text{m}$					

	1b-00	1b-20	1b-40	1b-60	1b-80	1b-100
binder	50 wt%	50 wt%	50 wt%	50 wt%	50 wt%	50 wt%
carbon black	50 wt%	40 wt%	30 wt%	20 wt%	10 wt%	
Dye 1b		10 wt%	20 wt%	30 wt%	40 wt%	50 wt%

## 2.4 Conclusions

Three solubility enhanced phthalocyanine dyes were synthesized, and the dye-based BMs were fabricated with the most soluble dye. The increase in solubility of the prepared dyes was attributed to bulky functional substituents at the peripheral positions of them. Since all dyes had high molar extinction coefficients, dye-based BMs absorbed light in the visible region with the small amounts of the dyes. In addition, the dyes including terminal alkoxy groups showed suitable thermal stability for commercial use due to terminal alkoxy groups are stable at postbaking temperature. The dielectric constants of the

BMs containing more than 30wt% of dyes were significantly lower than that of the BM prepared with carbon black only.

## 2.5 References

- [1] Chang SC. Improving pattern precision of chromium based black matrix by annealing. *Appl. Surf. Sci.* 2008; 254: 2244-2249
- [2] Koo HS, Chen M and Kawai T. Improvements in the optical and characteristics of black matrix films containing carbon nanotubes on color filters. *Diamond Relat. Mater.* 2009; 18: 533-536
- [3] Kuo KH, Chiu WY, Hsieh KH and Don TM. Novel UV-curable and alkali-soluble resins for light-shielding black matrix application. *Eur. Polym. J.* 2009; 45: 474-484
- [4] Jung J, Park Y, Jaung JY and Park J. Synthesis of new single black pigments based on azo and anthraquinone moieties for LCD black matrix. *Mol. Cryst. Liq. Cryst.* 2010; 529: 88-94
- [5] Sigiura T. Dyed color filters for liquid-crystal displays. *J. Soc Inf.* 1993; 1: 177-180
- [6] Choi J, Sakong C, Choi JH, Yoon C and Kim JP. Synthesis and

- characterization of some perylene dyes for dye-based LCD color filters. *Dyes Pigm.* 2011; 90: 82-88
- [7] Ağritaş MS. Non-aggregating phthalocyanines with bulky 2,4-di-tert-butylphenoxy-substituents. *Dyes Pigm.* 2007; 74: 490-493
- [8] Cheng G, Peng X, Hao G, Kennedy OV, Ivanov IN, Knappenberger K, Hill TJ, Rodgers MAJ and Kennedy ME. Synthesis, photochemistry, and electrochemistry of a series of phthalocyanines with graded steric hinderance. *J. Phys. Chem. A*; 107: 3503-3514
- [9] Erdoğmuş A and Nyokong T. Novel, soluble, fluxoro functional substituted zinc phthalocyanines; synthesis, characterization and photophysical properties. *Dyes Pigm.* 2010; 86: 174-181
- [10] Chen Y, Hanak M, Blau WJ, Dini D, Liu Y, Lin Y and Bai J. Soluble axially substituted phthalocyanines: synthesis and nonlinear optical response. *J. Mater. Sci.* 2006; 41: 2169-2185
- [11] Brewis M, Clarkson GJ, Humberstone P, Makhseed S and Mckeown NB. The Synthesis of some phthalocyanines and naphthalocyanines derived from sterically hindered phenols. *Chem. Eur. J.* 1998; 4: 1633-1640
- [12] Tau P and Nyokong T. Electrochemical characterization of tetra- and octa-substituted oxo(phthalocyaninato)titanium(IV) complex. *Electrochim. Acta.*

2007; 52: 3641-3650

[13] Kobayashi N. Design, synthesis, structure, and spectroscopic and electrochemical properties of phthalocyanines. *Bull. Chem. Soc. Jpn.* 2002; 75: 1-19

[14] Hacıvelioğlu F, Durmuş M, Yeşilot S, Gürek AG, Kılıç A and Ahsen V. The synthesis, spectroscopic and thermal properties of phenoxyclotriphosphazanyl-substituted phthalocyanines. *Dyes Pigm.* 2008; 79: 14-23

[15] Kim YD, Kim JP, Kwon OS and Cho IH. The synthesis and application of thermally stable dyes for ink-jet printed LCD color filters. *Dyes Pigm.* 2009; 81: 45-52

[16] Yoon C, Choi JH and Kim JP. Synthesis and examination of polymers to improve pattern clarity and resistance properties of phthalocyanine color pixels in liquid crystal display. *Bull. Korean. Chem. Soc.* 2011; 32: 1-4

[17] Tilley R. *Colour and the optical properties of materials* (1<sup>st</sup> edn). John Wiley: New York, 2000; 30-31



## **Chapter 3**

### **Analysis and characterization of dye-based black matrix film of low dielectric constant containing phthalocyanine and perylene dyes**

#### **3.1 Introduction**

Color filters (CF) are one of the important components in LCD devices, and can also be applied to light-emitting diode (LED) displays and organic light emitting diode (OLED) displays.[1, 2] The black matrix is a key component of LCD color filter, and it divides the red, green and blue pixels of the CF, and blocks light leaking from the areas between the RGB color patterns, enhancing contrast ratio.[3] In addition, BM prevents malfunction of thin film transistors (TFT) by minimizing the external incident light, which induces interference in the TFT electric signal.[4]

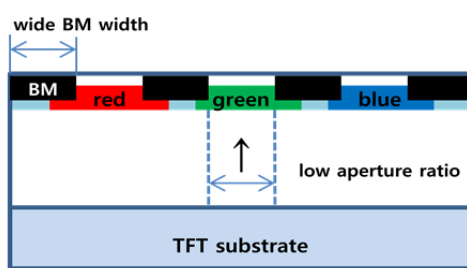
In the conventional structure of an LCD, as shown in Scheme 3.1, low aperture ratio caused by a wide width of the BM pattern limits the picture quality of the LCD. Therefore, to enhance picture quality and simplify the LCD structure, BM-on-TFT (BOT) structure is required, in which the BM is located

on the TFT array.[2] In LCDs with BOT structure, higher aperture ratio due to relatively narrow BM width allows more back light transmission, enhancing brightness and visibility. Materials of low dielectric constant are required instead of conventional BM materials such as Cr/CrO<sub>x</sub> and carbon black, since the CF is directly layered on the TFT in BOT structure.[4]

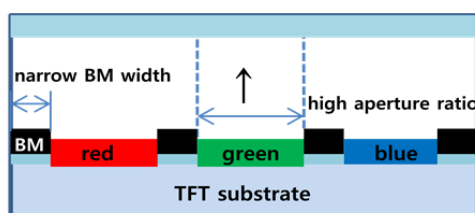
The most frequently used material for BMs is carbon black, which has advantages of high thermal stability and high light absorption. However, BMs fabricated with carbon black have high dielectric constants due to extended  $\pi$ -conjugation length in the carbon black molecules, causing electrical signal transduction errors on TFTs.[4] As shown in previous research, dyes have low dielectric constants compared with carbon black, and show much higher light absorption properties than organic pigments.[5] Therefore, dyes with high solubility in industrial solvents and high thermal stability can be excellent candidates for BMs of low dielectric constant.

BM can be fabricated with a single black material, or a mixture to make the black. As dyes generally have sharp absorption ranges, dye-based BMs need to be fabricated by material mixture methods. Dye-based BMs can be fabricated by mixing red, green and blue (RGB) dyes, or cyan, magenta and yellow (CMY) dyes, as well as by mixing dyes and carbon black.

In this study, greenish Zn-PC dyes and reddish PER dyes were synthesized and employed to fabricate BMs with low dielectric constant and light absorption in the whole visible region. The spectral, and thermal properties and solubility of the prepared dyes were investigated, and optical, thermal and dielectric properties of the dye-based BMs were examined. For further investigation of surface morphology of the BM films, dye-based BMs were probed by Field FE-SEM and AFM.



Conventional structure of LCD



BOT structure of LCD

Scheme 3.1. Conventional and BOT structures of LCD.

## 3.2 Experimental

### 3.2.1 General

1,8-Diazabicyclo-7-undecene (DBU), 3(4)-nitrophthalonitrile, 2,5-bis-(1,1-dimethylbutyl)-methoxyphenol and isoquinoline were purchased from TCI, and ZnCl<sub>2</sub>, perylene-3,4,9,10-tetracarboxylic dianhydride, 2,6diisopropylaniline, m-cresol, iodine, sulfuric acid, bromine, acetic acid, potassium carbonate anhydrous, phenol and 4-tert-butylphenol were purchased from Sigma-Aldrich and used as received. All the other reagents and solvents were of reagent-grade and obtained from commercial suppliers. Transparent glass substrates were provided by Paul Marienfeld GmbH & Co. KG, and acrylic binder was supplied by NDM Inc.

<sup>1</sup>H NMR spectra were recorded on a Bruker Avance 500 spectrometer at 500MHz using chloroform-d and tetramethylsilane (TMS), as the solvent and internal standard, respectively. Matrix-Assisted Laser Desorption/Ionization Time Of Flight (MALDI-TOF) mass spectra were collected on a Voyager-DE STR Biospectrometry Workstation with  $\alpha$ -cyano-4-hydroxy-cynamic acid

(CHCA) as the matrix. Absorption spectra were measured using an HP 8452A spectrophotometer. Differential scanning calorimetry (DSC) was conducted in nitrogen atmosphere at a heating rate of 10K/min using a TA instrument Differential Scanning Calorimeter Q1000. Thermogravimetric analysis (TGA) was conducted in nitrogen atmosphere at a heating rate of 10 °C min<sup>-1</sup> using a TA Instruments Thermogravimetric Analyzer 2050. Dielectric constants were measured using an Edward E306 thermal evaporator and an HP 4294A precision impedance analyzer. The thickness of the dye-based BM was measured using a KLA-TENCOR Nanospec AFT/200 alpha step.

### 3.2.2 Synthesis

#### 3.2.2.1 2(3)-Tetrakis(2,5-Bis(1,1-dimethylbutyl)-4-methoxyphenoxy)-phthalocyaninatozinc(II) (Zn-PC).

MALDI-TOF MS: m/z 1738.44 (100%, [M+2K]<sup>+</sup>). C<sub>106</sub>H<sub>132</sub>N<sub>8</sub>O<sub>8</sub>Zn Calcd. C, 74.38; H, 7.77; N, 6.55; O, 7.48% Found. C, 74.61; H, 8.04; N, 6.59; O, 7.35%.

#### 3.2.2.2 *N,N'*-Bis(2,6-diisopropylphenyl)-1-*p*-tert-butylphenoxy-perylene-

### *3,4,9,10-tetracarboxydiimide (PER)*

<sup>1</sup>H NMR (500Mhz, CDCl<sub>3</sub>): δ(ppm) 9.68 (d, 1H), 8.82 (m, 2H), 8.75 (m, 3H), 8.42 (s, 1H), 7.48 (m, 4H), 7.33 (m, 4H), 7.13 (d, 2H), 2.74 (septet, 4H), 1.36 (s, 9H), 1.16 (d, 24H). MALDI-TOF MS: m/z 860.28 (100%, [M+2K]<sup>+</sup>).

### *3.2.3 Preparation of dye-based black matrix*

The ink for the black matrix was composed of the dyes (0.014 or 0.033g), cyclohexanone (0.28 g), and acrylic binder (0.12g). The prepared dye-based inks were coated onto a transparent glass substrate using a MIDAS System SPIN-1200D spin coater. The coating speed was initially 100 rpm for 5 s, which was then increased to 500 rpm and kept constant for 20 s. The wet dye-coated black matrix was then dried at 80 °C for 20 min, prebaked at 150 °C for 10 min, and post-baked at 230 °C for 1h.

### *3.2.4. Measurement of spectral and optical properties*

The absorption spectra of the synthesized dyes and the transmittance spectra of the dye-based BM were measured using a UV-vis spectrophotometer. The optical density values were calculated from the transmittance spectra at 550nm and the thickness of the dye-based BMs.

### *3.2.5 Investigation of solubility*

The prepared dyes were added to cyclohexanone at various concentrations, and the solutions were sonicated for 5 min using an ultrasonic cleaner ME6500E. The solutions were left to stand for 48 h at room temperature, and checked for precipitation to determine the solubility of the dyes.

### *3.2.6 Measurement of thermal stability*

The thermal stability of the synthesized dyes was evaluated by DSC and

TGA. In DSC measurements, the prepared dyes were heated up to 250°C and held at this temperature for 3 min before cooling to room temperature. In TGA measurements, the prepared dyes were heated to 110°C and held at that temperature for 10 min to remove residual water and solvents. The dyes were then, heated to 220°C and held at that temperature for 30 min to simulate the thermal processing conditions of color filter manufacturing. The dyes were finally heated to 400°C to determine their degradation temperature. The temperature was raised at a rate of 10°C min<sup>-1</sup> in nitrogen atmosphere. To check the thermal stability of the dyes, the fabricated black matrices were heated to 230°C for 1 h in a forced convection oven (OF-02GW Jeitech Co., Ltd.). The differences in thickness values before and after heating were measured using a KLA-TENCOR Nanospec AFT/200 alpha step.

### *3.2.7 Field emission scanning electron microscopy and Atomic force microscopy*

The aggregation morphology of the dyes in black matrix was investigated

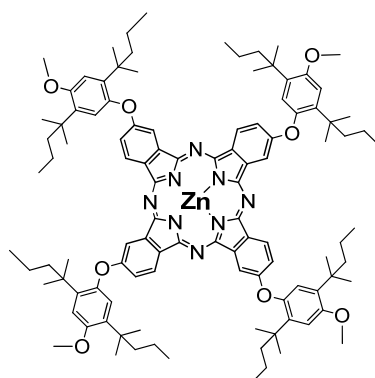


using a field emission scanning electron microscope (JSM 6700-F). The dye aggregates were observed at an acceleration voltage of 10kV and working distance (WD) of 6mm, and FE-SEM images of the dye-based black matrix were taken at 7000x magnification. The surface morphology of the dye-based BM (10 $\mu$ m x 10 $\mu$ m size) was observed using atomic force microscopy (Park science) in non-contact mode.

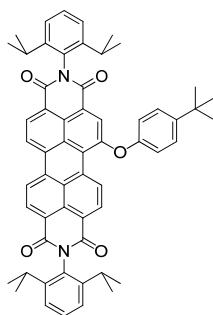
### 3.3 Results and Discussion

#### *3.3.1 Properties of dyes*

As shown in Figure 3.1, previously reported Zn-PC and PER dyes were synthesized as BM components by following reference synthetic routes.[6,7] No attempts to separate the mixture of 4 constitutional isomers of Zn-PC (C4h,Cs,C2v,C4h=12.5:50:25:12.5) were made.[8] The synthesized dyes were confirmed by H<sup>1</sup> NMR, MALDI-TOF spectroscopy and elemental analysis.



Zn-PC



PER

Fig. 3.1. Structure of Zn-PC and PER.

Figure 3.2 and Table 3.1 show the absorption spectra of Zn-PC and PER dyes in cyclohexanone, the industrial solvent of the LCD color filter. To apply dyes to the BM, they need to have broad and strong absorptions in the visible region.

The greenish Zn-PC dye displayed Q-band absorption in the 550-700 nm range, as well as B-band absorption in the 400-500 nm range, with an absorption maximum at 684 nm. The typical Q and B bands were due to  $\pi$ - $\pi^*$  transitions in the heteroaromatic 18- $\pi$  electron system, and the spectra of the dye were not much affected by the peripherally introduced substituents at the  $\beta$  position of the dye.[9] The reddish PER dye exhibited absorption in the 450-570 nm range with an absorption maximum at 528nm. The PER dye showed a slight bathochromic shift due to the electron donating power of the mono-substituted phenoxy moiety at the bay position of the dye.[10,11] As shown in Figure 3.2, the mixture of the two dyes in cyclohexanone nearly absorbed light in the whole visible region by combining the absorption ranges of each. The molar extinction coefficients of Zn-PC and PER dyes were 193588 and 62991, respectively, which are much higher than those of organic pigments. Therefore, the amounts of the dyes needed for BM can be decreased compared with organic pigments.

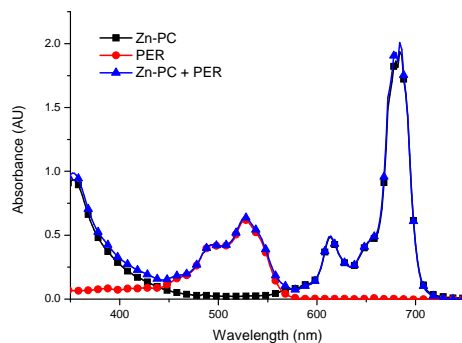


Fig. 3.2. Absorbtion spectra of Zn-PC and PER in cyclohexanone( $10^{-5}\text{molL}^{-1}$ ).

Table 3.1. Absorption maxima and molar extinction coefficients of the prepared dyes in cyclohexanone.

Dye	$\lambda_{\text{max}}$ (nm)	$\epsilon_{\text{max}}$ ( $\text{L mol}^{-1} \text{ cm}^{-1}$ )
Zn-PC	684	193588
PER	528	61991

The thermal properties of the dyes were investigated with TGA and DSC, as shown in Figure 3.3 and Figure 3.4. For dyes to be used as BM, dye molecules should be stable up to 230 °C for current industrial processes.[12,13] During the heating and cooling process in DSC measurements, no phase transitions due to melting or changing crystal structures were observed up to 250°C. In TGA measurements, the dyes showed less than 2 % weight loss after 1h at 230 °C.

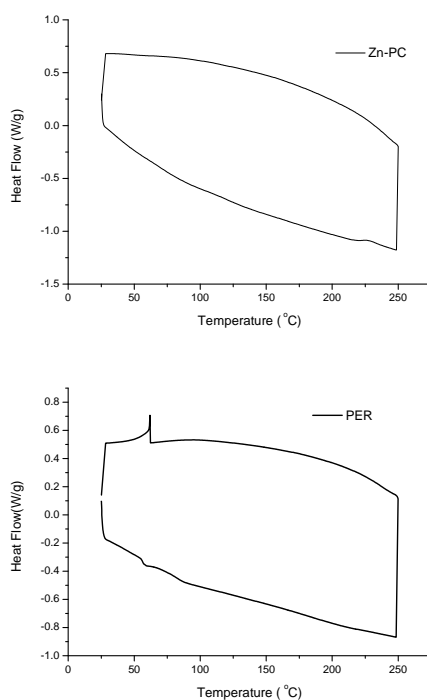


Fig. 3.3. Differential scanning calorimetry(DSC) measurements of the prepared dyes.

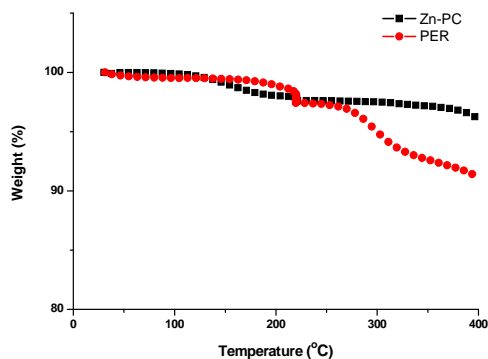


Fig. 3.4. Thermogravimetric analysis (TGA) of the prepared dyes.

These results were attributed to the fact that the dyes have mostly planar molecular structures including plenty of aromatic rings. Therefore this contributes to strong intermolecular  $\pi$ - $\pi$  stacked interactions, resulting in the high thermal stability of the dyes.[14,15,16] In addition, intermolecular interactions due to their high molecular weight and polar functional substituents increase thermal stability of the dyes.[17] From the TGA and DSC measurements, it is concluded that the dyes can endure LCD manufacturing process without phase transitions and degradations.

Table 3.2 lists the solubility of the dyes in cyclohexanone. The dyes need to be dissolved in industrial solvents to a concentration of at least 5wt% to be

applied for BM. The solubilities of Zn-PC dye and PER dye in cyclohexanone were 8wt% and 10wt%, respectively. The high solubility of the dyes was presumed to be due to the affinity between the ether linkages of the dyes and cyclohexanone molecules. In addition, bulky and polar substituents reduced the planarity of the dyes, enhancing their solubility. In particular, the substituents at the bay position of the PER dye induced twisting of the naphthalene subunits in the perylene core, reducing intermolecular aggregations and resulting in higher solubility in cyclohexanone than Zn-PC dye.[18,19]

Table 3.2. Solubility of the dyes in cyclohexanone at 20 °C.

	Zn-PC	PER
Cyclohexanone	8 wt%	10 wt%

### *3.3.2. Spectral and optical properties of dye-based black matrix*

The dyes in the film state should have broad and strong absorptions in the visible region. To investigate the light blocking property of the dye-based BM, film A (dye content : 7.6wt%, thickness : 12.5 $\mu\text{m}$  ) was prepared with the Zn-PC and PER dyes, in which the dyes were used to the extent of maximum solubility in cyclohexanone. The transmittance spectra of film A is shown in Figure 3.5. The prebaked Film A blocked the light in the whole visible region, except for 3% transmittance around 450nm and 6% transmittance around 580nm. The transmittance spectra of film A after post-baking was similar to that of film A after prebaking, except for a small increase in the transmittance around 580 nm. The high transmittance regions are consistent with the regions where both dyes have weak light absorptions.

To investigate the optical properties of film A, its optical density (OD) was measured and listed in Table 3. The OD can be expressed as follows.

$$\text{OD} = (\log 1/T)/d$$

where T and d are the transmittances at 550nm and the thickness of film,



respectively.[20]

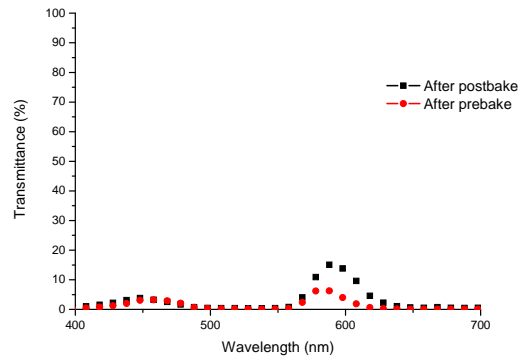


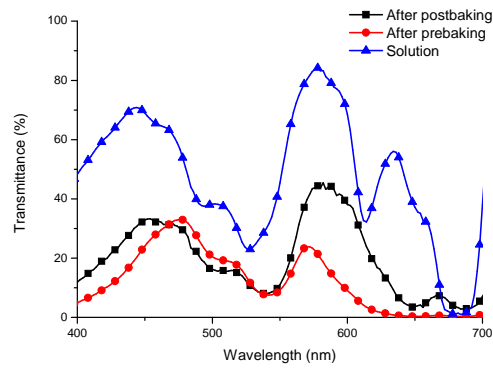
Fig. 3.5. Transmittance spectrum of film A.

Table 3.3. Optical density <sup>a</sup> of the prepared films.

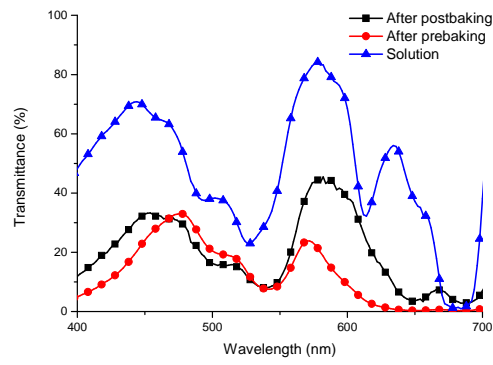
	After prebaking	After postbaking
Film A	0.233/ $\mu\text{m}$	0.226/ $\mu\text{m}$
Film B	0.085/ $\mu\text{m}$	0.083/ $\mu\text{m}$
Film C	0.095/ $\mu\text{m}$	0.092/ $\mu\text{m}$

<sup>a</sup> Optical density was investigated at 500nm

According to this, the OD of the film after prebaking and post-baking were 0.233/ $\mu\text{m}$  and 0.226/ $\mu\text{m}$ , respectively. In general, the OD of the BM film needs to be  $>2.5/\mu\text{m}$  for satisfactory industrial applications.[21] Therefore, for high OD of the dye-based film, the dye content in the solution has to be increased, and dispersants or surfactants might have to be used for this purpose. If the dye content in the film is increased up to the same content of carbon black or organic pigments in the conventional BM (50wt% of the BM resist), the calculated OD of dye-based BM would be 1.78/ $\mu\text{m}$ . This OD value is higher than that of organic pigment ( $\sim 1.2/\mu\text{m}$ ), while it is still lower than that of carbon black. Insufficient OD of dye-based BM can be enhanced by the fabrication of a hybrid BM, which includes dye and carbon black together. In a dye-carbon black hybrid BM, carbon black can also compensate for the narrow absorption ranges of the dye, preventing light leaking in visible regions.



Film B



Film C

Fig. 3.6. Transmittance spectrum of film B ( Zn-PC : PER = 2 mol:1 mol ) , film C ( Zn-PC : PER = 3 mol:1 mol) and solution (Zn-PC : PER = 1 mol:1 mol).

To investigate the spectral and optical properties of the BM film after the baking process, thin dye-based BMs with low dye content were prepared. By varying the ratio of Zn-PC to PER dyes, film B ( dye content : 3.5 wt%, Zn-PC : PER = 2mol : 1mol, thickness : 7.84  $\mu\text{m}$  ) and film C ( dye content : 3.7 wt%, Zn-PC : PER = 3mol : 1mol, thickness : 8.50  $\mu\text{m}$  ) were fabricated, and their transmittance spectra were measured. As shown in Figure 3.6, the films after post-baking exhibited increased transmittance values around 450nm and 580nm compared with the films after prebaking. In particular, marked increases in transmittance were shown in the 620-680nm range, where the Q-band of the Zn-PC dye is located. This is considered to occur due to the aggregations between Zn-PC dye molecules after post-baking. It is known that aggregates of Zn-PC dye show additional absorption peaks before the main Q band.[22,23,24] As shown in Figure 3.6, this phenomenon was confirmed by the low transmittance around 650nm of the post-baked films in comparison with the solution state, which meant that additional aggregation absorption peaks were formed after post-baking. Further proof of the Zn-PC dye aggregation is discussed in chapter 3.5. In the case of PER dyes, no definite dye aggregations after post-baking were deduced from the small changes of OD values and transmittances around 530nm during the baking process. The OD values of film

A, film B and film C are listed in Table 3.3.

### *3.3.3 Thermal properties of dye-based black matrix*

For the current LCD manufacturing process, the BM film needs to be stable up to 230 °C.[6] To test the thermal stability of the dye-based BMs, film C and the BM film without dyes were prepared and their retention rates were measured.

The retention rate of BM is defined as the ratio between the thickness of the film after prebaking and post-baking, and it needs to be >80% for satisfactory thermal stability. A 20% decrease of the film thickness was observed, mainly due to solvent vaporization during the post-baking process, as the boiling point of the solvent in this system is lower than the manufacturing temperature (230°C), and binders are known to be stable at this temperature.[20] As shown in Table 3.4, the retention rates of film C and film without dye were 80% and 83%, respectively. The retention rate of the dye-based film was almost the same as that of the film without dye, indicating that the dye-based film had sufficient

thermal stability. The results were attributed to the high thermal stability of the dye molecules, which was confirmed by TGA and DSC measurements. This was consistent with the results that changes of transmittance and OD between films after prebaking and post-baking were only due to aggregations of the dyes.

Table 3.4. Retention rates of film without dye and film C.

Retention rate (%)	
Film without dye	83
Film C	80

#### *3.3.4. Dielectric properties of dye-based black matrix*

The dielectric constant of BMs with BOT structure needs to be  $<7$  for satisfactory industrial application. However, the carbon black BM has a high dielectric constant of  $>20$ , which can cause malfunction of LCD TFTs with

BOT structure due to interference of the TFT electric signal with carbon black.[4] In order to investigate the dielectric property of the dye-based BM, film B(dye content : 3.5wt%, dielectric constant : 2.0) and film C(dye content : 3.7wt%, dielectric constant : 2.63) were prepared, and their dielectric constants at a frequency of 10kHz were measured. The dielectric constants of the prepared films and the previously reported film (dye content : 50wt%, dielectric constant : 4.23) are listed in table 3.5.[5] The dielectric constants of all films were  $<7$ , though the dye amount of the previously reported film was fifteen times greater than those of films B and C. Therefore, the dye-based BMs have sufficiently low dielectric constants regardless of the type and amount of dye. In addition, at the working frequency range (100-300 kHz), the dielectric constants of the BM can be further reduced due to lag in the charge transfer in the dye molecules.[25] This low dielectric character of dye makes it possible to manufacture hybrid-type BMs that include dye and carbon black. Hybrid-type BMs containing 20wt% carbon black and 30wt% dye is considered to have a dielectric constant of  $<7$  with good overall light absorption properties.

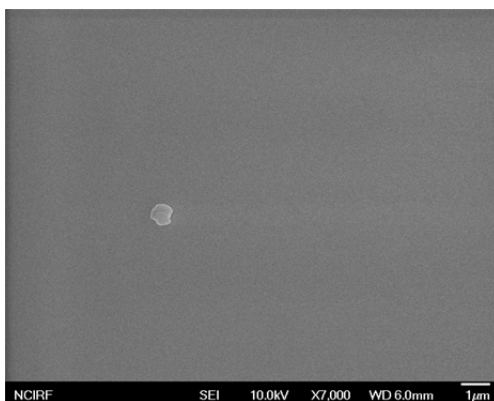
Table 3.5. Dielectric constants the dye-based black matrix at 10kHz.

	Film B	film C	Previously Reported film
Dielectric constant ( $\epsilon_r$ , average)	2.00	2.63	4.23

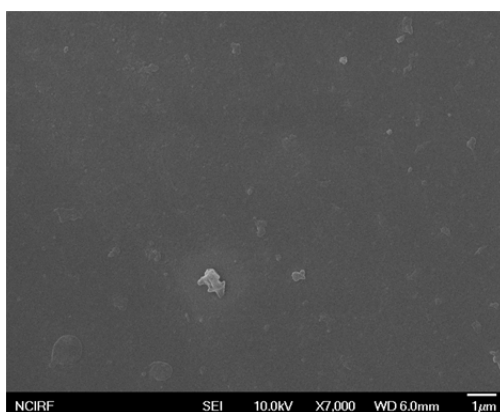
### 3.3.5. Surface investigation of BM film by FE-SEM and AFM

In order to investigate the surface morphology of the films after prebaking and post-baking, film B and film C were studied by using FE-SEM and AFM. The FE-SEM and AFM images are shown in the Figure 3.7 and Figure 3.8, respectively and the Rq (root mean square average roughness) values of the films are listed in Table 3.6.

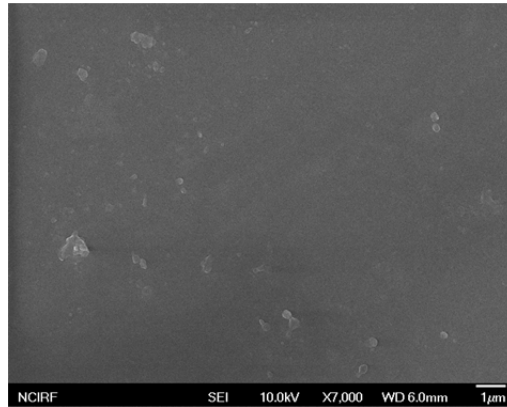




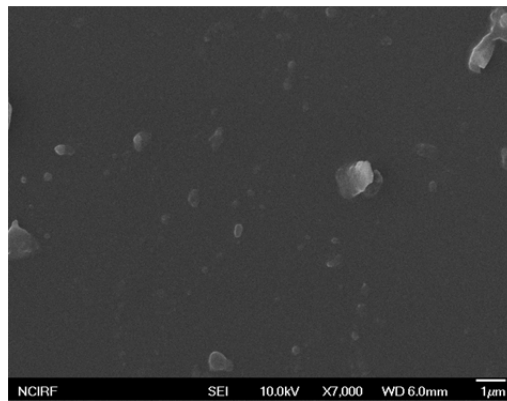
Film B after prebaking



Film B after postbaking



Film C after prebaking



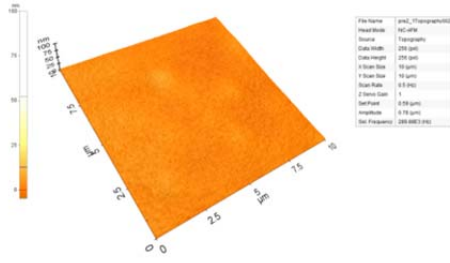
Film C after postbaking

Fig. 3.7. SEM images of film B and film C.

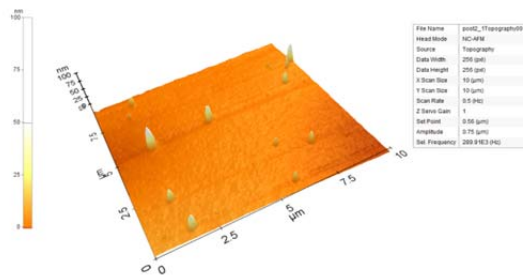
As shown in FE-SEM images, the aggregation of the dyes on both films after post-baking increased compared to that after prebaking. As discussed earlier, this aggregation was attributed to the stacking of Zn-PC dyes, and accordingly, film C, which contains more Zn-PC dyes, showed the higher aggregation. These results are thought to arise from the differences in the molecular structure and solubility of Zn-PC and PER dye. The substituted moiety at the bay position of PER dye twists the core of the dye, breaking its planarity.[19] However, the planar structure of Zn-PC dye was maintained in spite of substitutions at its peripheral positions. Therefore the strong  $\pi$ - $\pi$  interactions between the planes of Zn-PC dye molecules were still formed, giving more aggregates. In addition, Zn-PC dyes have a higher tendency to aggregate during the evaporation of solvents due to the lower solubility in industrial solvents.

The aggregates on the films are shown three-dimensionally in the AFM images. In films B and C after post-baking, aggregates were grown perpendicular to the plane of the films. This was due to the disk-like shapes of Zn-PC dyes, which led to columnar structures.[26] From the Rq values of the films, surface roughness of the films can be inferred; generally, films with Rq value between 1.3nm and 25nm are known to have smooth surfaces.[27] The Rq values of film B after prebaking and post-baking were 1.52nm and 2.30nm,

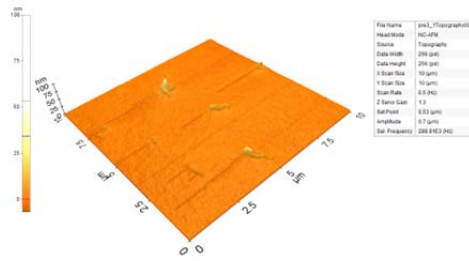
respectively, and the Rq values of film C after prebaking and post-baking were 1.97nm and 2.61nm, respectively. Though the films after post-baking have increased Rq values, they are considered to have sufficiently smooth faces for application in for BMs. Also, no definite phase separations were observed in microscopic images, which meant that dyes were properly blended except for dye aggregations.



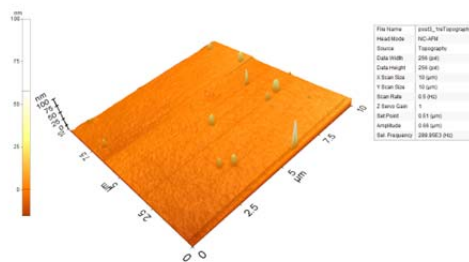
Film B after prebaking



Film B after postbaking



Film C after prebaking



Film C after postbaking

Fig. 3.8. AFM images of film B and film C.

Table 3.6. Rq of the prepared films.

	film B		Film C	
	After prebaking	After postbaking	After prebaking	After postbaking
Rq	1.52	2.30	1.97	2.61

### 3.4 Conclusion

The dye-based BM films were fabricated with greenish phthalocyanine and reddish perylene dyes. The high thermal stability of the dye-based BM was attributed to the rigid molecular structures of the dyes. In addition, due to the low dielectric characteristics of the dye, the dielectric constants of the dye-based BMs were significantly lower than that of the BM prepared with carbon black only. However, the low solubility of the dyes in industrial solvents and dye aggregations in the baking process limited the input of the dye in the BM resist, resulting in low light absorption of the dye-based BM. By fabricating hybrid-type BM that includes dye and carbon black together, the light

absorption property of the BM would be improved compared to the dye-based BM, satisfying the property requirements of BMs.

### 3.5 References

- [1] Tsuda K. Color filters for LCDs. *Displays* 1993; 14: 115-24.
- [2] Sabnis RW. Color filter technology for liquid crystal displays. *Displays* 1999; 20: 119-29.
- [3] Chang SC. Improving pattern precision of chromium based black matrix by annealing. *Appl. Surf. Sci.* 2008; 254: 2244-2249.
- [4] Jung J, Park Y, Jaung JY and Park J. Synthesis of new single black pigments based on azo and anthraquinone moieties for LCD black matrix. *Mol. Cryst. Liq. Cryst.* 2010; 529: 88-94
- [5] Lee W, Yuk SB, Choi J, Jung DH, Choi S, Park J and Kim JP. Synthesis and characterization of solubility enhanced metal-free phthalocyanines for liquid crystal display black matrix of low dielectric constant. *Dyes Pigm.* 2012; 92: 942-948.
- [6] Choi J, Sakong C, Choi JH, Yoon C and Kim JP. Synthesis and characterization of some perylene dyes for dye-based LCD color filters. *Dyes*



Pigm. 2011; 90: 82-88.

[7] Choi J, Kim SH, Lee W, Yoon C and Kim JP. Synthesis and Characterization of Thermally Stable Dyes with Improved Optical Properties for Dye-based LCD Color Filters. *New J. Chem.* 2012; 36: 812-818.

[8] Erdoğan A and Nyokong T. Novel, soluble, fluoro functional substituted zinc phthalocyanines; synthesis, characterization and photophysical properties. *Dyes Pigm.* 2010; 86: 174-181.

[9] Brewis M, Clarkson GJ, Humberstone P, Makhseed S and Mckeown NB. The Synthesis of some phthalocyanines and naphthalocyanines derived from sterically hindered phenols. *Chem. Eur. J.* 1998; 4: 1633-1640.

[10] Langhals H, Blanke P. An approach to novel NIR dyes utilising  $\alpha$ -effect donor groups. *Dyes Pigm.* 2003; 59: 109–116.

[11] Zhao C, Zhang Y, Li R, Li X, Jiang J. Di(alkoxy)-and Di(alkylthio)-Substituted Perylene-3,4,9,10-tetracarboxy Diimides with Tunable Electrochemical and Photophysical Properties. *J. Org. Chem.* 2007; 72: 2402-2410.

[12] Ohmi T. Manufacturing process of flat display. *JSME Int J Ser B (Jpn Soc Mech Eng)*. 2004; 47: 422-428.

[13] Takamatsu T, Ogawa S, Ishii M. Color filter fabrication technology for

LCDs. Sharp Tech J 1991; 50: 69-72.

[14] Kobayashi N. Design, synthesis, structure, and spectroscopic and electrochemical properties of phthalocyanines. Bull. Chem. Soc. Jpn. 2002; 75: 1-19.

[15] Kim JH, Masaru M, Fukunishi K. Three dimensional molecular stacking and functionalities of aminonaphthoquinone by intermolecular hydrogen bondings and interlayer  $\pi$ - $\pi$  interactions. Dyes Pigm. 1998; 40: 53-57.

[16] Thetford D, Cherryman J, Chorlton AP, Docherty R. Theoretical molecular modeling calculations on the solid state structure of some organic pigments. Dyes Pigm. 2004; 63: 259-276.

[17] Kim YD, Kim JP, Kwon OS, Cho IH. The synthesis and application of thermally stable dyes for ink-jet printed LCD color filters. Dyes Pigm. 2009; 81: 45-52.

[18] Ma YS, Wang CH, Zhao YJ, Yu Y, Han CX, Qiu XJ, Shi Z. Perylene diimide dyes aggregates: Optical properties and packing behavior in solution and solid state. Supramolecular chemistry 2007; 19: 141-149.

[19] Würthner F, Sautter A, Thalacker C. Substituted Diazadibenzoperylenes: New functional building blocks for supramolecular chemistry. Angew. Chem. 2000; 112: 1298-1301.

- [20] Kuo KH, Chiu WY, Hsieh KH and Don TM. Novel UV-curable and alkali-soluble resins for light-shielding black matrix application. *Eur. Polym. J.* 2009; 45: 474-484.
- [21] Koo HS, Chen M and Kawai T. Improvements in the optical and characteristics of black matrix films containing carbon nanotubes on color filters. *Diamond Relat. Mater.* 2009; 18: 533-536.
- [22] Yanik H, Aydın D, Durmuş M and Ahsen V. Peripheral and non-peripheral tetrasubstituted aluminium, gallium and indium phthalocyanines: Synthesis, photophysics and photochemistry. *J. Photochem. Photobiol. A-Chem.* 2009; 206: 18-26.
- [23] M. Durmus and T. Nyokong, *Inorg.* The synthesis, fluorescence behaviour and singlet oxygen studies of new water-soluble cationic gallium(III) phthalocyanines. *Chem. Commun.* 2007; 10: 332-338.
- [24] Li H, Jensen TJ, Fronczek FR and Vincente MGH. Syntheses and Properties of a Series of Cationic Water-Soluble Phthalocyanines. *J. Med. Chem.* 2008; 51: 502-511.
- [25] Tilley R. *Colour and the optical properties of materials* (1<sup>st</sup> edn). John Wiley: New York, 2000; 30-31.

[26] Zucchi G, Donnio B and Geerts YH. Remarkable miscibility between disk-like and lathlike mesogen. *Chem. Mat.* 2005; 17: 4273-4277.

[27] Miller JD, Veeramasuneni S, Drelich J, Yalamanchili MR and Yamauchi G. Effect of roughness as determined by atomic force microscopy on the wetting properties of PTFE thin films. *Polymer Eng Sci.* 1996; 36: 1849-1855.

## Chapter 4

### **The effect of five-membered heterocyclic bridges and ethoxyphenyl substitution on the performance of phenoxazine-based dye-sensitized solar cells**

#### 4.1 Introduction

Dye-sensitized solar cells (DSSCs) have attracted considerable attention as promising solar devices since Grätzel et al. reported Ru-based photosensitizers in 1991 [1]. The Ru complex dyes typical used as sensitizers in DSSCs have shown high electronic conversion efficiencies of over 11% with good stability [2]. However, high production cost and difficulties in purification have limited their development for large-scale applications. Recently, more attention has been paid to sensitizers without Ru (metal-free organic dyes and organometallic dyes) due to their lower cost, easier modification and purification, high molar extinction coefficient, and environmental friendliness. As such, sensitizers without Ru such as triphenylamine [3], indoline [4], cyanine [5], coumarin [6], perylene [7], porphyrin [8], phthalocyanine [9], and phenothiazine [10] have

been extensively studied. Among these, porphyrin derivatives have shown high electronic conversion efficiency (12.3%) [7].

For efficient DSSCs, organic dyes should have broad and red-shifted absorptions in the visible region. Accordingly, most organic dyes have the structure of donor-conjugated bridges-acceptor (D- $\pi$ -A) to obtain a broad and red-shifted absorption spectrum. Among the various conjugated bridges, furan and thiophene have displayed the most remarkable results, showing wide and red-shifted absorption spectra, as well as high molar extinction coefficients [11]. In addition, to achieve enhanced photovoltaic performance, organic dyes with an additional donor (D-D-A or D-D- $\pi$ -A) have been suggested [12]. The introduction of an additional donor group could increase the electron-donating capability, which would improve electron injection and charge separation. Phenoxazine (POZ) includes electron-rich oxygen and nitrogen atoms in a heterocyclic ring, which displays high electron-donating ability [13]. It also shows sufficient electrochemical properties, which implies that POZ could be a promising sensitizer in DSSCs [14]. However, despite these advantages, POZ-based sensitizers have not been reported extensively.

In this research, to study effects of conjugated bridges with a POZ moiety on photovoltaic performance, five-membered heterocyclic rings were introduced as

a conjugated bridge unit to POZ molecules. The addition of these bridge units could extend the conjugation of the dye molecule, which red-shifted the absorption spectrum and increased the molar absorptivity of the dyes. Furthermore, to improve the donating power and molar extinction coefficient, an ethoxy phenyl ring was substituted in the 7 position of the POZ-furan dye as an additional donor.

Based on these strategies, three organic dyes (**WS1**, **WS2** and **WS3**) were designed and synthesized. The photophysical and electrochemical properties of the synthesized dyes were investigated in detail and density functional theory (DFT) calculations were also performed. Photovoltaic cells were assembled with the synthesized dyes and their photovoltaic properties were analyzed. In addition, electrochemical impedance spectroscopy (EIS) was used to study the interfacial charge transport process in the photovoltaic cells.

## 4.2 Experimental

### *4.2.1 Materials and reagents*

Phenoxazine, N-bromosuccinimide and 4-ethoxyphenylboronic acid were purchased from TCI and used as received without further purification. 1-bromobutane, 5-formyl-2-furan-boronic acid, 5-formyl-2-thiophene-boronic acid, tetrakis(triphenylphosphine) palladium(0), phosphorus oxychloride, 4-ethoxyphenylboronic acid, cyanoacetic acid and piperidine were purchased from Sigma-Aldrich and used as received without further purification. All solvents (chloroform, tetrahydrofuran, dimethylformamide, dimethyl sulfoxide, dichloromethane, 1, 2-dichloroethane and acetonitrile) were obtained from Sigma-Aldrich and used as received. Other chemicals were reagent grade and used without further purification.

#### *4.2.2 Analytical instruments and measurements*

$^1\text{H}$  NMR and  $^{13}\text{C}$  NMR spectra were recorded on a Bruker Avance 300, 500 and 600MHz using DMSO with the chemical shift against TMS (Seoul National University National Center for Inter-University Research Facilities). Mass data were measured using a JEOL JMS 600W mass spectrometer (Seoul National University National Center for Inter-University Research Facilities). UV-vis spectra were measured with a Hewlett-Packard 8425A



spectrophotometer. Cyclic voltammetry spectra were obtained using a three-electrode cell with a 273A potentiostat (Princeton applied research, Inc.). Measurements were performed using Ag wire ( $\text{Ag}/\text{Ag}^+$ ), glassy carbon and platinum wire as the reference, working and counter electrodes, respectively, in  $\text{CH}_2\text{Cl}_2$  solution containing 0.1M tetrabutylammonium tetrafluoroborate (TBATFB) as the supporting electrolyte. A standard ferrocene/ferrocenium ( $\text{Fc}/\text{Fc}^+$ ) redox couple was employed to calibrate the oxidation peak. Photocurrent-voltage measurements were performed using a Keithley model 2400 source measure unit. A 1000W Xe lamp (Spectra-physics) served as a light source, and it was adjusted using an NREL-calibrated silicon solar cell equipped with a KG-5 filter to approximate AM 1.5G sunlight intensity. The incident photon-to-current conversion efficiency (IPCE) was measured as a function of the wavelength from 300nm to 800nm using a specially designed IPCE system for dye-sensitized solar cells (PV measurements, Inc.). A 75W Xe lamp was employed as a light source to generate a monochromatic beam. The electrical impedance spectra (EIS) of the DSSCs under dark with 0.60V forward bias were measured with an impedance analyzer (Compactstat, IVIUM Tech) at frequencies of  $10^{-1} - 10^6$  Hz. The magnitude of the alternative signal

was 10 mV. The impedance parameters were determined by fitting the impedance spectra using Z-view software.

#### *4.2.3 Fabrication of dye-sensitized solar cells and measurements*

A Photoanode paste was prepared for a screen-printing process. The final composition of the paste comprised TiO<sub>2</sub> nanopowder (1 g), ethyl cellulose (0.5 g), terpineol (3.3 mL), and acetic acid (0.16 mL). After that, pre-washed FTO glass was coated by a doctor blade process and then heated at 70 °C for 30 minutes for drying. After the printing, the TiO<sub>2</sub> films were heated in four steps of 325 °C, 375 °C, 450 °C, and 500 °C for 5, 5, 15, and 15 minutes, respectively, using a high-temperature furnace (Lab house Co.). For the post-treatment, the coated and sintered TiO<sub>2</sub> films were immersed in TiCl<sub>4</sub> solution (40 mM in water) for 30 min. at 70 °C. After washing, the films were annealed at 500 °C for 30 minutes. Counter electrodes were prepared by spin coating method using 5 mM H<sub>2</sub>PtCl<sub>6</sub> solution (in ethanol) on one-holed FTO glass and heated at 400 °C for 20 min. After cooling at 60 °C, the TiO<sub>2</sub> electrodes were immersed in EtOH/CH<sub>2</sub>Cl<sub>2</sub> solution containing the dyes at 0.5 mM for 48 h at ambient temperature. After dye absorption, the photoanodes were washed using

anhydrous ethanol and dried under nitrogen flow. The dye-covered photoelectrode and Pt-electrode were assembled using ionomer surlyn with a hot-press at 80 °C. After assembling, the electrolyte solution (composed of 0.6 M BMII, 0.05 M I<sub>2</sub>, 0.1 M LiI, and 0.5 M TBP in acetonitrile solvent) was injected into the one-holed FTO glass using a capillarity vacuum technique, and the hole was sealed with a cover-glass using the same surlyn. A black mask aperture was placed on the front electrode for better analysis of the photovoltaic characteristics. The active area of the dye-coated TiO<sub>2</sub> film was *ca.* 0.24 cm<sup>2</sup>, which was measured by analyzing the images from a CCD camera (moticom 1000). The TiO<sub>2</sub> film thickness was measured by an  $\alpha$ -step surface profiler (KLA Tencor).

Photocurrent–voltage (I–V) measurements were performed using a Keithley model 2400 source measure unit. A class-A solar simulator (Newport) equipped with a 150 W Xe lamp was used as the light source. The light intensity was adjusted with an NREL-calibrated Si solar cell with a KG-5 filter for approximating the light intensity of 1 sun. Photocurrent–voltage measurements of the dye-sensitized solar cells were performed with an aperture mask by following a reported method. Incident photon-to-current conversion efficiency (IPCE) was measured as a function of wavelength from 300 to 1000 nm using a

specially designed IPCE system for dye-sensitized solar cells (PV measurements, Inc.). A 75 W xenon lamp was used as the light source for generating monochromatic beams. Calibration was performed using a silicon photodiode, which was calibrated based on the NIST-calibrated photodiode G425 standard. The IPCE values were measured under halogen bias light at a low chopping speed of 10 Hz. All calculations were carried out using Gaussian 09 software. Optimized geometries, energy levels, and frontier molecular orbitals of the dyes' HOMOs and LUMOs were calculated at the B3LYP/6-31G (d,p) level.

#### *4.2.4 Synthesis of dyes*

##### *4.2.4.1 10-Butyl-10H-phenoxazine (I)*

Sodium hydroxide (7.36g, 0.184mol) and 1-bromobutane (6.62g, 0.048mol) were slowly added to a phenoxazine (4.0g, 0.022mol) solution in dry DMSO (50mL) at room temperature and stirred for 24h. Then, the reaction mixture was poured into water and extracted with ethyl acetate. The organic phase was separated and dried over anhydrous MgSO<sub>4</sub>. After removing the solvent, the

residue was purified by column chromatography using ethyl acetate-hexane (1:10; v/v) as the eluent to give **1**, colorless viscous liquid (4.78g, 91%).

$^1\text{H}$  NMR (500MHz,  $d_6$ -DMSO) :  $\delta$  = 6.81 (d,  $J$  = 8.7Hz, 2H), 6.63-6.67 (m, 4H), 3.53 (t,  $J$  = 7.7 Hz, 2H), 1.50-1.54 (m, 2H), 1.38-1.43 (m, 2H), 0.94 ppm (t,  $J$  = 7.3 Hz, 3H).

#### 4.2.4.2 10-Butyl-10H-phenoxazine-3-carbaldehyde (**2**)

$\text{POCl}_3$  (0.55mL, 0.006mol) was added dropwise to a solution of **1** (1.29g, 0.005mol) and dry DMF (5mL) in dry 1,2-dichloroethane (10.7mL) in an ice water bath with temperature below 15°C. The reaction was heated to room temperature and refluxed at 90°C for 48h. The mixture was quenched with dilute NaOH (aq) and extracted with water and dichloromethane (DCM). The organic phase was dried with anhydrous  $\text{MgSO}_4$ , and then the solvent was removed in vacuo. The residue was purified by column chromatography using ethyl acetate-hexane (1:6; v/v) to give **3**, yellow oil (0.957g, 71.6%).

$^1\text{H}$  NMR (500MHz,  $d_6$ -DMSO) :  $\delta$  = 9.64 (s, 1H), 7.41 (dd,  $J$  = 8.3, 1.8 Hz, 1H), 7.00 (s, 1H), 6.68-6.87 (m, 5H), 3.62 (t,  $J$  = 7.9 Hz, 2H), 1.52-1.56 (m, 2H), 1.40-1.45 (m, 2H), 0.95 ppm (t,  $J$  = 7.3 Hz, 3H).

#### 4.2.4.3 3-Bromo-10-butyl-10H-phenoxazine (**3a**)

**1** (1.488g, 0.0062mol) and N-bromosuccinimide (1.106g, 0.0062mol) were dissolved in chloroform (30mL), and the reaction was stirred for 1h at ambient temperature. The reaction was quenched with water and extracted with water and DCM. The organic phase was collected and the solvent was removed by rotary evaporation. The residue was purified by column chromatography using hexane to give **3a**, white solid (1.48g, 75%).

<sup>1</sup>H NMR (500MHz, d<sub>6</sub>-DMSO) : δ = 7.0-6.96 (m, 1H), 6.86-6.80 (m, 2H), 6.69-6.59 (m, 4H), 3.52-3.47 (m, 2H), 1.53-1.46 (m, 2H), 1.44-1.35 (m, 2H), 0.90-0.91 ppm (m, 3H).

#### 4.2.4.4 3,7-Dibromo-10-butyl-10H-phenoxazine (**3b**)

**3b** as a white solid (1.72g, 70%) was synthesized according to the procedure described for the synthesis of **3a**. N-bromosuccinimide (2.21g, 0.0124mol) was added to a solution of **1** (1.49g, 0.0062mol) in chloroform (30mL) at ambient temperature. Eluent : hexane.

<sup>1</sup>H NMR (500MHz, d<sub>6</sub>-DMSO) : δ = 7.0 (d, J = 8.6 Hz, 2H), 6.83 (s, 2H), 6.54 (d, J = 8.7 Hz, 1H), 3.50 (t, J = 7.5 Hz, 2H), 1.50-1.45 (m, 2H), 1.40-1.36 (m, 2H), 0.92 ppm (t, J = 7.3 Hz, 3H).

#### 4.2.4.5 5-(10-Butyl-10H-phenoxazin-3-yl)furan-2-carbaldehyde (**4a**)

Under nitrogen atmosphere, a mixture of **3a** (2.21g, 0.0069mol), 5-formyl-2-furan-boronic acid (1.12g, 0.0080mol), 2M aqueous of K<sub>2</sub>CO<sub>3</sub> (8.66mL), Pd(PPh<sub>3</sub>)<sub>4</sub> (0.4g, 0.00035mol) in dry THF (100mL) was stirred for 1/2 h and refluxed at 80 °C overnight. The reaction was extracted with DCM, water and brine. The organic phase was dried with anhydrous MgSO<sub>4</sub>, and then the solvent was removed in vacuo. The residue was purified by column chromatography using DCM-hexane (5:1; v/v) to give **4a**, orange oil (1.13g, 49%).

<sup>1</sup>H NMR (500MHz, d<sub>6</sub>-DMSO) : δ = 9.53 (s, 1H), 7.60 (s, 1H), 7.33 (d, J = 8.4 Hz, 1H), 7.12 (s, 1H), 7.11 (s, 1H), 6.86 (t, J = 7.9 Hz, 1H), 6.78 (d, J = 8.5 Hz, 1H), 6.74-6.66 (m, 3H), 3.59 (t, J = 7.6 Hz, 2H), 1.57-1.52 (m, 2H), 1.45-1.40 (m, 2H), 0.95 ppm (t, J = 7.3 Hz, 3H).

#### 4.2.4.6 5-(10-Butyl-10H-phenoxazin-3-yl)thiophene-2-carbaldehyde (**4b**)

**4b** as an orange oil (1.53g, 42%) was synthesized according to the procedure described for the synthesis of **4a**. 5-formyl-2-thiophene-boronic acid (1.95g, 0.0124mol) was added under nitrogen atmosphere to a solution of **3a** (3.32g,

0.0104mol), 2M aqueous K<sub>2</sub>CO<sub>3</sub> (13mL), Pd(PPh<sub>3</sub>)<sub>4</sub> (0.61g, 0.00053mol) in dry THF (100mL). Eluent : DCM-hexane (5:1; v/v).

<sup>1</sup>H NMR (300MHz, d<sub>6</sub>-DMSO) : δ = 9.84 (s, 1H), 7.96 (s, 1H), 7.59 (s, 1H), 7.26 (d, J = 8.3 Hz, 1H), 7.09 (s, 1H), 6.88-6.84 (m, 1H), 6.75-6.66 (m, 4H), 3.59 (t, J = 7.9 Hz, 2H), 1.55-1.48 (m, 2H), 1.46-1.38 (m, 2H), 0.95 ppm (t, J = 7.2 Hz, 3H).

#### 4.2.4.7 3-(5-Formyl-2-furan)-7-bromo-10-butyl-10H-phenoxazine (**4c**)

**4c** as an orange oil (1.03g, 41%) was synthesized according to the procedure described for the synthesis of **4a**. 5-formyl-2-furan-boronic acid (1.02g, 0.0072mol) was added under nitrogen atmosphere to a solution of **3b** (2.41g, 0.0061mol), 2M aqueous K<sub>2</sub>CO<sub>3</sub> (15.25mL), Pd(PPh<sub>3</sub>)<sub>4</sub> (0.71g, 0.00061mol) in dry THF (100mL). Eluent : DCM-hexane (5:1; v/v).

<sup>1</sup>H NMR (500MHz, d<sub>6</sub>-DMSO) : δ = 9.53 (s, 1H), 7.60 (s, 1H), 7.35 (d, J = 8.4 Hz, 1H), 7.13 (m, 2H), 7.02 (d, J = 8.4 Hz, 1H), 6.85 (s, 1H), 6.82 (d, J = 8.6 Hz, 1H), 6.68 (d, J = 8.7 Hz, 1H), 3.58 (t, J = 7.5 Hz, 2H), 1.54-1.50 (m, 2H), 1.43-1.39 (m, 2H), 0.94 ppm (t, J = 7.3 Hz, 3H).



4.2.4.8 *5-(3-(4-Ethoxyphenyl)-10-butyl-10H-phenothiazin-7-yl)furan-2-carbaldehyde (5a)*

A mixture of **4c** (0.5g, 0.0012mol), 2M aqueous K<sub>2</sub>CO<sub>3</sub> (6ml), Pd(PPh<sub>3</sub>)<sub>4</sub> (0.07g, 0.00006mol) in dry THF (15mL) was refluxed for 1/2 h. 4-ethoxyphenylboronic acid (0.28g, 0.0017mol) dissolved in dry THF (5mL) was added to the reaction mixture and refluxed for 15h. The mixture was quenched with water and extracted with DCM. The organic phase was dried with anhydrous MgSO<sub>4</sub>, and then the solvent was removed in vacuo. The residue was purified by column chromatography using DCM-ethyl acetate (10:1; v/v) to give **5a**, orange oil (0.29g, 53%).

<sup>1</sup>H NMR (500MHz, d<sub>6</sub>-DMSO) : δ = 9.52 (s, 1H), 7.57 (s, 1H), 7.49 (d, J = 8.7 Hz, 2H), 7.34 (d, J = 8.4 Hz, 2H), 7.13-7.07 (m, 3H), 6.94 (d, J = 8.7 Hz, 2H), 6.91 (s, 1H), 6.77 (t, J = 8.7 Hz, 2H), 4.06-4.00 (m, 2H), 3.62 (t, J = 7.5 Hz, 2H), 1.58-1.56 (m, 2H), 1.45-1.43 (m, 2H), 1.34 (t, J = 7 Hz, 3H), 0.97 ppm (t, J = 7.3 Hz, 3H).

4.2.4.9 *(E)-(10-Butyl-10H-phenoxazin-3-yl)-2-cyanoacrylic acid (POX)*

**3** (0.23g, 0.00086mol), cyanoacetic acid (0.22g, 0.0026mol) and piperidine (0.18mL, 0.00347mol) were added to anhydrous CH<sub>3</sub>CN (100mL). After the

mixture was refluxed for 8h, the solution was extracted with DCM and 0.1M HCl aqueous solution. The organic phase was dried over anhydrous MgSO<sub>4</sub>, and the solvent was removed in vacuo. The crude product was purified by column chromatography using DCM- methanol (5:1; v/v) to give **POX**, red solid (0.22g, 75%).

<sup>1</sup>H NMR (600MHz, d<sub>6</sub>-DMSO) : δ = 7.97 (s, 1H), 7.48 (d, J = 8.5 Hz, 1H), 7.36 (s, 1H), 6.85 (t, J = 7.6 Hz, 1H), 6.69-6.78 (m, 4H), 3.59 (t, J = 7.6 Hz, 2H), 1.50-1.55 (m, 2H), 1.37-1.43 (m, 2H), 0.93 ppm (t, J = 7.3 Hz, 3H) ;

<sup>13</sup>C NMR (150MHz, d<sub>6</sub>-DMSO) : δ = 164.1, 152.2, 143.8, 143.6, 137.8, 130.9, 130.6, 124.3, 123.7, 122.6, 117.2, 115.3, 114.5, 112.9, 111.7, 98.0, 42.9, 26.7, 19.2, 13.7 ppm ;

m/z (FAB) 334.1316 ((M<sup>+</sup>), C<sub>20</sub>H<sub>18</sub>N<sub>2</sub>O<sub>3</sub> requires 334.1317).

#### 4.2.4.10 (E)-3-(5-(10-Butyl-10H-phenoxazin-3-yl)furan-2-yl)-2-cyanoacrylic acid (**WS1**)

**WS1** (0.13g, 54%) was synthesized according to the procedure described for the synthesis of **POX**. **4a** as a dark red solid (0.2g, 0.0006mol), cyanoacetic acid (0.15g, 0.0018mol), and piperidine (0.24mL, 0.0024mol) were added to anhydrous CH<sub>3</sub>CN (50mL). Eluent : DCM-methanol (9:1; v/v).

$^1\text{H}$  NMR (500MHz,  $d_6$ -DMSO) :  $\delta$  = 7.97 (s, 1H), 7.48 (s, 1H), 7.41 (d, J = 8 Hz, 1H), 7.19-7.17 (m, 2H), 6.87-6.84 (m, 1H), 6.81 (d, J = 9 Hz, 1H), 6.74-6.72 (m, 1H), 6.70-6.68 (m, 2H), 3.60 (t, J = 7.5 Hz, 2H), 1.58-1.52 (m, 2H), 1.46-1.39 (m, 2H), 0.95 ppm (t, J = 7.5 Hz, 3H) ;

$^{13}\text{C}$  NMR (125MHz,  $d_6$ -DMSO) :  $\delta$  = 163.5, 158.0, 146.4, 143.7, 143.2, 136.4, 133.9, 131.1, 126.2, 123.7, 121.1, 121.0, 120.4, 116.4, 114.6, 111.9, 111.8, 110.6, 108.0, 42.6, 26.1, 18.7, 13.2 ppm ;

m/z (FAB) 400.1422 ((M<sup>+</sup>), C<sub>24</sub>H<sub>20</sub>N<sub>2</sub>O<sub>4</sub> requires 400.1423).

4.2.4.11 (E)-3-(5-(10-Butyl-10H-phenoxazin-3-yl)thiophene-2-yl)-2-cyanoacrylic acid (**WS2**)

**WS2** (0.43g, 79%) as a dark red solid was synthesized according to the procedure described for the synthesis of **POX. 4b** (0.46g, 0.0013mol), cyanoacetic acid (0.33g, 0.0039mol), and piperidine (0.51mL, 0.0052mol) were added to anhydrous CH<sub>3</sub>CN (100mL). Eluent : DCM-methanol (10:1; v/v).

$^1\text{H}$  NMR (500MHz,  $d_6$ -DMSO) :  $\delta$  = 8.43 (s, 1H), 7.96 (s, 1H), 7.63 (s, 1H), 7.25 (d, J = 8.5 Hz, 1H), 7.08 (s, 1H), 6.87 (t, J = 7.5 Hz, 1H), 6.77-6.69 (m, 4H), 3.61 (t, J = 6.5 Hz, 2H), 1.59-1.53 (m, 2H), 1.47-1.40 (m, 2H), 0.96 ppm (t, J = 7 Hz, 3H) ;

$^{13}\text{C}$  NMR (75MHz,  $d_6$ -DMSO) :  $\delta$  = 163.2, 151.9, 145.8, 143.8, 143.1, 141.0, 133.8, 132.6, 131.3, 124.2, 123.8, 123.2, 122.1, 121.0, 116.2, 114.6, 111.9, 111.6, 66.4, 26.0, 18.8, 13.2 ppm ;

m/z (FAB) 417.1281 ((M + H<sup>+</sup>), C<sub>24</sub>H<sub>21</sub>N<sub>2</sub>O<sub>3</sub> S requires 417.1273).

*4.2.4.12(E)-3-(5-(4-Methoxyphenyl)-10-butyl-10H-phenoxazin-7-yl)furan-2-yl)-2 cyanoacrylic acid (WS3)*

**WS3** (0.25g, 72%) as a dark purple solid was synthesized according to the procedure described for the synthesis of **POX. 5a** (0.3g, 0.00066mol), cyanoacetic acid (0.17g, 0.002mol) and piperidine (0.26mL, 0.0026mol) were added to anhydrous CH<sub>3</sub>CN (100mL). Eluent : DCM-methanol (5:1; v/v).

$^1\text{H}$  NMR (500MHz,  $d_6$ -DMSO) :  $\delta$  = 7.98 (s, 1H), 7.54 (d, J = 8.5 Hz, 2H), 7.49 (s, 1H), 7.44(d, J = 8.5, 1H), 7.22-7.20 (m, 2H), 7.13 (d, J = 8 Hz, 1H), 6.95 (m, 3H), 6.86 (d, J = 8.5 Hz, 1H), 6.80 (d, J = 8.5 Hz, 1H), 4.06-4.05 (m, 2H), 3.65 (t, J = 7 Hz, 2H), 1.59-1.57 (m, 2H), 1.48-1.43 (m, 2H), 1.34(d, J = 7 Hz, 3H), 0.97 ppm (t, J = 7 Hz, 3H) ;

$^{13}\text{C}$  NMR (75MHz,  $d_6$ -DMSO) :  $\delta$  = 163.5, 158.1, 157.3, 146.4, 143.6, 143.5, 136.5, 133.7, 132.8, 130.5, 129.8, 126.3, 121.3, 121.0, 120.4, 120.4, 116.4, 114.2, 112.3, 112.1, 111.9, 110.6, 108.2, 62.5, 42.2, 26.2, 18.8, 14.1, 13.3 ppm ;

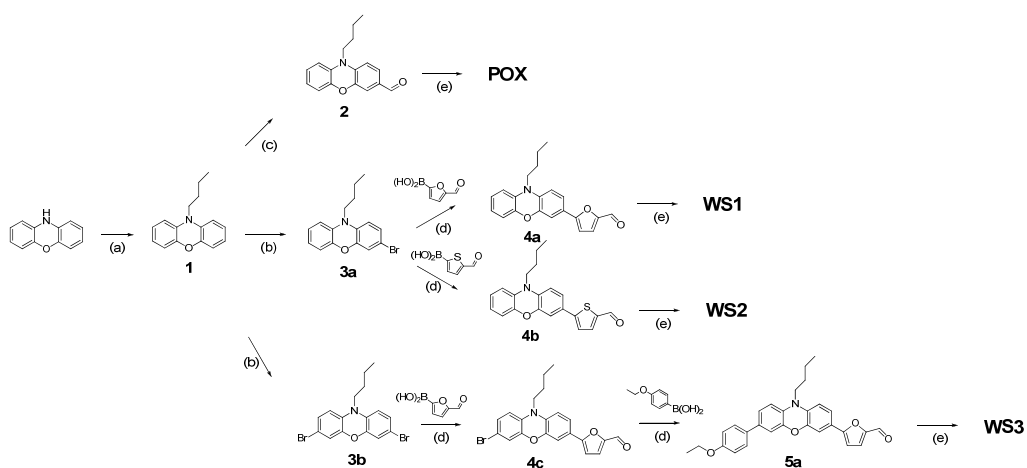
m/z (FAB) 500.2002 ((M<sup>+</sup>), C<sub>32</sub>H<sub>28</sub>N<sub>2</sub>O<sub>5</sub> requires 500.1998).

## 4.3 Results and Discussion

### 4.3.1. Synthesis

The synthetic routes of POZ dyes are shown in Scheme 4.1 and the synthesized dyes and reference dyes (POX) were shown in Fig. 4.1. The POZ syntheses first involved an alkylation reaction on POZ nitrogen atom and a butyl chain was introduced to the POZ moiety to give intermediate **1**. The bromination of **1** was performed by varying the amount of N-bromosuccinimide (NBS) to provide mono-brominated **3a** and dibrominated **3b**, respectively. The Suzuki coupling reactions of **3a** were carried out with 5-formyl-2-furanboronic acid or 5-formyl-2-thiopheneboronic acid, which produced **4a** and **4b**, respectively. The Suzuki coupling reaction of **3b** to give **4c** followed the procedure performed with **3a**, and subsequently, an additional Suzuki coupling reaction of **4c** with 4-ethoxyphenylboronic acid gave **5a**. The final compounds (**WS1**, **WS2**, and **WS3**) were obtained by the Knoevenagel reactions of the corresponding aldehydes (**4a**, **4b**, and **5a**) with cyanoacetic acid in the presence

of piperidine [15]. The reference dye (**POX**) was obtained by previously reported synthetic routes. The structures of all the synthesized intermediates and dyes were identified by  $^1\text{H}$  NMR, and the final products were additionally confirmed by  $^{13}\text{C}$  NMR and HRMS.



Scheme 4.1. Synthesis of **POX**, **WS1**, **WS2**, and **WS3**: (a) 1-iodobutane, NaOH, DMSO (b) NBS,  $\text{CHCl}_3$  (c)  $\text{POCl}_3$ , DMF,  $\text{CHCl}_3$  (d) 2M aqueous of  $\text{K}_2\text{CO}_3$ ,  $\text{Pd}(\text{pPh}_3)_4$ , THF (e) cyanoacetic acid, piperidine, acetonitrile.

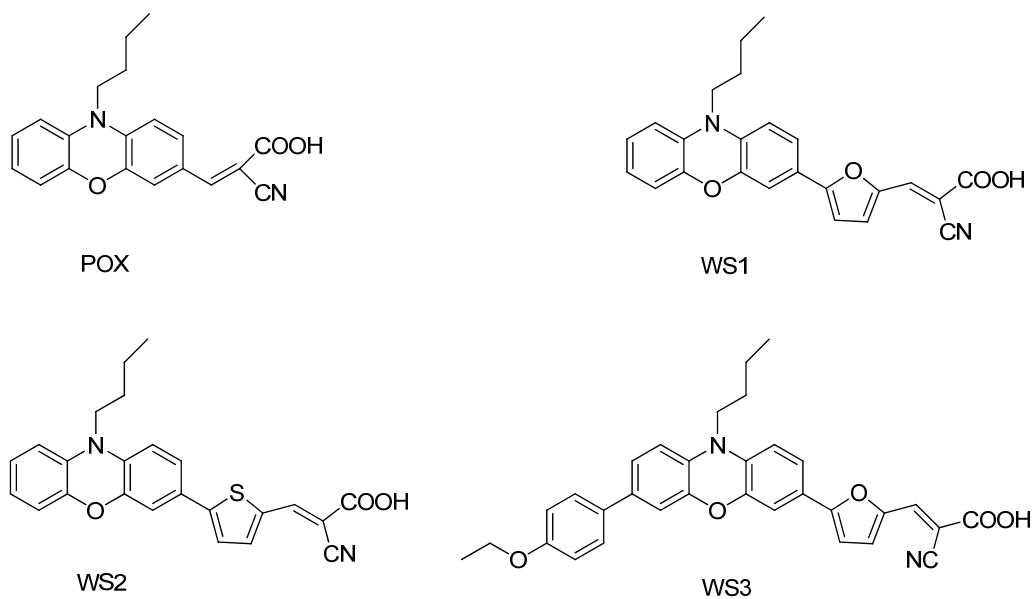


Fig. 4.1. Structure of **POX**, **WS1**, **WS2**, and **WS3**.

#### 4.3.2. Photophysical properties

The absorption spectra of the dyes in EtOH/CH<sub>2</sub>Cl<sub>2</sub> solution and on the TiO<sub>2</sub> surface are shown in Fig. 4.2, and the corresponding photophysical data are listed in Table 4.1. All the dyes exhibited two major absorption bands, which appeared at below 350nm and 400-550nm, respectively. The former band in the UV region is ascribed to a localized aromatic  $\pi$ - $\pi^*$  transition, and the latter band

in the visible region is due to the intramolecular charge-transfer (ICT) transition from the donor to the acceptor. The absorption maxima ( $\lambda_{\text{max}}$ ) of **WS1**, **WS2**, and **WS3** are 452, 455, and 475 nm, respectively. The absorption spectrum of **WS3**, which included both the additional donor and bridge moiety, was red-shifted more than 10nm compared to those of **WS1** and **WS2**, which included the bridge unit only. This was attributed to the better delocalization of electrons over the  $\pi$ -conjugated molecules by both the electron-rich furan and the ethoxy phenyl ring. The molar extinction coefficient at  $\lambda_{\text{max}}$  of **WS1**, **WS2**, and **WS3** were 19063, 19209, and 26335  $\text{M}^{-1}\text{cm}^{-1}$ , respectively. These are higher than those of structurally similar phenothiazine dyes (PT 5, 17600  $\text{M}^{-1}\text{cm}^{-1}$ ) as well as standard ruthenium dye (N719, 14000 $\text{M}^{-1}\text{cm}^{-1}$ ), which afford the use of thinner  $\text{TiO}_2$  film for efficient electron diffusion. Among these dyes, **WS3** exhibited the highest molar extinction coefficient. This result indicated that the ethoxy phenyl ring is beneficial to the conjugation and absorption properties of **WS3**, despite the large dihedral angle between the POZ core and ethoxy phenyl ring (Table 4.2). The red-shifts in the absorption spectra and high molar extinction coefficients of the dyes have a tendency to increase with enhancement of the electron density in the bridge unit and additional donor.



Thus, their introduction to the POZ moiety is favorable for enhancing the light harvest and photocurrent generation of the dyes.

The absorption spectra of the dyes absorbed on TiO<sub>2</sub> film are blue-shifted compared to those in solution, and there is a larger blue-shift in **WS3** (9nm) than in **WS1** and **WS2** (3nm). This might be due to the H-aggregation of the dyes or the deprotonation of carboxylic acid upon the adsorption onto the TiO<sub>2</sub> surface [16]. **WS3** showed almost the same absorbance on the TiO<sub>2</sub> surface compared to **WS1** and **WS2**, although it exhibited a much higher molar extinction coefficient in solution. As shown in Table 4.2 and Table 4.3, this is due to the non-planar structure of **WS3** caused by the introduction of the ethoxy phenyl ring, which inhibits the adsorption of the dye on the TiO<sub>2</sub> surface. The optimized geometry of the dye in the ground state revealed that the POZ core of all the dyes had planar structures with small torsion angles (0.82-1.07°). On the other hand, there were considerable differences in the dihedral angles between the POZ core and the substituents. **WS1** had almost planar structure with a small dihedral angle (0.29°) between the core of the dye and the furan moiety, while, the planarity of **WS2** and **WS3** decreased significantly due to the large dihedral angle between the POZ core and the adjacent bridge unit or donor moiety; the dihedral angle between thiophene and the POZ core in **WS2** was

19.36°, and that between the ethoxy phenyl ring and the POZ core in **WS3** was 37.35°. **WS3** had the most twisted molecular geometry of the dyes, which led to less adsorption and decreased absorbance of the dye on the TiO<sub>2</sub> surface (Table 4.3).

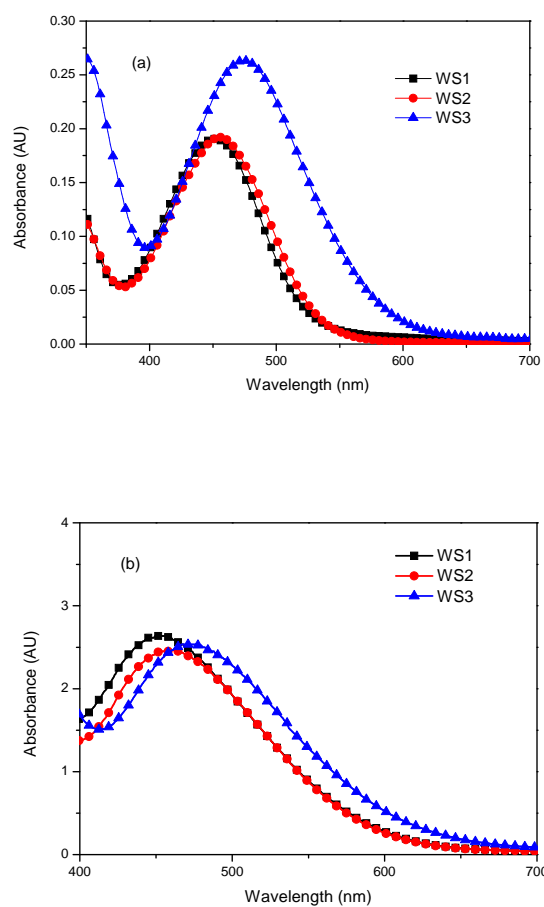


Fig. 4.2. Absorbtion spectra of **WS1**, **WS2**, and **WS3** in (a) EtOH/CH<sub>2</sub>Cl<sub>2</sub> (7 : 2; v/v) (10<sup>-5</sup>molL<sup>-1</sup>) and (b) on TiO<sub>2</sub>.

Table 4.1. Photophysical and electrochemical properties of **WS1**, **WS2** and **WS3** dyes.

Dye	Absorption <sup>a</sup>			Oxidation potential data <sup>c</sup>		
	$\lambda_{\max}/\text{nm}$	$\epsilon/\text{M}^{-1}\text{cm}^{-1}$ (at $\lambda_{\max}$ )	$\lambda_{\text{abs}}^{\text{b}}/\text{nm}$ (on $\text{TiO}_2$ )	$E_{\text{ox}}/\text{V}$ (vs. NHE)	$E_{0-0}^{\text{d}}/\text{V}$	$E_{\text{ox}} - E_{0-0}/\text{V}$ (vs. NHE)
<b>WS1</b>	452	19063	449	0.88	2.36	-1.48
<b>WS2</b>	455	19209	452	0.89	2.33	-1.44
<b>WS3</b>	475	26335	466	0.81	2.13	-1.31

<sup>a</sup> Measured in  $1 \times 10^{-5}$  EtOH/CH<sub>2</sub>Cl<sub>2</sub> solutions at room temperature.

<sup>b</sup> Measured on TiO<sub>2</sub> film. <sup>c</sup> Measured in CH<sub>2</sub>Cl<sub>2</sub> containing 0.1 M tetrabutylammonium tetrafluoroborate. (TBABF<sub>4</sub>) electrolyte (working electrode: glassy carbon; counter electrode: Pt; reference electrode: Ag/Ag<sup>+</sup>; calibrated with ferrocene/ferrocenium (Fc/Fc<sup>+</sup>) as an internal reference and converted to NHE by addition of 630 mV.)

<sup>d</sup> Estimated from onset wavelength in absorption spectra

Table 4.2. Optimized structures, dihedral angles and electronic distributions in HOMO and LUMO levels of the prepared dyes.

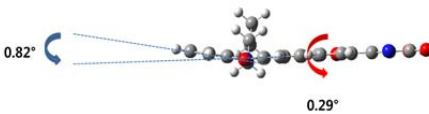
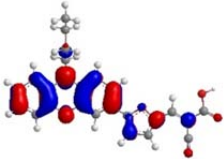
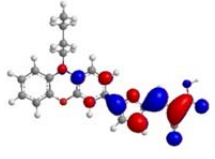

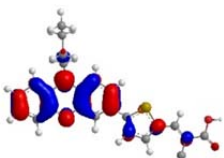
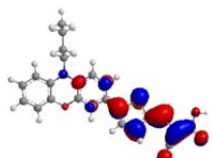
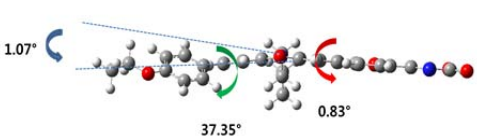
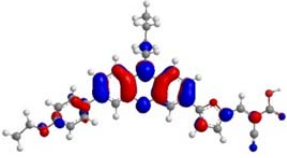

Dye	Optimized structure	HOMO	LUMO
<b>WS1</b>	 <p>0.82° 0.29°</p>		
<b>WS2</b>	 <p>0.45° 19.36°</p>		
<b>WS3</b>	 <p>1.07° 37.35° 0.83°</p>		

Table 4.3. DSSC performance parameters of **POX**, **WS1**, **WS2**, and **WS3**<sup>a</sup>.

Dye <sup>b</sup>	J <sub>sc</sub> (mA/cm <sup>2</sup> )	V <sub>oc</sub> (mV)	FF (%)	η (%)	Dye amount <sup>c</sup> (10 <sup>-7</sup> mol cm <sup>-2</sup> )
<b>POX</b>	9.88	663.5	73.22	4.80	-
<b>WS1</b>	11.72	653.0	68.76	5.26	2.05
<b>WS2</b>	11.11	628.3	70.38	4.91	1.89
<b>WS3</b>	11.35	639.9	67.09	4.87	1.34
<b>N719</b>	14.71	728.3	72.85	7.80	-

<sup>a</sup> Measured under AM 1.5 irradiation G (100 mW cm<sup>-1</sup>); 0.2 cm<sup>2</sup> working area. <sup>b</sup> Dyes were maintained at 0.5 mM in EtOH/CH<sub>2</sub>Cl<sub>2</sub> solution, with 10 mM CDCA co-adsorbent. Electrolyte comprised 0.7 M 1-propyl-3-methyl-imidazolium iodide (PMII), 0.2 M LiI, 0.05 M I<sub>2</sub>, 0.5 M TBP in acetonitrile-valeronitrile (v/v, 85/15) for organic dyes. <sup>c</sup> Dyes' adsorption on TiO<sub>2</sub> were measured by a colorimetric method using 0.1 M NaOH aqueous-DMF (1:1) mixed solutions to wash the dyes from 8 μm thick TiO<sub>2</sub> film.

#### 4.3.3. Electrochemical properties

The electrochemical properties and energy levels of the prepared dyes are provided in Table 4.1 and Fig. 4.3. The oxidation potentials of the dyes were

measured using cyclic voltammetry (CV), and the C-V curves of the dyes are shown in Fig. 4.4. The HOMO levels of the prepared dyes correspond to the first oxidation potential versus a normal hydrogen electrode (*vs.* NHE) calibrated by  $\text{Fc}/\text{Fc}^+$  (with 640 mV *vs.* NHE). All of the HOMO levels of the dyes ranged from 0.81 eV to 0.88 eV (*vs.* NHE) and were sufficiently positive compared to the redox potential of  $\text{I}^-/\text{I}_3^-$  (0.4 V *vs.* NHE), implying that the oxidized dyes can be effectively regenerated by the redox electrolyte [17]. The LUMO levels of the dyes were obtained by subtracting the zeroth-zeroth energy ( $E_{0-0}$ ) from  $E_{\text{ox}}$ , in which the zeroth-zeroth energy of the dyes is determined from the inflection point at the end of the visible absorption spectrum of the dyes. All of the LUMO levels of the dyes were more negative than the conduction band energy level ( $E_{\text{cb}}$ ) of  $\text{TiO}_2$  (-0.5 *vs.* NHE), indicating that the excited electrons of the dyes can be efficiently injected into the conduction band of  $\text{TiO}_2$ , and oxidized dyes are simultaneously formed [17]. As shown in Table 4.1, **WS3** had a more negative HOMO level and a more positive LUMO level than **WS1** and **WS2**. This might be attributed to the extension of conjugation induced by the additional donating group. Consequently, the gap between the HOMO and LUMO decreased, and the absorption spectra became red-shifted.

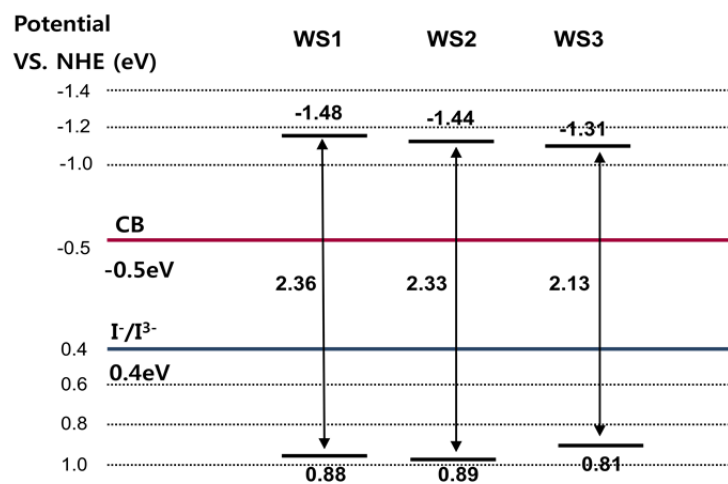


Fig. 4.3. Dyes' HOMO and LUMO energy levels.

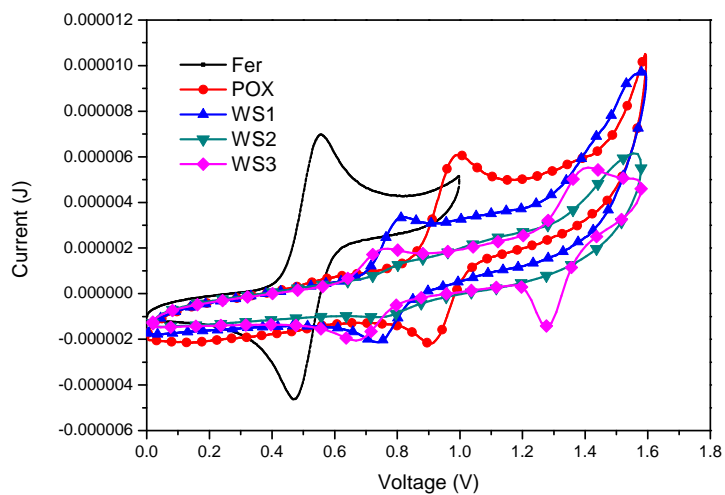


Fig. 4.4. CV curves of  $\text{Fc}/\text{Fc}^+$ , **POX**, **WS1**, **WS2**, and **WS3** in  $\text{CH}_2\text{Cl}_2$ .

#### 4.3.4. Photovoltaic properties

DSSCs were fabricated using the dyes as sensitizers, and their photovoltaic properties were measured under the standard AM 1.5G irradiation conditions ( $100\text{mW cm}^{-2}$ ). The effects of the five-membered heterocyclic bridges and the ethoxyphenyl substitution on the performance of the cells were evaluated by measuring their conversion efficiency relative to the reference dye (**POX**). The IPCE spectra and photocurrent-voltage (J-V) curves are shown in Fig. 4.5, and the corresponding data are listed in Table 4.3. All the dyes showed high maximum IPCE values at 400-500nm, which were 73.4%, 69.7%, and 73.2% for **WS1**, **WS2**, and **WS3**, respectively. These values were higher than that of standard ruthenium dye (N719, 69.6%). Therefore, all the dyes can effectively convert visible light into photocurrent in the absorption ranges. The IPCE spectra of **WS1** and **WS2** showed broadened and red-shifted ranges compared to that of **POX**, and the onsets of their IPCE spectra were extended to 750nm. The bridge units introduced to the POZ moiety red-shifted the spectra of the dyes due to the extension of conjugation, increasing light harvest in the long wavelength region. **WS3**, which had an additional donor, showed a similar



IPCE spectrum to that of **WS1**. This might be attributed to the fact that the absorption spectrum of **WS3** on TiO<sub>2</sub> was largely blue-shifted compared to that of **WS1**. In addition, it is known that a larger amount of dye adsorbed on TiO<sub>2</sub> leads to a broader IPCE spectrum [18]. Thus, the lesser amount of adsorption of **WS3** on the TiO<sub>2</sub> surface also contributed the relatively narrow IPCE spectrum of the dye. The short-circuit current ( $J_{sc}$ ) values increased in the order of **POX** < **WS2** < **WS3** < **WS1**, and this trend correlated with the broadness of the IPCE spectrum. Consequently, the introduced bridge units improved  $J_{sc}$  and the conversion efficiency, while the introduction of the additional donor group to the POZ moiety had little effect on  $J_{sc}$ .

The open-circuit voltage ( $V_{oc}$ ) values of the cells fabricated with the dyes increased in the order of **WS2** < **WS3** < **WS1** < **POX**. The  $V_{oc}$  values of the cells based on **WS1-3** are lower than that based on **POX**. As shown in previous studies, this might be explained by the increased interaction caused by the introduction of a heterocyclic bridge unit from  $\pi$ - $\pi$  interaction between the dye molecules and/or the interaction between the heteroatom in the bridge unit and iodine [19, 11c]. These interactions enhanced the charge recombination at the dye/dye or dye/electrolyte interface, resulting in low  $V_{oc}$  values of the cells. As shown in Fig. 4.6, this tendency was also shown in the dark currents of the cells

made with the dyes. The dark current is defined as the relatively small electric current flowing out of a system without illumination and lower dark current indicates decreased recombination and high  $V_{oc}$ . Thus, the low dark current of the cell with **POX** corresponds with the highest  $V_{oc}$ , whereas the high dark current of the cell with **WS2** is consistent with the lowest  $V_{oc}$ .

To explain the correlation between the  $V_{oc}$  of the cells and the dyes, electrochemical impedance spectroscopy (EIS) [20] was carried out in the dark under a forward bias of -0.60 V. The Nyquist plots of the DSSCs fabricated with the dyes are shown in Fig. 4.7. In the Nyquist plot, the major semicircle at the intermediate frequency represents the charge transfer impedance at the  $TiO_2$ /dye/electrolyte interface. The charge recombination resistance can be estimated by the radius of the major semicircle at the intermediate frequency, with a larger radius of the major semicircle meaning a smaller charge recombination rate [21]. The charge recombination resistance increased in the order of **WS2** < **WS3** < **WS1** < **POX**, which is in accordance with the  $V_{oc}$  values in the DSSCs made with the dyes. As the charge recombination between injected electrons and the electrolyte increased,  $V_{oc}$  increased as well. As shown in Fig. 4.8, this result coincides with the electron lifetime vs dark bias voltage. The electron lifetime increased in the order of **WS2** < **WS3**  $\approx$  **WS1** < **POX** <

**N719**. Longer electron lifetime indicates improved charge recombination resistance between the injected electrons and electrolyte, with a consequent increase in the  $V_{oc}$  [22]. The results suggest that the introduction of the furan bridge unit retards the charge recombination more effectively compared to the thiophene bridge unit, leading to a longer electron lifetime and a higher  $V_{oc}$ .

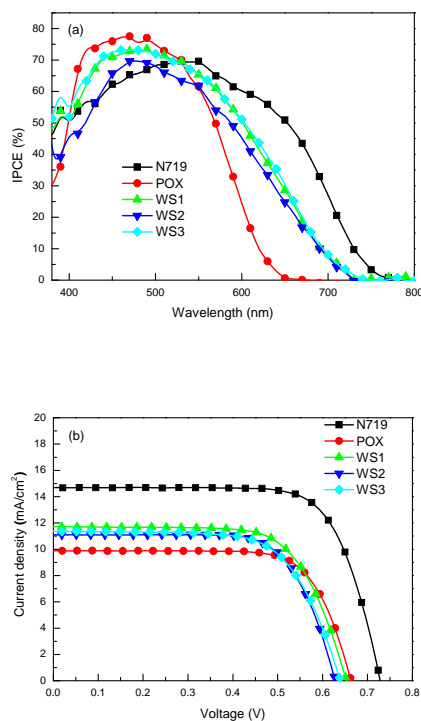


Fig. 4.5. (a) IPCE spectra DSSCs based on **POX**, **WS1**, **WS2**, **WS3**, and **N719** and (b) the DSSCs'  $J-V$  curves under AM 1.5G simulated sunlight ( $100 \text{ mWcm}^{-2}$ ).

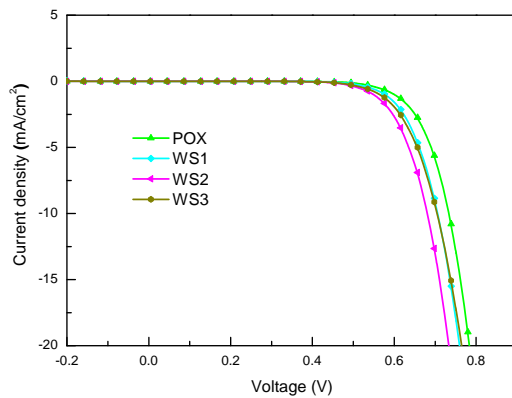


Fig. 4.6. DSSCs'  $J$ - $V$  curves based on **POX**, **WS1**, **WS2**, and **WS3** in the dark.

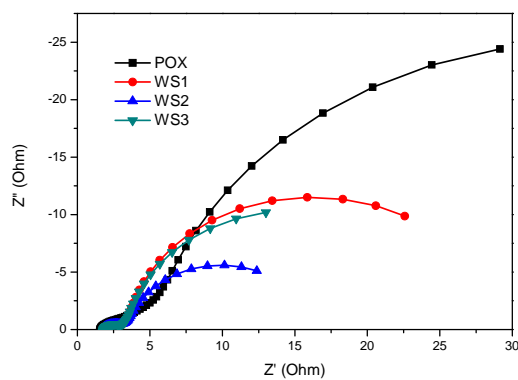


Fig. 4.7. Impedance spectra of DSSCs based on **POX**, **WS1**, **WS2**, and **WS3**;

Nyquist plots measured at 0.60 V forward bias in the dark.

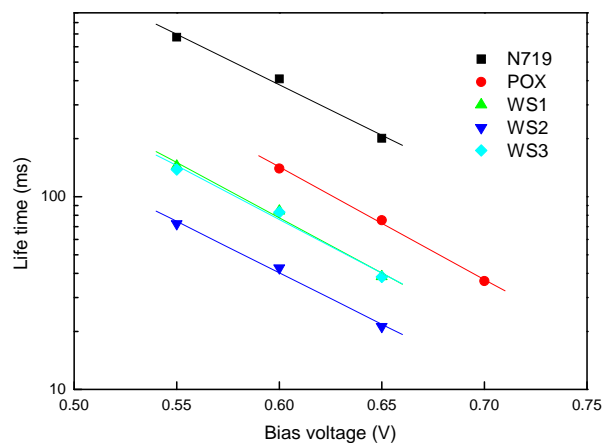


Fig. 4.8. Electron lifetime of **N719**, **POX**, **WS1**, **WS2**, and **WS3** as a function of bias voltage.

#### 4.4 Conclusion

The first design and synthesis of three novel phenoxazine-based organic dyes (**WS1**, **WS2** and **WS3**) has been done to study the effects of the various bridge units and an additional donor on the performance of DSSCs. The introduction of the heterocyclic bridge units (furan and thiophene) extended the conjugation

and red-shifted the absorption spectra of the dyes, improving  $J_{sc}$ . Consequently, the DSSCs based on **WS1** with the furan unit and **WS2** with the thiophene unit showed higher overall conversion efficiencies in comparison with the reference dye (**POX**) without the bridge unit. The most effective bridge unit was furan, which had a higher recombination resistance and  $V_{oc}$  value. **WS3** with the ethoxy phenyl ring as an additional donor showed more red-shift in the absorption, whereas the planarity of the dye was reduced by the large dihedral angle between the ethoxy phenyl ring and the POZ core. This non-planar structure of the dye led to less adsorption of the dye on the  $TiO_2$  surface, which limited the  $J_{sc}$  enhancement. The DSSC based on **WS1** with the furan bridge unit exhibited the highest overall conversion efficiency of 5.26% ( $J_{sc} = 11.72$  mA/cm<sup>2</sup>,  $V_{oc} = 653$  mV,  $FF = 68.76$ ).

#### 4.5 References

- [1] O'Regan B, Grätzel M. A low-cost, high-efficiency solar cell based on dye-sensitized colloidal  $TiO_2$  films. *Nature* 1991; 353: 737-40
- [2] (a) Grätzel M. Dye-sensitized solar cells. *Journal of Photochemistry and*

Photobiology C 2003; 4: 145-53

(b) Grätzel M. Conversion of sunlight to electric power by nanocrystalline dye-sensitized solar cells. *Journal of Photochemistry and Photobiology A* 2004; 164(3): 3-14

(c) Park N-G, Kim K. Transparent solar cells based on dye-sensitized nanocrystalline semiconductors. *Physica Status Solidi (a)* 2008; 205(8): 1895-904

[3] (a) Zeng WD, Cao Y, Bai Y, Wang Y, Shi Y, Zhang M, et al. Efficient dye-sensitized solar cells with an organic photosensitizer featuring orderly conjugated ethylenedioxythiophene and dithienosilole blocks. *Chemistry of materials* 2010; 22: 1915-25

(b) Hagberg DP, Yum J-H, Lee H, De Angelis F, Marinado T, Karlsson KM. Molecular engineering of organic sensitizers for dye-sensitized solar cell applications. *Journal of the American Chemical Society* 2008; 130: 6259-66

(c) Zhang G, Bala H, Cheng Y, Shi D, Lv X, Yu Q, et al. High efficiency and stable dye-sensitized solar cells with an organic chromophore featuring a binary  $\pi$ -conjugated spacer. *Chemical Communications* 2009; 16: 2198-200

(d) Ko S-B, Cho A-N, Kim M-J, Lee C-R, Park N-G. Alkyloxy substituted organic dyes for high voltage dye-sensitized solar cell: effect of alkyloxy chain length on open-circuit voltage. *Dyes and Pigments* 2012; 94: 88-98

[4] Ito S, Miura H, Uchida S, Takata M, Sumioka K, Liska P. High-conversion efficiency organic dye-sensitized solar cells with a novel indoline dye. *Chemical Communications* 2008; 41: 5194-6

[5] Chen Z, Li F, Huang C. Organic D- $\pi$ -A dyes for dye-sensitized solar cell. *Current Organic Chemistry* 2007; 11: 1241-58

[6] Wang Z-S, Cui Y, Dan-oh Y, Kasada C, Shinpo A, Hara K. Thiophene-functionalized coumarin dye for efficient dye-sensitized solar cells: electron lifetime improved by coadsorption of deoxycholic acid. *Journal of Physical Chemistry C* 2007; 111(19): 7224-30

[7] Li C, Yum J-H, Moon S-J, Herrmann A, Eickemeyer F, Pschirer NG, et al. An improved perylene sensitizer for solar cell applications. *Chemosuschem* 2008; 1(7): 615-8

[8] (a) Yella A, Lee H-W, Tsao HN, Yi C, Chandiran AK, Nazeeruddin MK, et al. Porphyrin-sensitized solar cells with cobalt (II/III)-Based redox electrolyte



exceed 12 percent efficiency. *Science* 2011; 334: 629-34

(b) Martínez-Díaz MV, de la Torre G, Torres T. Lighting porphyrins and phthalocyanines for molecular photovoltaics. *Chemical Communications* 2010; 46: 7090-108

(c) Walter MG, Rudine AB, Wamser CC. Porphyrins and phthalocyanines in solar photovoltaic cells. *Journal of Porphyrins and Phthalocyanines* 2010; 14: 759-92

(d) Bessho T, Zakeeruddin SM, Yeh C-Y, Diau EW-G, Grätzel M. Highly efficient mesoscopic dye-sensitized solar cells based on donor–acceptor-substituted porphyrins. *Angewante Chemie International Edition* 2010; 49: 6646-9

[9] Mori S, Nagata M, Nakahata Y, Yasuta K, Goto R, Kimura M, et al. Enhancement of incident photon-to-current conversion efficiency for phthalocyanine-sensitized solar cells by 3D molecular structuralization. *Journal of the American Chemical Society* 2010; 132: 4054-5

[10] (a) Tian H, Yang X, Chen R, Pan Y, Li L, Hagfeldt A, Sun L. Phenothiazine derivatives for efficient organic dye-sensitized solar cells. *Chemical*

Communications 2007; 3741-3

(b) Kim SH, Sakong C, Chang JB, Kim B, Ko MJ, Kim DH, Hong KS, Kim JP.

The effect of N-substitution and ethylthio substitution on the performance of phenothiazine donors in dye-sensitized solar cells. *Dyes and Pigments* 2013; 97: 262-71

(c) Kim SH, Kim HW, Sakong C, Namgoong JW, Park SW, Ko MJ, Lee CH,

Lee WI, Kim JP. Effect of five-membered heteroaromatic linkers to the performance of phenothiazine-based dye-sensitized solar cells. *Organic letters* 2011; 13: 5784-87

[11] (a) Eu S, Hayashi S, Umeyama T, Oguro A, Kawasaki M; Kadota N, Matano Y, Imahori H. Effects of 5-membered heteroaromatic spacers on structures of porphyrin films and photovoltaic properties of porphyrin-sensitized TiO<sub>2</sub> cells. *Journal of Physical Chemistry C* 2007; 111: 3528-37

(b) Lin JT, Chen P, Yen Y, Hsu Y, Chou H, Yeh MP. Organic dyes containing furan moiety for high-performance dye-sensitized solar cells. *Organic letters* 2009; 11: 97-100

[12] (a) Li G, Zhou YF, Cao XB, Bao P, Jiang KJ, Lin Y, Yang ML. Novel TPD-based organic D- $\pi$ -A dyes for dye-sensitized solar cells. *Chemical Communications* 2009; 16: 2201-3

- (b) Wu Y, Zhang X, Li W, Wang Z, Tian H, Zhu W. Hexylthiophene-featured D–A– $\pi$ –A structural indoline chromophores for coadsorbent-free and panchromatic dye-sensitized solar cells. *Advanced Energy Materials* 2012; 2: 149-56
- [13] (a) Tian H, Yang X, Cong J, Chen R, Liu J, Hao Y, Hagfeldt A, Sun L. Tuning of phenoxazine chromophores for efficient organic dye-sensitized solar cells. *Chemical Communications* 2009; 41: 6288-90
- (b) Tian H, Yang X, Chen R, Hagfeldt A, Sun L. A metal-free “black dye” for panchromatic dye-sensitized solar cells. *Energy & Environmental Science* 2009; 2: 674-77
- [14] Karlsson KM, Jiang X, Eriksson KS, Gabrielsson E, Rensmo H, Hagfeldt A, et al. Phenoxazine dyes for dye-sensitized solar cells: relationship between molecular structure and electron lifetime. *Chemistry-A European Journal* 2011; 17: 6415-24
- [15] (a) Hara K, Wang Z-S, Sato T, Furube A, Katoh R, Sugihara H, et al. Oligothiophene-containing coumarin dyes for efficient dye-sensitized solar cells. *Journal of Physical Chemistry B* 2005; 109: 15476-82
- (b) Mikroyannidis JA, Kabanakis A, Balraju P, Sharma GD. Novel broadly absorbing sensitizers with cyanovinylene 4-nitrophenyl segments and various

anchoring groups: synthesis and application for high-efficiency dye-sensitized solar cells. *Journal of Physical Chemistry C* 2010; 114: 12355-63

[16] (a) Lin L-Y, Tsai C-H, Wong K-T, Huang T-w, Hsieh L, Liu S-h, et al. Organic dyes containing coplanar diphenyl-substituted dithienosilole core for efficient dye-sensitized solar cells. *Journal of Organic Chemistry* 2010; 75: 4778-85

(b) Chen R, Yang X, Tian H, Sun L. Tetrahydroquinoline dyes with different spacers for organic dye-sensitized solar cells. *Journal of Photochemistry and Photobiology A* 2007; 189: 295-300

[17] Hagfeldt A, Grätzel M. Light-induced redox reactions in nanocrystalline systems. *Chemical Reviews* 1995; 95(1): 49-68

[18] Sakong C, Kim SH, Yuk SB, Namgoong JW, Park SW, Ko MJ, Kim DH, Hong KS, Kim JP. Influence of solvent and bridge structure in alkylthio-substituted triphenylamine dyes on the photovoltaic properties of dye-sensitized solar cells. 2012; 7: 1817-26

[19] Sakong C, Kim HJ, Kim SH, Namgoong JW, Park JH, Ryu J, Kim B, Ko MJ, Kim JP. Synthesis and applications of new triphenylamine dyes with donor-donor-(bridge)-acceptor structure for organic dye-sensitized solar cells. *New Journal of Chemistry* 2012; 36: 2025-32

- [20] (a) Wang Q, Moser J-E, Grätzel M. Electrochemical impedance spectroscopic analysis of dye-sensitized solar cells. *Journal of Physical Chemistry B* 2005; 109: 14945-53
- (b) Bisquert J. Chemical capacitance of nanostructured semiconductors: its origin and significance for nanocomposite solar cells. *Physical Chemistry Chemical Physics* 2003; 5: 5360-4
- [21] (a) Kern R, Sastrawan R, Ferber L, Stangl R, Luther J. Modeling and interpretation of electrical impedance spectra of dye solar cells operated under open-circuit conditions. *Electrochimica Acta* 2002; 47: 4213-25
- (b) Kuang D, Ito S, Wenger B, Klein C, Moser JE, Humpry-Baker R, Zakeeruddin SM, Grätzel M. High molar extinction coefficient heteroleptic ruthenium complexes for thin film dye-sensitized solar cells. *Journal of the American Chemical Society* 2006; 128: 4146-54
- [22] Kuang D, Uchida S, Humpry-Baker R, Zakeeruddin SM, Grätzel M. Organic dye-sensitized ionic liquid based solar cells: remarkable enhancement in performance through molecular design of indoline sensitizers. *Angewante Chemie International Edition* 2008; 47: 1923-7

## **Chapter 5**

### **The effects of the number of anchoring groups and *N*-substitution on the performance of phenoxazine dyes in dye-sensitized solar cells**

#### **5.1 Introduction**

The demand for environmentally friendly energy sources continues to increase due to depletion of traditional energy sources and due to environmental consideration. One of the attractive candidates of these new energy sources is solar energy, which is clean, renewable and limitless. Dye-sensitized solar cells (DSSCs) have been considered as one of the promising energy harvesting devices since the report of Ru-based photosensitizers in 1991 by Grätzel et al [1]. The Ru complex sensitizers (N3, N719 and black dye) have shown high photoelectric conversion efficiencies of over 11% under AM 1.5 conditions [2]. Compared with them, metal-free organic dyes and organometallic dyes have advantages including lower cost, easier modification and purification, environmental friendliness and high molar extinction coefficient. The highest conversion efficiencies of organic dyes (10% [3]) and organometallic dyes

(12.3% [4]) demonstrated that non-Ru dyes could be promising sensitizers for realizing highly efficient DSSCs. For these reasons, sensitizers containing coumarin [5], carbazole [6], fluorene [7], hemicyanine [8], indoline [9], merocyanine [10], perylene [11], polyene [12], porphyrin [4,13], phthalocyanine [14], triphenylamine [3,15] have been extensively studied.

Phenoxazine (POZ)-based sensitizers have exhibited higher conversion efficiencies than triphenylamine (TPA) and phenothiazine (PTZ)-based sensitizers, which are structurally similar [16,17,18]. This is because POZ-based sensitizers, with electron-rich nitrogen and oxygen heteroatoms, have stronger electron-donating ability than TPA and PTZ-based sensitizers. POZ-based sensitizers also show sufficient electrochemical properties for use in DSSCs [19]. However, despite their potential for application to DSSCs, POZ-based sensitizers have not been studied extensively.

We report the introduction of an additional cyanoacrylic acid moiety in the 7-position of the POZ chromophore as the second anchoring group. Compared to mono-anchoring sensitizers, this di-anchoring sensitizer has increased electron pathways and extended conjugations of the POZ moiety. Therefore, the short-circuit current ( $J_{sc}$ ) can be improved by the bathochromic shift of the absorption spectrum. However, the di-anchoring dyes have exhibited lower open-circuit

voltages ( $V_{oc}$ ) compared to the mono-anchoring dyes. Therefore, to improve  $V_{oc}$  of cells based on di-anchoring dyes, a bulky methoxyphenyl ring was introduced to the POZ nitrogen atom. The steric hinderance by these bulky groups was expected to reduce dye aggregation and suppress the electron recombination between the electrons injected on the  $TiO_2$  and the holes in the electrolyte to result in high  $V_{oc}$ .

Four POZ derivatives were designed and synthesized, *i.e.*, **POX**, **WB**, **WH1** and **WH2** as shown in Fig. 5.1. To examine the effects of the additional anchoring group and the *N*-substituents on the performance of DSSCs, photophysical and electrochemical properties of the dyes and photovoltaic performance of the cells based on these dyes were analyzed. In addition, electrochemical impedance spectroscopy (EIS) was used to investigate interfacial charge transport process. Density functional theory (DFT) calculations were also performed for further analysis of the results.



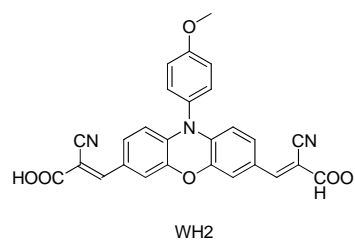
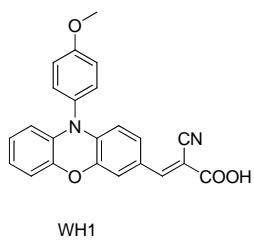
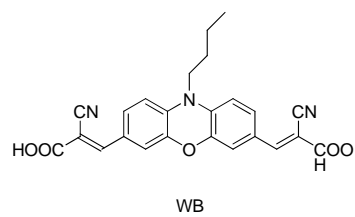
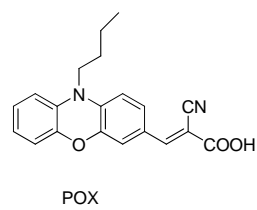


Fig. 5.1. Structure of **POX**, **WB**, **WH1** and **WH2**.

## 5.2 Experimental

### *5.2.1 Materials and reagents*

Phenoxazine, 1-bromobutane, 4-iodoanisole, copper-tin alloy, 18-crown-6, phosphorus oxychloride, cyanoacetic acid and piperidine were purchased from Sigma-Aldrich and used as received without further purification. All solvents (dimethylformamide, 1,2-dichlorobenzene, dimethyl sulfoxide, dichloromethane, 1,2-dichloroethane and acetonitrile) were obtained from Sigma-Aldrich and used as received. Other chemicals were reagent grade and used without further purification.

### *5.2.2 Analytical instruments and measurements*

$^1\text{H}$  NMR and  $^{13}\text{C}$  NMR spectra were recorded on a Bruker Advance 500 and 600MHz (Seoul National University National Center for inter-University Research Facilities) with the chemical shift against TMS. Mass data were measured with a JEOL JMS 600W mass spectrometer (Seoul National University National Center for inter-University Research Facilities). ATR-FTIR

spectra were recorded on a Nicolet 6700 spectrometer by using the window ZnSe/diamond ATR accessory. UV-vis spectra and photoluminescence spectra were recorded on a Hewlett-Packard 8425A spectrophotometer and a Shimadzu RF-5301PC spectrofluorometer, respectively. Cyclic voltammetry spectra were obtained using a three-electrode cell with a 273A potentiostat (Princeton applied research, Inc.). Measurements were taken using a Ag wire ( $\text{Ag}/\text{Ag}^+$ ), a glassy carbon and a platinum wire as the reference, working and counter electrodes, respectively, in the DMF solution containing 0.1M tetrabutylammonium tetrafluoroborate (TBATFB) as the supporting electrolyte. A standard ferrocene/ferrocenium ( $\text{Fc}/\text{Fc}^+$ ) redox couple was used to calibrate the oxidation peak. Photocurrent-voltage measurements were performed using a Keithly model 2400 source measure unit. Incident photon-to-current conversion efficiency (IPCE) was measured as a function of wavelength from 300nm to 1000nm using a specially designed IPCE system for dye-sensitized solar cells (PV measurements, Inc.). Electrical impedance spectra (EIS) of DSSCs under dark with 0.55 V forward bias and under illumination at an open-circuit voltage were measured with an impedance analyzer (Compactstat, IVIUM Tech) at frequencies of  $10^{-1} - 10^6$  Hz. The magnitude of the alternative signal was 10

mV. Impedance parameters were determined by fitting the impedance spectra using the Z-view software.

### 5.2.3 Fabrication of dye-sensitized solar cells and measurements

The nanocrystalline TiO<sub>2</sub> working electrode was comprised of a TiO<sub>2</sub> transparent layer (20 nm, synthesized) and a TiO<sub>2</sub> scattering layer (250 nm, G1). The Pt-coated counter electrode was prepared by a reported procedure [20]. TiO<sub>2</sub> electrodes were immersed in THF solution containing the dyes at 0.5 mM for 40 h at ambient temperature. They were then washed with ethanol and dried under a stream of nitrogen. The working and counter electrodes were sealed with Surlyn (60µm, Dupont) and electrolyte was injected through a hole in the counter electrode. The electrolyte was comprised of 0.7 M 1-propyl-3-methylimidazolium iodide (PMII, synthesized), 0.2 M LiI (Aldrich), 0.05 M I<sub>2</sub> (Aldrich), and 0.5 M 4-*tert*-butylpyridine (Aldrich) in a mixed solvent of acetonitrile and valeronitrile (v/v, 85/18). The active area of the dye-coated TiO<sub>2</sub> film was *ca.* 0.24 cm<sup>2</sup>, measured by analyzing the images from a CCD camera (moticam 1000). TiO<sub>2</sub> film thickness was measured by an  $\alpha$ -step surface profiler (KLA tencor).

Photocurrent–voltage (I–V) measurements were performed using a Keithley model 2400 source measure unit. A class-A solar simulator (Newport) equipped with a 150 W Xe lamp was used as the light source. Light intensity was adjusted with an NREL-calibrated Si solar cell with KG-5 filter for approximating 1 sunlight intensity. Photocurrent–voltage measurements of the dye-sensitized solar cells were performed with an aperture mask following a reported method. Incident photon-to-current conversion efficiency (IPCE) was measured as a function of wavelength from 300 to 1000 nm using a specially designed IPCE system for dye-sensitized solar cells (PV measurements, Inc.). A 75 W xenon lamp was used as the light source for generating monochromatic beams. Calibration was performed using a silicon photodiode, which was calibrated based on the NIST-calibrated photodiode G425 standard. IPCE values were measured under halogen bias light at a low chopping speed of 10 Hz. All calculations were carried out using the Gaussian 09 software. Optimized geometries, energy levels, and frontier molecular orbitals of the dyes' HOMOs and LUMOs were calculated at the B3LYP/6-31G (d,p) level.

#### 5.2.4 Synthesis of dyes

##### 5.2.4.1 10-Butyl-10H-phenoxazine (**1**)

To a phenoxazine (1.5g, 0.0082mol) solution in dry DMSO (22.5mL), sodium hydroxide (2.76g, 0.069mol) and 1-bromobutane (1.89g, 0.0137mol) were slowly added at room temperature and stirred for 24h. Then the reaction mixture was poured into water and extracted with ethyl acetate. The organic phase was separated and dried over anhydrous MgSO<sub>4</sub>. After removing the solvent, the residue was purified by column chromatography using ethyl acetate-hexane (1:10; v/v) as the eluent to give **1**, colorless viscous liquid (1.8g, 92%). <sup>1</sup>H NMR (500MHz, d<sub>6</sub>-DMSO) : δ = 6.81 (d, J = 8.7Hz, 2H), 6.63-6.67 (m, 4H), 3.53 (t, J = 7.7 Hz, 2H), 1.50-1.54 (m, 2H), 1.38-1.43 (m, 2H), 0.94 ppm (t, J = 7.3 Hz, 3H).

##### 5.2.4.2 10-(4-Methoxyphenyl)-10H-phenoxazine (**2**)

Under nitrogen atmosphere, phenoxazine (1.5g, 0.0082mol), 4-iodoanisole (2.88g, 0.0123mol), CuSn (1.49g, 0.0082mol), K<sub>2</sub>CO<sub>3</sub> (3.4g, 0.0246mol) and 18-crown-6 (0.38g, 0.00145mol) were dissolved in dry 1,2-dichlorobenzene (60mL). The mixture was heated under refluxed for 48h under nitrogen

atmosphere. Then the reaction mixture was filtered and washed with dichloromethane (DCM). The filtrate was extracted with DCM, water and NH<sub>4</sub>OH. The organic phase was collected and dried over anhydrous MgSO<sub>4</sub>. After removing solvent, the residue was purified by column chromatography using DCM-hexane (1:3; v/v) to give **2**, viscous pale yellow liquid (1.42g, 81.6%).

<sup>1</sup>H NMR (300MHz, d<sub>6</sub>-DMSO) : δ = 7.30 (d, J = 8.6 Hz, 2H), 7.18 (d, J = 8.6 Hz, 2H), 6.62-6.72 (m, 6H), 5.85 (d, J = 9.2 Hz, 2H), 3.83 ppm (s, 3H).

#### 5.2.4.3 10-Butyl-10H-phenoxazine-3-carbaldehyde (**3**)

To a solution of **1** (2.57g, 0.01mol) and dry DMF (5mL) in dry 1,2-dichloroethane (21.4mL) in an ice water bath, POCl<sub>3</sub> (1.1mL, 0.012mol) was added dropwise below 15 °C. The reaction was heated to room temperature and heated under refluxed at 90 °C for 48h. The mixture was quenched with dilute NaOH (aq) and extracted with water and DCM. The organic phase was dried with anhydrous MgSO<sub>4</sub> and then the solvent was removed in vacuo. The residue was purified by column chromatography using ethyl acetate-hexane (1:6; v/v) to give **3**, yellow oil (1.91g, 71.6%).

<sup>1</sup>H NMR (500MHz, d<sub>6</sub>-DMSO) : δ = 9.64 (s, 1H), 7.41 (dd, J = 8.3, 1.8 Hz, 1H), 7.00 (s, 1H), 6.68-6.87 (m, 5H), 3.62 (t, J = 7.9 Hz, 2H), 1.52-1.56 (m, 2H), 1.40-1.45 (m, 2H), 0.95 ppm (t, J = 7.3 Hz, 3H).

#### 5.2.4.4 10-Butyl-10H-phenoxazine-3,7-dicarbaldehyde (**4**)

**4** as an orange solid (1.46g, 49.5%) was synthesized according to the procedure described above for the synthesis of **3**. To a solution of **1** (2.57g, 0.01mol) and dry DMF (5mL) in dry 1,2-dichloroethane (21.4mL) in an ice water bath, POCl<sub>3</sub> (9.17mL, 0.1mol) was added dropwise below 15 °C. Eluent : DCM- methanol (7:1; v/v).

<sup>1</sup>H NMR (500MHz, d<sub>6</sub>-DMSO) : δ = 9.68 (s, 2H), 7.44 (dd, J = 8.3, 1.8 Hz, 2H), 7.05 (s, 2H), 6.94 (d, J = 8.4 Hz, 2H), , 3.68 (t, J = 7.7 Hz, 2H), 1.52-1.57 (m, 2H), 1.41-1.45 (m, 2H), 0.95 ppm (t, J = 7.3 Hz, 3H).

#### 5.2.4.5 10-(4-Methoxyphenyl)-10H-phenoxazine-3-carbaldehyde (**5**)

**5** as a yellow solid (0.41g, 76.2%) was synthesized according to the procedure described above for the synthesis of **3**. To a solution of **2** (0.48g, 0.0017mol) and dry DMF (0.39mL) in dry 1,2-dichloroethane (21.4mL) in an ice water bath, POCl<sub>3</sub> (1.1mL, 0.012mol) was added dropwise below 15 °C. Eluent : DCM.



$^1\text{H}$  NMR (500MHz,  $\text{d}_6$ -DMSO) :  $\delta$  = 9.62 (s, 1H), 7.36 (d, J = 9 Hz, 2H), 7.21-7.25 (m, 3H), 7.09 (s, 1H), 6.67-6.77(m, 3H), 5.96 (d, J = 8.5 Hz, 1H), 5.89 (d, J = 8 Hz, 1H), 3.85 ppm (s, 3H).

#### 5.2.4.6 10-(4-Methoxyphenyl)-10H-phenoxazine-3,7- dicarbaldehyde (**6**)

**6** as an orange solid (0.27g, 46%) was synthesized according to the procedure described above for the synthesis of **3**. To a solution of **2** (0.48g, 0.0017mol) and dry DMF (1.4mL) in dry 1,2-dichloroethane (10mL) in an ice water bath,  $\text{POCl}_3$  (9.17mL, 0.1mol) was added dropwise below  $15^\circ\text{C}$ . Eluent : DCM.

$^1\text{H}$  NMR (500MHz,  $\text{d}_6$ -DMSO) :  $\delta$  = 9.67 (s, 2H), 7.42 (d, J = 8.5 Hz, 2H), 7.29 (dd, J = 8.5, 1.5 Hz, 2H), 7.24 (d, J = 7 Hz, 2H), 7.16 (s, 2H), 6.02 (d, J = 8 Hz, 2H), 3,86 ppm (s, 3H).

#### 5.2.4.7 (E)-(10-Butyl-10H-phenoxazin-3-yl)-2-cyanoacrylic acid (**POX**)

**3** (0.46g, 0.00173mol), cyanoacetic acid (0.44g, 0.0052mol) and piperidine (0.35mL, 0.00693mol) were added to anhydrous  $\text{CH}_3\text{CN}$  (100mL). After the mixture was refluxed for 8h, the solution was extracted with DCM and 0.1M HCl aqueous solution. The organic phase was dried over anhydrous  $\text{MgSO}_4$  and the solvent was removed in vacuo. The crude product was purified by column

chromatography using DCM- methanol (5:1; v/v) to give **POX**, red solid (0.43g, 75%). mp 232-233 °C .

<sup>1</sup>H NMR (600MHz, d<sub>6</sub>-DMSO) : δ = 7.97 (s, 1H), 7.48 (d, J = 8.5 Hz, 1H), 7.36 (s, 1H), 6.85 (t, J = 7.6 Hz, 1H), 6.69-6.78 (m, 4H), 3.59 (t, J = 7.6 Hz, 2H), 1.50-1.55 (m, 2H), 1.37-1.43 (m, 2H), 0.93 ppm (t, J = 7.3 Hz, 3H) ;

<sup>13</sup>C NMR ( 150MHz, d<sub>6</sub>-DMSO) : δ = 164.1, 152.2, 143.8, 143.6, 137.8, 130.9, 130.6, 124.3, 123.7, 122.6, 117.2, 115.3, 114.5, 112.9, 111.7, 98.0, 42.9, 26.7, 19.2, 13.7 ppm ;

m/z (FAB) 334.1316 ((M<sup>+</sup>), C<sub>20</sub>H<sub>18</sub>N<sub>2</sub>O<sub>3</sub> requires 334.1317).

ATR-FTIR (cm<sup>-1</sup>): 2221 (cyano, C≡N stretching band), 1686 (carbonyl, C=O stretching band).

#### 5.2.4.8 3,3'- (10-Butyl-10H-phenoxazin-3,6-diyl) bis[2-cyanoacrylic acid] (**WB**)

**WB** as a dark red solid (0.56g, 57.3%) was synthesized according to the procedure described above for the synthesis of **POX. 4** (0.67g, 0.0023mol), cyanoacetic acid (1.04g, 0.0138mol) and piperidine (1.35mL, 0.021mol) were added to anhydrous CH<sub>3</sub>CN (75mL). Eluent : DCM- methanol (2:1; v/v). mp 279-280 °C .

$^1\text{H}$  NMR (600MHz,  $d_6$ -DMSO) :  $\delta$  = 7.97 (s, 2H), 7.48 (d, J = 8.4 Hz, 2H), 7.36 (s, 2H), 6.85 (t, J = 7.5 Hz, 2H), 6.69-6.78 (m, 8H), 3.59 (t, J = 7.6 Hz, 2H), 1.50-1.55 (m, 2H), 1.37-1.43 (m, 2H), 0.93 ppm (t, J = 7.3 Hz, 3H) ;

$^{13}\text{C}$  NMR (150MHz,  $d_6$ -DMSO) :  $\delta$  = 163.7, 152.0, 143.6, 135.6, 130.6, 129.4, 125.3, 116.8, 115.4, 112.9, 43.3, 26.8, 19.2, 13.7 ppm ;

m/z (FAB) 429.1325 ((M<sup>+</sup>), C<sub>24</sub>H<sub>19</sub>N<sub>3</sub>O<sub>5</sub> requires 429.1325).

ATR-FTIR (cm<sup>-1</sup>): 2220 (cyano, C≡N stretching band), 1680 (carbonyl, C=O stretching band).

#### 5.2.4.9 (*E*)-10-((4-Methoxyphenyl)-10H-phenoxazin-3-yl)-2-cyanoacetic acid (**WH1**)

**WH1** as a red solid (0.37g, 77%) was synthesized according to the procedure described above for the synthesis of **POX. 5** (0.4g, 0.00126mol), cyanoacetic acid (0.32g, 0.0038mol) and piperidine (0.43mL, 0.00504mol) were added to anhydrous CH<sub>3</sub>CN (100mL). Eluent : DCM- methanol (20:1; v/v). mp 266-267°C.

$^1\text{H}$  NMR (600MHz,  $d_6$ -DMSO) :  $\delta$  = 7.97 (s, 1H), 7.49 (s,1H), 7.36 (d, J = 8.6 Hz, 2H), 7.30 (d, J = 8.6 Hz, 1H), 7.20 (d, J = 8.6 Hz, 2H), 6.79 (d, J = 7.9 Hz,

1H), 6.74 (t, J = 7.5 Hz, 1H), 6.68 (t, J = 7.7 Hz, 1H), 5.89-5.91 (m, 2H), 3.84 ppm (s, 3H) ;

<sup>13</sup>C NMR (150MHz, d<sub>6</sub>-DMSO) : δ = 163.9, 159.4, 152.4, 143.1, 143.0, 138.9, 132.3, 131.0, 130.6, 129.0, 124.3, 123.9, 122.9, 116.9, 116.5, 115.4, 114.7, 113.9, 112.7, 98.2, 55.4 ppm ;

m/z (FAB) 384.1115 ((M<sup>+</sup>), C<sub>23</sub>H<sub>16</sub>N<sub>2</sub>O<sub>4</sub> requires 384.1110).

ATR-FTIR (cm<sup>-1</sup>): 2225 (cyano, C≡N stretching band), 1679 (carbonyl, C=O stretching band).

5.2.4.10 3,3'-10-((4-Methoxyphenyl)-10H-phenoxazin-3,6-diyl) bis[2-cyanoacrylic acid] (**WH2**)

**WH2** as a dark red solid (0.59g, 53.7%) was synthesized according to the procedure described above for the synthesis of **POX. 6** (0.79g, 0.0023mol), cyanoacetic acid (1.06g, 0.0138mol) and piperidine (1.58mL, 0.02mol) were added to anhydrous CH<sub>3</sub>CN (75mL). Eluent : DCM-methanol (2:1; v/v). mp 272-273 °C.

<sup>1</sup>H NMR (600MHz, d<sub>6</sub>-DMSO) : δ = 8.01 (s, 2H), 7.53 (s, 2H), 7.43 (d, J = 8.8 Hz, 2H), 7.38 (d, J = 8.6 Hz, 2H), 7.24 (d, J = 8.9 Hz, 2H), 6.0 (d, J = 8.5 Hz, 2H), 3.85 ppm (s, 3H).

$^{13}\text{C}$  NMR (150MHz,  $d_6$ -DMSO) :  $\delta$  = 163.5, 159.7, 151.8, 143.1, 137.1, 130.7, 129.6, 128.2, 125.8, 116.7, 115.4, 113.8, 55.5 ppm ;

m/z (FAB) 479.1120 ((M<sup>+</sup>), C<sub>27</sub>H<sub>17</sub>N<sub>3</sub>O<sub>6</sub> requires 479.1117).

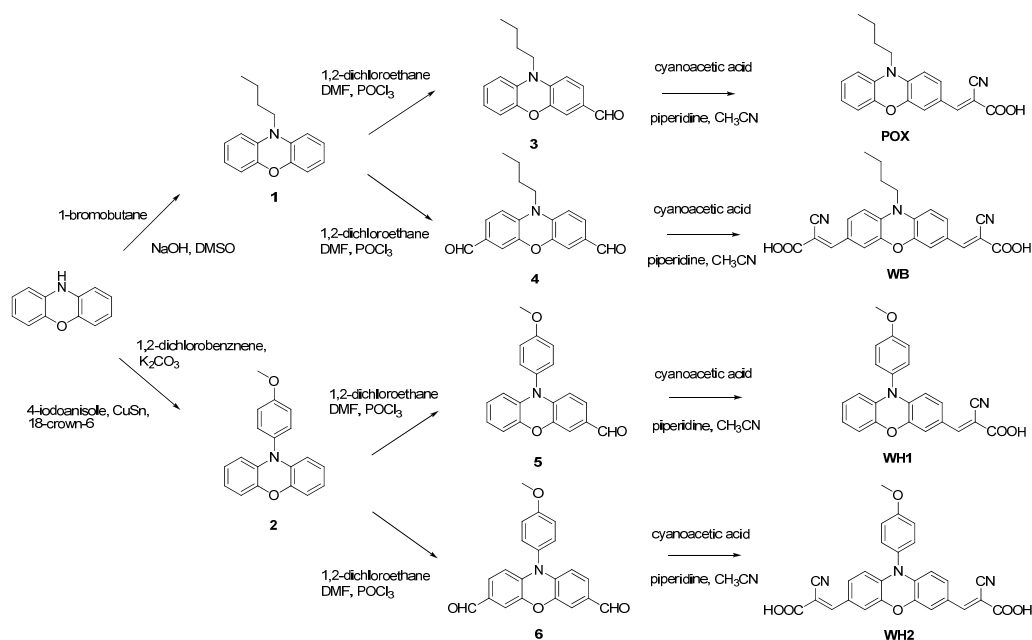
ATR-FTIR (cm<sup>-1</sup>): 2220 (cyano, C≡N stretching band), 1679 (carbonyl, C=O stretching band).

## 5.3 Results and Discussion

### 5.3.1. Synthesis of dyes

The detailed synthesis routes to the POZ type dyes are shown in Scheme 5.1. The POZ dyes were initially modified by *N*-alkylation or *N*-arylation of commercially available POZ. *N*-alkylation was performed in DMSO with 1-bromobutane and NaOH as the base, giving intermediate **1**. *N*-arylation was also performed by the Ullmann reaction, which produced the methoxyphenyl substituted phenoxazine, intermediate **2**. The intermediates **1** and **2** were subsequently formylated via the Vilsmeier-Haack reaction to synthesize intermediates **3-6**. During the formylation reactions, the number of introduced

aldehyde groups was controlled by varying the amount of  $\text{POCl}_3$ . Finally, the dyes (**POX**, **WB**, **WH1** and **WH2**) were synthesized by Knoevenagel condensations of the corresponding aldehydes on the intermediate moieties with cyanoacetic acid [21]. The structures of all the synthesized intermediates and dyes were confirmed by  $^1\text{H}$  NMR and the final products were additionally identified by  $^{13}\text{C}$  NMR and HRMS.



Scheme 5.1. Synthesis of **POX**, **WB**, **WH1** and **WH2**.

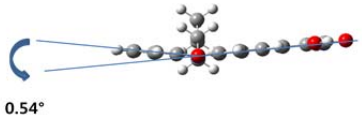
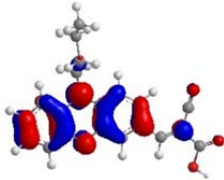
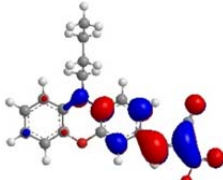
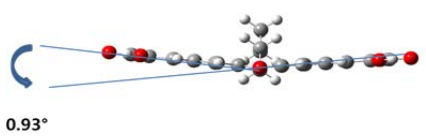
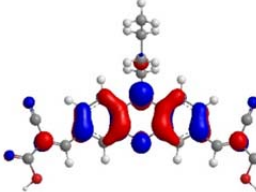
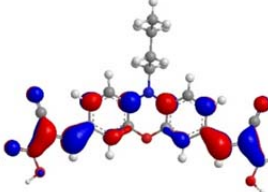
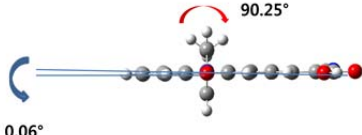
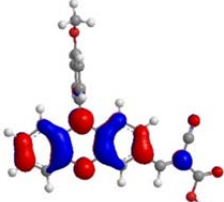
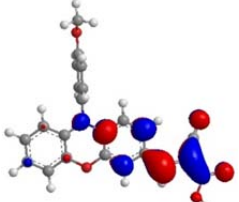
### 5.3.2. Density functional theory (DFT) calculations

To explain the structural properties of the dyes, their geometrically optimized structures were calculated using the density functional theory (DFT) at the B3LYP/6-31G(d,p) level. The optimized structures with torsion angle and electron density of the HOMOs and LUMOs of the dyes are shown in Table 5.1. In the optimized structures, the POZ moieties of all the dyes exhibited almost planar structures with small torsion angles (0.06-0.93°). These planar structures enhanced the aromatic character of the heterocyclic atom, increasing the degree of electronic resonance between donor and acceptor moieties in the dye molecules. On the other hand, the planar structure can increase the stacking of the dye molecules, inducing more dye aggregation. The methoxyphenyl substituent located on the POZ nitrogen atom made a large dihedral angle of about 90° with the POZ core. This large dihedral angle caused large steric hinderance that suppressed aggregations among dye molecules. However, this gave a small  $\pi$ -system overlap between the substituent and the POZ core, which limited the HOMO delocalization over the methoxy phenyl substituent. All of the electron distributions of the HOMO orbitals of the dyes were mostly localized over the POZ moiety, whereas those of the LUMO orbitals were

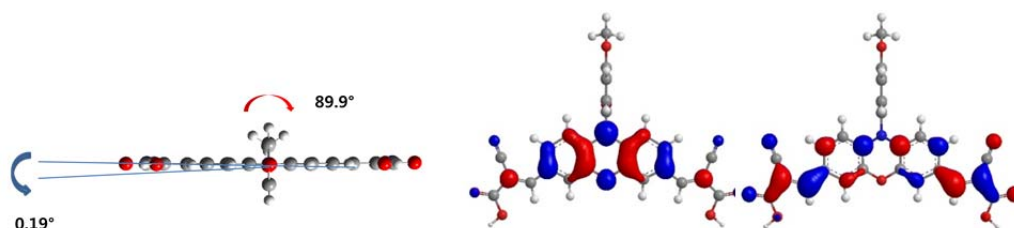
mainly localized in the cyanoacrylic acid and its adjacent phenyl ring. The results indicated that the HOMO-LUMO excitation induced by light irradiation can effectively move the electron distribution from the POZ moiety to the cyanoacrylic acid moiety. Photoinduced electrons can be efficiently transferred from the dye to the  $\text{TiO}_2$  surface by this electron separation.



Table 5.1. Optimized structures, dihedral angles and electronic distributions in HOMO and LUMO levels of the prepared dyes.

Dye	Optimized structure	HOMO	LUMO
<b>POX</b>	 <p>0.54°</p>		
<b>WB</b>	 <p>0.93°</p>		
<b>WH1</b>	 <p>0.06°</p> <p>90.25°</p>		

## WH2



### 5.3.3. Photophysical properties of the dyes in solution and on TiO<sub>2</sub> film

The absorption spectra of the four dyes in THF solution and on the TiO<sub>2</sub> surface are shown in Fig. 5.2 and the corresponding photophysical data are listed in Table 5.2. All the dyes exhibited two major absorption bands at around 310nm and 480nm, respectively. The former band at the shorter wavelength is due to the localized aromatic  $\pi$ - $\pi^*$  transition, and the latter band at the longer wavelength is attributed to the intramolecular charge-transfer (ICT) transition from the donor to the acceptor. The absorption maxima ( $\lambda_{\text{max}}$ ) of **POX**, **WB**, **WH1** and **WH2** are 464, 498, 458 and 498 nm, respectively. Di-anchoring dyes (**WB** and **WH2**) were red-shifted in their absorption spectra, compared to the corresponding mono-anchoring dyes (**POX** and **WH1**). This is due to the extension of electron delocalization over the whole molecule caused by the introduction of an additional anchoring moiety. **WH1** including the *N*-

methoxyphenyl ring showed a slight blue-shift in its absorption spectrum, compared to **POX** including the *N*-butyl chain. As shown in the calculation study, this is because the *N*-methoxyphenyl ring, which is perpendicular to the POZ plane, gave a poor orbital overlap, which led to inefficient conjugation [19]. The molar extinction coefficients at  $\lambda_{\text{max}}$  of **POX**, **WB**, **WH1** and **WH2** were 38957, 34229, 37224 and 47893  $\text{M}^{-1}\text{cm}^{-1}$ , respectively. These are higher than those of conventional TPA and PTZ dyes so the light harvesting of the dyes and photocurrent generation of the cells are increased. As shown in Fig. 5.2, di-anchoring dyes showed intermediate shoulders in their absorption spectra at around 400 nm. This might be attributed to the formation of localized electron transitions in the dye molecules induced by the additional anchoring group. This phenomenon is also shown in absorption spectra of the dyes on  $\text{TiO}_2$  surface.

The absorption spectra of the dyes absorbed on  $\text{TiO}_2$  films are blue-shifted compared to those of the dyes in solution. H-aggregation of the dyes or deprotonation of carboxylic acid upon adsorption onto the  $\text{TiO}_2$  surfaces has been suggested as the cause of a blue-shift of the spectrum [22]. The absorption maxima of the dyes on  $\text{TiO}_2$  were similarly ranked as those of the dyes in solution. The dyes with the *N*-methoxyphenyl ring showed lower absorbance

than the dyes with the *N*-butyl chain. This was ascribed to the lower adsorption of the dyes with the *N*-methoxyphenyl ring due to the large steric hinderance.

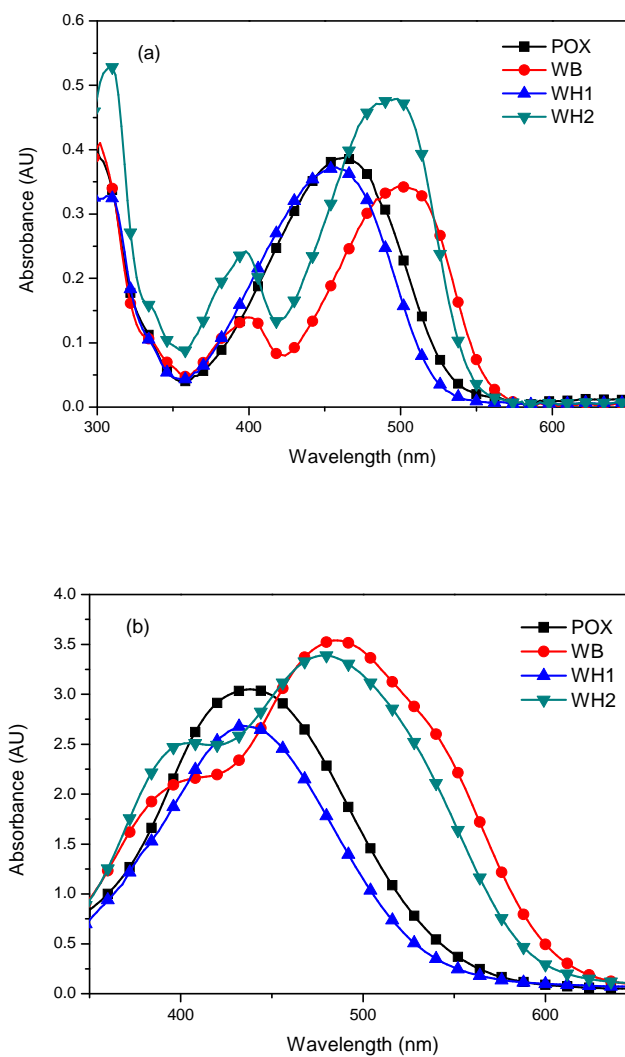


Fig. 5.2. Absorption spectra of **POX**, **WB**, **WH1** and **WH2** in (a) THF ( $10^{-5}$  molL<sup>-1</sup>) and (b) on TiO<sub>2</sub>.

Table 5.2. Photophysical and electrochemical properties of **POX**, **WB**, **WH1** and **WH2**.

Dye	Absorption <sup>a</sup>		Emission <sup>a</sup>		Oxidation potential data <sup>c</sup>		
	$\lambda_{\max}/\text{nm}$	$\epsilon/\text{M}^{-1}\text{cm}^{-1}$ (at $\lambda_{\max}$ )	$\lambda_{\text{abs}}^{\text{b}}/\text{nm}$ (on $\text{TiO}_2$ )	$\lambda_{\max}/\text{nm}$	$E_{\text{ox}}/\text{V}$ (vs. NHE)	$E_{0-0}^{\text{d}}/\text{V}$	$E_{\text{ox}} - E_{0-0}/\text{V}$ (vs. NHE)
<b>POX</b>	464	38957	444	558	1.01	2.38	-1.37
<b>WB</b>	498	34229	482	565	1.14	2.29	-1.15
<b>WH1</b>	458	37224	426	555	1.06	2.42	-1.36
<b>WH2</b>	498	47893	494	554	1.16	2.33	-1.17

<sup>a</sup> Measured in  $1 \times 10^{-5}$  THF solutions at room temperature.

<sup>b</sup> Measured on  $\text{TiO}_2$  film. <sup>c</sup> Measured in DMF containing 0.1 M tetrabutylammonium tetrafluoroborate. ( $\text{TBABF}_4$ ) electrolyte (working electrode: glassy carbon; counter electrode: Pt; reference electrode:  $\text{Ag}/\text{Ag}^+$ ; calibrated with ferrocene/ferrocenium ( $\text{Fc}/\text{Fc}^+$ ) as an internal reference and converted to NHE by addition of 630 mV [23]).

<sup>d</sup>  $E_{0-0}$  was determined from the intersections of absorption and emission spectra.

#### 5.3.4. Electrochemical properties

The electrochemical properties and energy levels of the synthesized dyes are provided in Table 5.2 and Fig. 5.3. The oxidation potentials of the dyes (Fig. 5.4) were measured by cyclic voltammetry (CV). The HOMO levels of the four dyes correspond to the first oxidation potential versus normal hydrogen

electrode (vs. NHE) calibrated by  $\text{Fc}/\text{Fc}^+$  (with 640 mV vs. NHE). All the HOMO levels of the dyes ranged from 1.01 eV to 1.16 eV (vs. NHE) and were much more positive than the redox potential of  $\text{I}/\text{I}_3^-$  (0.4 V vs. NHE) [24]. Therefore, the oxidized dyes were sufficiently regenerated by the redox electrolyte. Their LUMO levels, corresponding to excited state oxidation potentials, were calculated by  $E_{\text{ox}} - E_{0-0}$ , where  $E_{0-0}$  is the zeroth-zeroth energy of the dye estimated from the intersection between the normalized absorption and emission spectra (Fig. 5.5 and Fig. 5.6). The LUMO levels of the dyes ranged from -1.15 to -1.37 and were more negative than the conduction bands edge of  $\text{TiO}_2$  (-0.5 vs. NHE) [24], thus indicating that the excited electrons of the dyes can be efficiently injected into the conduction band of  $\text{TiO}_2$ .

The LUMO levels of the di-anchoring dyes were more positive than those of mono-anchoring dyes possibly due to the extension of conjugation induced by the additional anchoring group. Consequently, although the additional anchoring group made the HOMO level of the di-anchoring group slightly more positive, the HOMO-LUMO gap decreased and the absorption spectra were red-shifted.

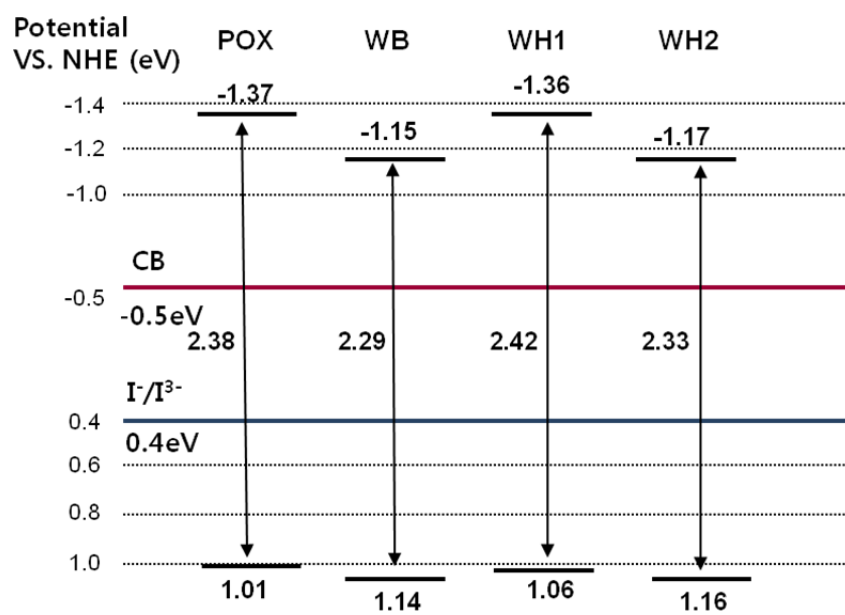


Fig. 5.3. Dyes' HOMO and LUMO energy levels.

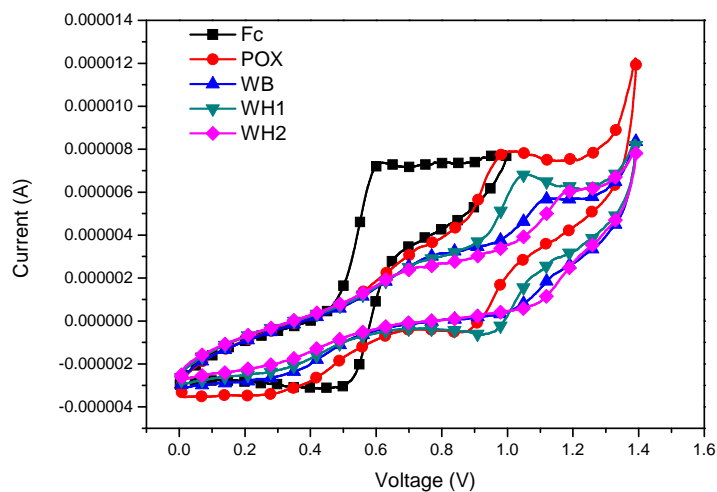


Fig.5.4. CV curves of  $\text{Fc}/\text{Fc}^+$ , **POX**, **WB**, **WH1** and **WH2** in DMF.

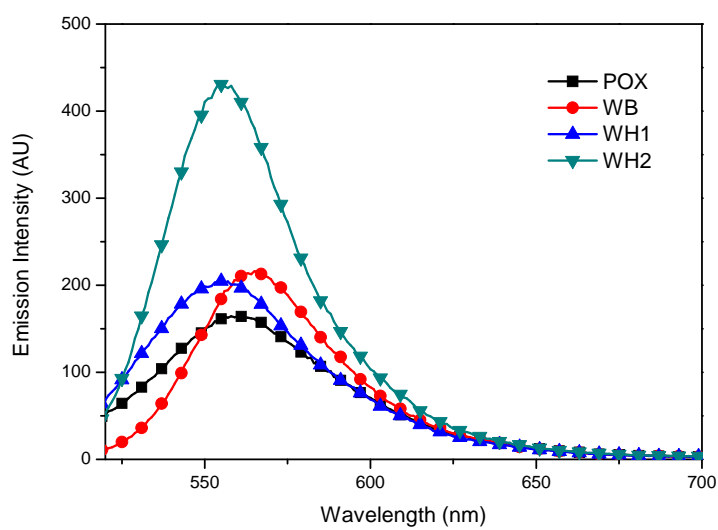


Fig. 5.5. Emission spectra of **POX**, **WB**, **WH1** and **WH2** in THF.



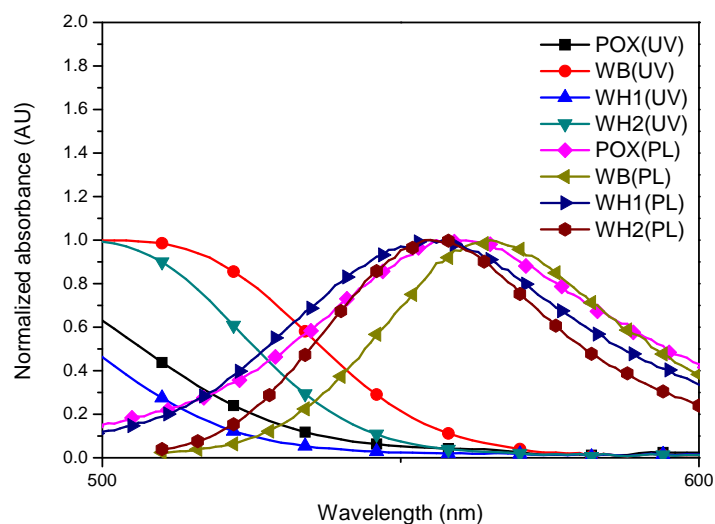


Fig. 5.6. Normalized absorption and emission spectra of **POX**, **WB**, **WH1** and **WH2** in THF.

### 5.3.5. Photovoltaic properties

DSSCs were fabricated using the synthesized dyes according to the methods described in the experimental section and their photovoltaic properties were measured under standard AM 1.5G irradiation conditions ( $100\text{mW cm}^{-2}$ ). The incident photon-to-current conversion (IPCE) spectra and photocurrent-voltage (J-V) curves are shown in Fig. 5.7 and corresponding data are listed in Table

5.3. The highest IPCE values of the cells with all dyes were over 79% in the absorption range ca. 400-600 nm. All the dyes could efficiently convert visible light to photocurrent in the spectral ranges. The  $J_{sc}$  values of the dyes were ranked **WH1** < **WH2** < **POX** < **WB** and this trend was in agreement with the broadness of IPCE spectrum. IPCE spectra of the cells with the di-anchoring dyes were broader than those with mono-anchoring dyes, promoting higher  $J_{sc}$  values. This result indicated that the di-anchoring dyes with broad and red-shifted spectra could inject more electrons effectively into the TiO<sub>2</sub> conduction band. On the other hand, the *N*-substituted methoxyphenyl ring decreased the donating ability of the dyes because it had a poor orbital overlap with the POZ moiety [19]. Therefore, the cells based on the dyes with the *N*-methoxyphenyl ring showed narrower IPCEs compared to those with the *N*-butyl chain, resulting in lower  $J_{sc}$  values. Photovoltaic properties of DSSCs were affected by the amount of the dye adsorbed onto the TiO<sub>2</sub> surface. As shown in Table 5.3, the dyes with the *N*-methoxyphenyl ring were less absorbed than those with the *N*-butyl chain because of their bulky structures. As a result, the cells with **WH1** and **WH2** showed narrower IPCE spectra and lower  $J_{sc}$  values than those with **POX** and **WB**, respectively.

$V_{oc}$  values increased in the order of **WB** < **WH2** < **POX** < **WH1**. The cells fabricated with the di-anchoring dyes showed lower  $V_{oc}$  values compared to those with the mono-anchoring dyes. The di-anchoring dyes transfer more protons to the  $TiO_2$  surface upon adsorption [25]. Thus, the high concentration of the protons changes the  $TiO_2$  surface to a more positive state, lowering the conduction band edges of  $TiO_2$  and lowering  $V_{oc}$  [26, 27]. To confirm the binding of the di-anchoring dyes, their FT-IR spectra on the  $TiO_2$  surface were measured (Fig. 5.8). The FT-IR spectra of the di-anchoring dyes showed that the broad band at  $1685\text{ cm}^{-1}$  assigned to the carboxylic groups of free dyes disappeared as the dyes were adsorbed on the  $TiO_2$ , indicating their double-anchoring behavior [28]. The DSSCs based on the dyes with the *N*-methoxyphenyl ring showed higher  $V_{oc}$  than those with the *N*-butyl chain. This was due to the bulky methoxyphenyl ring that suppressed dye aggregation and the recombination between the injected electrons on  $TiO_2$  and the electrolyte. Consequently **WH1**, the mono-anchoring dye with the *N*-methoxyphenyl ring, showed the highest  $V_{oc}$ , and **WB**, the di-anchoring dye with the *N*-butyl chain, showed the lowest  $V_{oc}$ . The dark currents of all DSSCs were also measured (Fig. 5.9); their trends were in good agreement with the  $V_{oc}$  ranks of the dyes. Dark current is defined as the relatively small electric current flowing out of a system

without illumination; a higher dark current is accountable for increased recombination and low  $V_{oc}$ . Thus, as shown in Fig. 5.9, the low dark current of the cell with **WH1** is consistent with the highest  $V_{oc}$ , whereas the high dark current of the cell with **WB** is consistent with the lowest  $V_{oc}$ .

All four dyes exhibited almost the same overall conversion efficiencies and the  $\eta$  values of **POX**, **WB**, **WH1** and **WH2** were 4.97%, 5.03%, 5.09% and 4.86%, respectively. This similarity is ascribed to the trade-off relationship between  $V_{oc}$  and  $J_{sc}$  for the cells based on the synthesized dyes. The best overall conversion efficiency was achieved by the cell fabricated with WH1 ( $\eta = 5.09\%$ ,  $J_{sc} = 10.11 \text{ mA/cm}^2$ ,  $V_{oc} = 690 \text{ mV}$ ,  $FF = 72.23\%$ ).

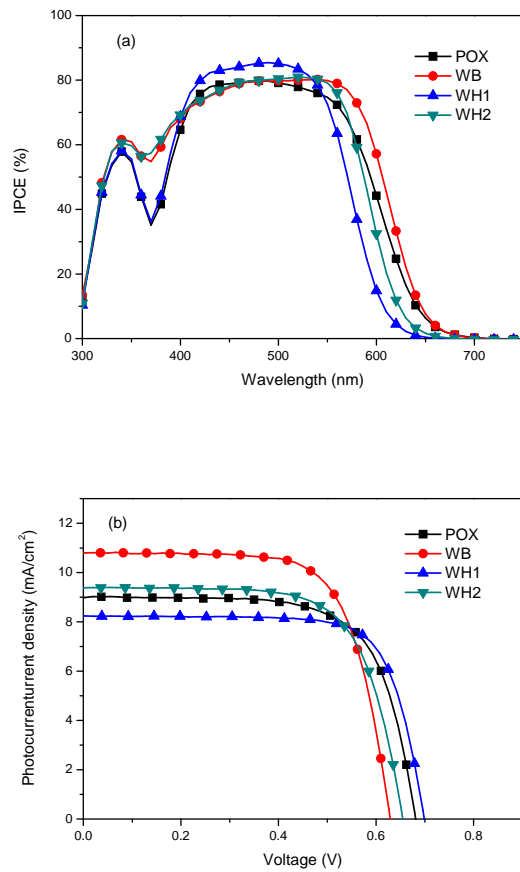


Fig. 5.7. (a) IPCE spectra DSSCs based on **POX**, **WB**, **WH1** and **WH2** and (b) the DSSCs'  $J-V$  curves under AM 1.5G simulated sunlight ( $100 \text{ mWcm}^{-2}$ ).

Table 5.3. DSSC performance parameters of **POX**, **WB**, **WH1**, and **WH2**.<sup>a</sup>

Dye <sup>b</sup>	J <sub>sc</sub> (mA/cm <sup>2</sup> )	V <sub>oc</sub> (V)	FF (%)	η (%)	Dye amount <sup>c</sup> (10 <sup>-7</sup> mol cm <sup>-2</sup> )
<b>POX</b>	11.19	0.68	64.97	4.97	1.4207
<b>WB</b>	11.79	0.65	65.10	5.02	1.8653
<b>WH1</b>	10.11	0.69	72.23	5.09	1.2744
<b>WH2</b>	10.75	0.66	67.5	4.86	1.2370
<b>N719</b>	14.89	0.78	63.18	7.69	-

<sup>a</sup> Measured under AM 1.5 irradiation G (100 mW cm<sup>-1</sup>); 0.236~0.3 cm<sup>2</sup> working area. <sup>b</sup> Dyes were maintained at 0.5 mM in THF solution, with 10 mM CDCA co-adsorbent. Electrolyte comprised 0.7 M 1-propyl-3-methyl-imidazolium iodide (PMII), 0.2 M LiI, 0.05 M I<sub>2</sub>, 0.5 M TBP in acetonitrile-valeronitrile (v/v, 85/15) for organic dyes. <sup>c</sup> Dyes' adsorption on TiO<sub>2</sub> were measured by a colorimetric method using 0.1 M NaOH aqueous-DMF (1:1) mixed solutions to wash the dyes from 8 μm thick TiO<sub>2</sub> film.

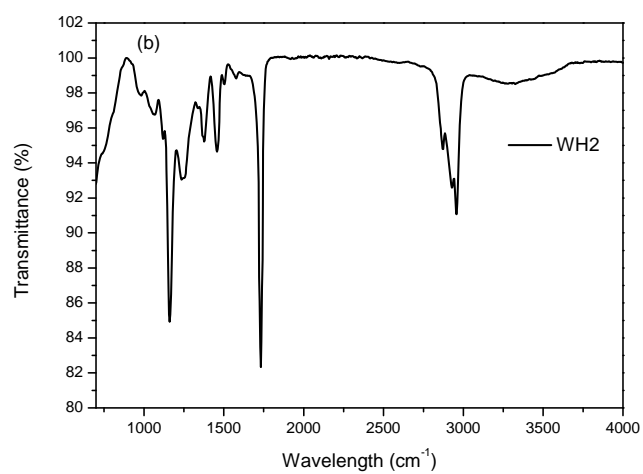
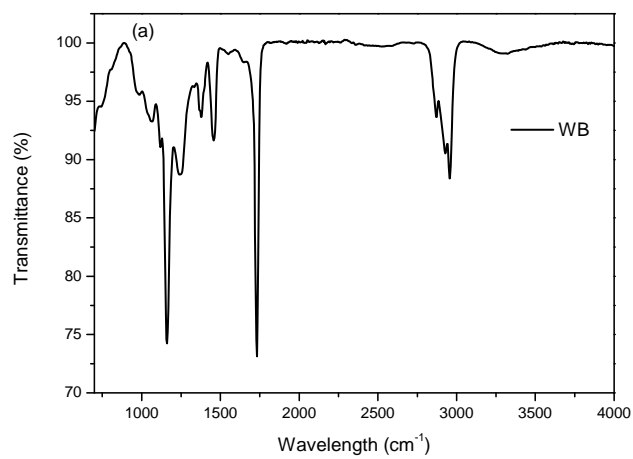


Fig. 5.8. FT-IR spectra of (a) **WB** absorbed on TiO<sub>2</sub> and (b) **WH2** absorbed on TiO<sub>2</sub>.

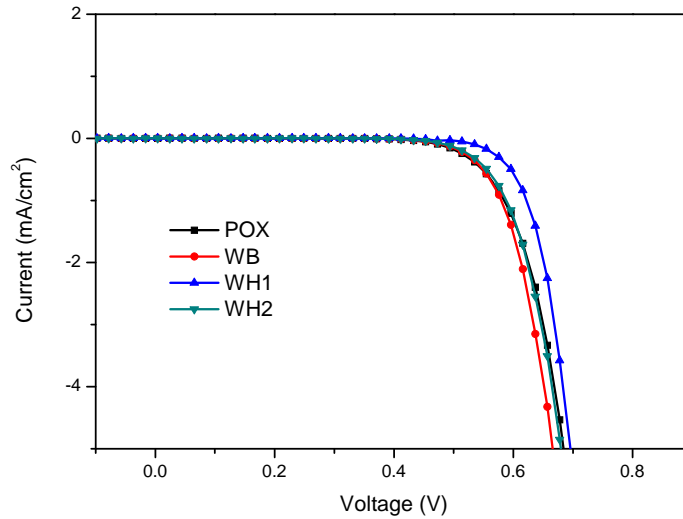


Fig. 5.9. DSSCs'  $J-V$  curves based on **POX**, **WB**, **WH1** and **WH2** in the dark.

### 5.3.6. Electrochemical impedance spectroscopy

To elucidate the correlation between the  $V_{oc}$  of the cell and the dye, electrochemical impedance spectroscopy (EIS) [29] was carried out in the dark and under illumination. A Nyquist plot in the dark under a forward bias of 0.55V with frequency range of 0.1Hz-100kHz and a Bode phase plot under AM 1.5GmWcm<sup>-2</sup> illumination are shown in Fig. 5.10.



The major semicircle in the Nyquist plot indicate charge recombination resistance at the  $\text{TiO}_2$  surface; a larger radius of the major semicircle means a larger charge recombination resistance [30]. The radius of the major semicircle in the Nyquist plot increased in the order of **WB** < **WH2** < **POX** < **WH1**, implying increasing resistance to charge recombination. This result coincides with the increase of  $V_{oc}$  in the DSSCs based on the dyes, as the suppression of electron recombination between the injected electrons and electrolyte improves  $V_{oc}$ . This trend is in agreement with results of the electron lifetime vs dark bias voltage (Fig. 5.11). Electron lifetime is calculated by multiplying the resistance by the chemical capacitance (Fig. 5.12 and Table 5.4). The chemical capacitances of the dyes were almost similar, so that electron lifetimes were mainly dependent on the resistances. Thus, longer electron lifetimes imply increased resistance between the injected electrons and the electrolyte, which consequently improves the  $V_{oc}$  [31].

A Bode phase plot is also related to the charge transfer resistance at the  $\text{TiO}_2$ /dye/electrolyte interface. The frequency of the characteristic peak in the Bode phase plot increased in the order of **WH1** < **POX** < **WH2** < **WB**. A lower characteristic frequency in the Bode phase plot means a slower charge recombination rate and higher  $V_{oc}$ . As the reciprocal of the characteristic

frequency is correlated with electron lifetime, electron lifetime increased in the order of **WB** < **WH2** < **POX** < **WH1** [32]. This sequence of the electron lifetime calculated from the Bode phase plot also indicated increasing resistance to recombination. These results suggest that the introduction of the methoxy phenyl ring improved  $V_{oc}$ , whereas the introduction of the additional anchoring group decreased  $V_{oc}$ .

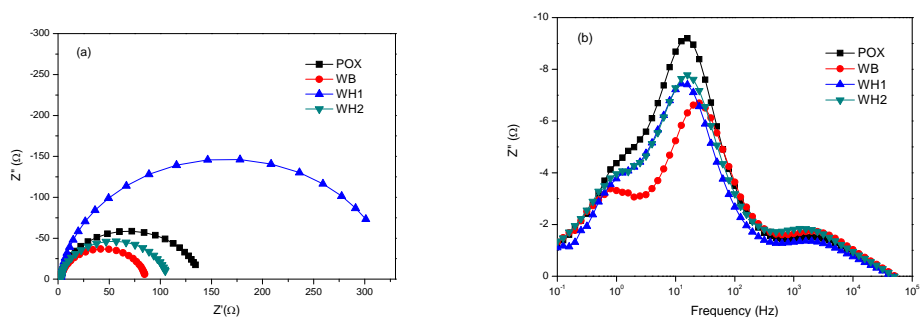


Fig. 5.10. Impedance spectra of DSSCs based on **POX**, **WB**, **WH1**, and **WH2**.

(a) Nyquist plots measured at 0.55 V forward bias in the dark, (b) Bode phase plots measured under illuminations (AM 1.5G).

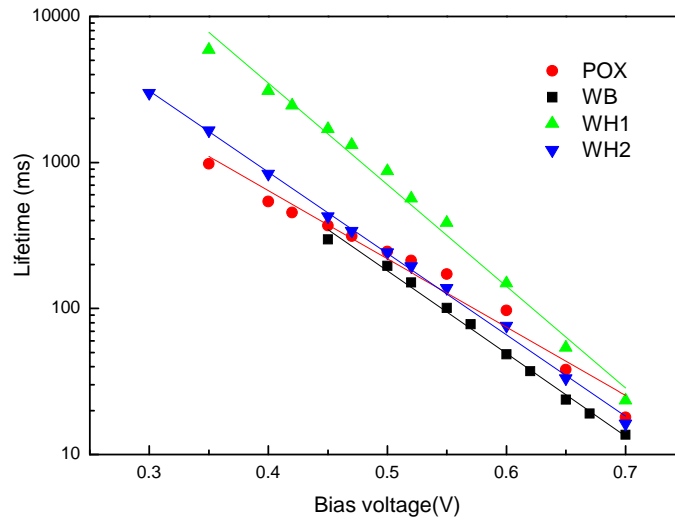


Fig. 5.11. Electron lifetime of **POX**, **WB**, **WH1**, and **WH2** as a function of bias voltage.

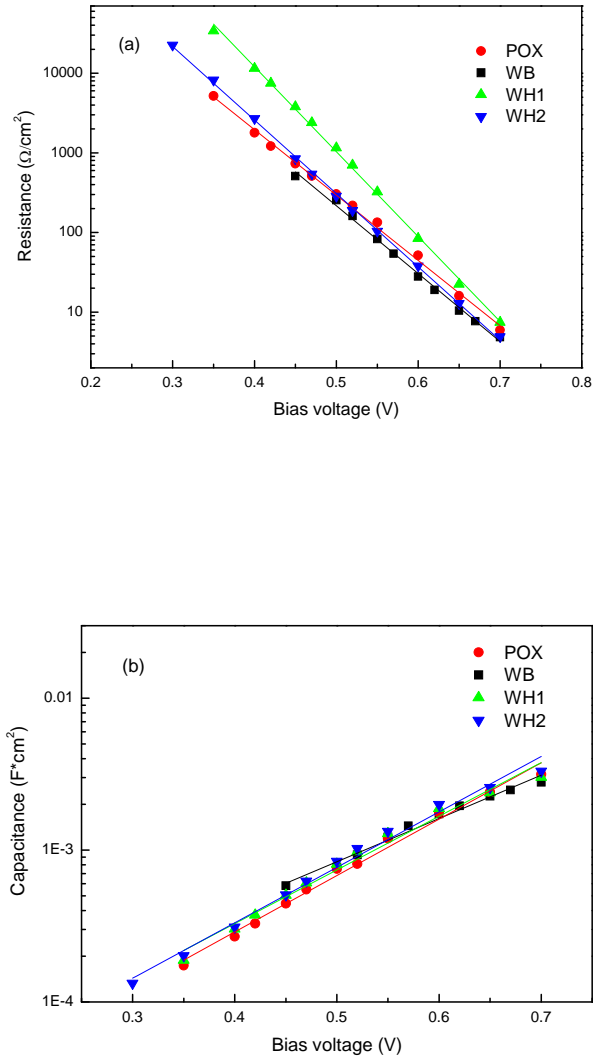


Fig. 5.12. (a) Resistance and (b) capacitance of **POX**, **WB**, **WH1** and **WH2** as a function of bias voltage.

Table 5.4. Lifetime calculations of **POX**, **WB**, **WH1** and **WH2**.

Device	Rs <sup>a</sup>	R2 <sup>a</sup>	C2 <sup>a</sup>	<b>R2*C2</b> <b>Life time</b> <b>(ms)</b>
<b>POX</b>	4.94	18.44	6.16*E <sup>-04</sup>	11.35
<b>WB</b>	4.99	13.26	5.22*E <sup>-04</sup>	6.92
<b>WH1</b>	4.58	15.07	8.42*E <sup>-04</sup>	12.68
<b>WH2</b>	4.98	15.29	6.93*E <sup>-04</sup>	10.60

<sup>a</sup>Rs, R2 (Rrec) and C2 are the ohmic serial resistance, charge transfer resistance at TiO<sub>2</sub>/dye/electrolyte interface and chemical capacitance, respectively.

## 5.4 Conclusion

Four new organic sensitizers with POZ dyes (**POX**, **WB**, **WH1** and **WH2**) were designed and synthesized to investigate the effects of an additional anchoring group and the *N*-substituent on the performance of DSSCs.

The introduction of the additional anchoring group extended the conjugation of the dyes, leading to the red-shifts of their absorption spectra. The di-anchoring dyes transferred more electrons to the TiO<sub>2</sub> electrode, increasing the  $J_{sc}$  value. The introduction of the methoxyphenyl ring located on the POZ nitrogen atom caused steric hinderance due to the large dihedral angle between the *N*-substituent and the POZ core. As a result, the electron recombination between the injected electron and the electrolyte was retarded, improving the  $V_{oc}$  value.

On the other hand, the di-anchoring dyes transferred more protons to the TiO<sub>2</sub> surface compared to the mono-anchoring dyes. This lowered the Fermi level of the TiO<sub>2</sub> and the  $V_{oc}$  of the cells. The adsorption of dyes with the *N*-methoxyphenyl ring was limited by their bulky structures. Therefore, the dyes

with the *N*-methoxyphenyl ring showed lower  $J_{sc}$  values compared to the dyes with the butyl chain.

Consequently, introduction of the additional anchoring group enhanced  $J_{sc}$ , but decreased  $V_{oc}$ . To improve the lowered  $V_{oc}$  caused by the di-anchoring system, a methoxyphenyl ring was introduced on the POZ core. The introduction of the 4-methoxyphenyl ring increased the  $V_{oc}$ , but decreased the  $J_{sc}$  simultaneously. Thus, with the increases and decreases of  $J_{sc}$  and  $V_{oc}$ , all DSSCs fabricated with the dyes showed similar overall conversion efficiencies, and the cells based on **WH1** showed the best overall conversion efficiency ( $\eta = 5.09\%$ ,  $J_{sc} = 10.11 \text{ mA/cm}^2$ ,  $V_{oc} = 690 \text{ mV}$ ,  $FF = 72.23\%$ ).

## 5.5 References

- [1] O'Regan B, Grätzel M. A low-cost, high-efficiency solar cell based on dye-sensitized colloidal TiO<sub>2</sub> films. *Nature* 1991; 353: 737-40
- [2] (a) Grätzel M. Dye-sensitized solar cells. *Journal of Photochemistry and Photobiology C* 2003; 4: 145-53
- (b) Grätzel M. Conversion of sunlight to electric power by nanocrystalline dye-

sensitized solar cells. *Journal of Photochemistry and Photobiology A* 2004; 164(3): 3-14

(c) Park N-G, Kim K. Transparent solar cells based on dye-sensitized nanocrystalline semiconductors. *Physica Status Solidi (a)* 2008; 205(8): 1895-904

[3] Zeng WD, Cao Y, Bai Y, Wang Y, Shi Y, Zhang M, et al. Efficient dye-sensitized solar cells with an organic photosensitizer featuring orderly conjugated ethylenedioxythiophene and dithienosilole blocks. *Chemistry of materials* 2010; 22: 1915-25

[4] Yella A, Lee H-W, Tsao HN, Yi C, Chandiran AK, Nazeeruddin MK, et al. Porphyrin-sensitized solar cells with cobalt (II/III)-Based redox electrolyte exceed 12 percent efficiency. *Science* 2011; 334: 629-34

[5] Wang Z-S, Cui Y, Dan-oh Y, Kasada C, Shinpo A, Hara K. Thiophene-functionalized coumarin dye for efficient dye-sensitized solar cells: electron lifetime improved by coadsorption of deoxycholic acid. *Journal of Physical Chemistry C* 2007; 111(19): 7224-30

[6] Koumura N, Wang Z-S, Miyashita M, Uemura Y, Sekiguchi H, Cui Y, et al. Substituted carbazole dyes for efficient molecular photovoltaics: long electron lifetime and high open circuit voltage performance. *Journal of Materials*



Chemistry 2009; 19: 4829-36

[7] Kim S, Lee JK, Kang SO, Ko J, Yum J-H, Fantacci S, et al. Molecular engineering of organic sensitizers for solar cell applications. *Journal of the American Chemical Society* 2006; 128(51): 16701-7

[8] Stathatos E, Lianos P, Laschewsky A, Ouari O, Van Cleuvenbergen P. Synthesis of a hemicyanine dye bearing two carboxylic groups and its use as a photosensitizer in dye-sensitized photoelectrochemical cells. *Chemistry of Materials* 2001; 13: 3888-92

[9] Ito S, Miura H, Uchida S, Takata M, Sumioka K, Liska P. High-conversion efficiency organic dye-sensitized solar cells with a novel indoline dye. *Chemical Communications* 2008; 41: 5194-6

[10] Tang J, Wu W-J, Hua JH, Li X, Tian H. Starburst triphenylamine-based cyanine dye for efficient quasi-solid-state dye-sensitized solar cells. *Energy & Environmental Science* 2009; 2: 982-90

[11] Li C, Yum J-H, Moon S-J, Herrmann A, Eickemeyer F, Pschirer NG, et al. An improved perylene sensitizer for solar cell applications. *ChemSuschem* 2008; 1(7): 615-8

[12] Hara K, Sato T, Katoh R, Furube A, Yoshihara T, Murai M, et al. Novel conjugated organic dyes for efficient dye-sensitized solar cells. *Advanced*

Functional Materials 2005; 15(2): 246-52

[13] (a) Martínez-Díaz MV, de la Torre G, Torres T. Lighting porphyrins and phthalocyanines for molecular photovoltaics. Chemical Communications 2010; 46: 7090-108

(b) Walter MG, Rudine AB, Wamser CC. Porphyrins and phthalocyanines in solar photovoltaic cells. Journal of Porphyrins and Phthalocyanines 2010; 14: 759-92

(c) Bessho T, Zakeeruddin SM, Yeh C-Y, Diau EW-G, Grätzel M. Highly efficient mesoscopic dye-sensitized solar cells based on donor-acceptor-substituted porphyrins. Angewante Chemie International Edition 2010; 49: 6646-9

[14] Mori S, Nagata M, Nakahata Y, Yasuta K, Goto R, Kimura M, et al. Enhancement of incident photon-to-current conversion efficiency for phthalocyanine-sensitized solar cells by 3D molecular structuralization. Journal of the American Chemical Society 2010; 132: 4054-5

[15] (a) Hagberg DP, Yum J-H, Lee H, De Angelis F, Marinado T, Karlsson KM. Molecular engineering of organic sensitizers for dye-sensitized solar cell applications. Journal of the American Chemical Society 2008; 130: 6259-66

(b) Zhang G, Bala H, Cheng Y, Shi D, Lv X, Yu Q, et al. High efficiency and

stable dye-sensitized solar cells with an organic chromophore featuring a binary  $\pi$ -conjugated spacer. *Chemical Communications* 2009; 16: 2198-200

(c) Ko S-B, Cho A-N, Kim M-J, Lee C-R, Park N-G. Alkyloxy substituted organic dyes for high voltage dye-sensitized solar cell: effect of alkyloxy chain length on open-circuit voltage. *Dyes and Pigments* 2012; 94: 88-98

[16] Tian H, Yang X, Cong J, Chen R, Liu J, Hao Y, Hagfeldt A, Sun L. Tuning of phenoxazine chromophores for efficient organic dye-sensitized solar cells. *Chemical Communications* 2009; 41: 6288-90

[17] Tian H, Yang X, Chen R, Pan Y, Li L, Hagfeldt A, Sun L. Phenothiazine derivatives for efficient organic dye-sensitized solar cells. *Chemical Communications* 2007: 3741-3

[18] Tian H, Yang X, Chen R, Hagfeldt A, Sun L. A metal-free "black dye" for panchromatic dye-sensitized solar cells. *Energy & Environmental Science* 2009; 2: 674-77

[19] Karlsson KM, Jiang X, Eriksson KS, Gabrielsson E, Rensmo H, Hagfeldt A, et al. Phenoxazine dyes for dye-sensitized solar cells: relationship between molecular structure and electron lifetime. *Chemistry-A European Journal* 2011; 17: 6415-24

[20] Park SW, Son K-I, Ko MJ, Kim K, Park NG. Effect of donor moiety in

organic sensitizer on spectral response, electrochemical and photovoltaic properties. *Synthetic Metals* 2009; 159: 2571-7

[21] (a) Hara K, Wang Z-S, Sato T, Furube A, Katoh R, Sugihara H, et al. Oligothiophene-containing coumarin dyes for efficient dye-sensitized solar cells. *Journal of Physical Chemistry B* 2005; 109: 15476-82

(b) Mikroyannidis JA, Kabanakis A, Balraju P, Sharma GD. Novel broadly absorbing sensitizers with cyanovinylene 4-nitrophenyl segments and various anchoring groups: synthesis and application for high-efficiency dye-sensitized solar cells. *Journal of Physical Chemistry C* 2010; 114: 12355-63

[22] (a) Lin L-Y, Tsai C-H, Wong K-T, Huang T-w, Hsieh L, Liu S-h, et al. Organic dyes containing coplanar diphenyl-substituted dithienosilole core for efficient dye-sensitized solar cells. *Journal of Organic Chemistry* 2010; 75: 4778-85

(b) Chen R, Yang X, Tian H, Sun L. Tetrahydroquinoline dyes with different spacers for organic dye-sensitized solar cells. *Journal of Photochemistry and Photobiology A* 2007; 189: 295-300

[23] Hagberg DP, Edvinsson T, Marinado T, Boschloo G, Hagfeldt A, Sun L. A novel organic chromophore for dye-sensitized nanostructured solar cells. *Chemical Communications* 2006: 2245-7

- [24] Hagfeldt A, Grätzel M. Light-induced redox reactions in nanocrystalline systems. *Chemical Reviews* 1995; 95(1): 49-68
- [25] Nazeeruddin MK, De Angelis F, Fantacci S, Selloni A, Viscardi G, Liska P, Ito S, Takeru B, Grätzel M. Combined experimental and DFT-TDDFT computational study of photoelectrochemical cell ruthenium sensitizers. *Journal of the American Chemical Society* 2005; 127: 16835-47
- [26] Yang YS, Kim HD, Ryu J-H, Kim KK, Park SS, Ahn K-S, Kim JH. Effects of anchoring groups in multi-anchoring organic dyes with thiophene bridge for dye-sensitized solar cells. *Synthetic Metals* 2011; 161: 850-55
- [27] Shang H, Luo Y, Guo X, Huang X, Zhan X, Jiang K, Meng Q. The effect of anchoring group number on the performance of dye-sensitized solar cells. *Dyes and Pigments* 2010; 87: 249-56
- [28] (a) Heredia D, Natera J, Gervaldo M, Otero L, Fungo F, Lin C-Y, Wong K-T. Spirobifluorene-bridged donor/acceptor dye for organic dye-sensitized solar cells. *Organic letters* 2010; 12: 12-15
- (b) Abotto A, Manfredi N, Marinzi C, De Angelis F, Mosconi E, Yum J-H, Xianxi Z, Nazeeruddin MK, Grätzel M. Di-branched di-anchoring organic dyes for dye-sensitized solar cells. *Energy & Environmental Science* 2009; 2: 1094-1101

- [29] (a) Wang Q, Moser J-E, Grätzel M. Electrochemical impedance spectroscopic analysis of dye-sensitized solar cells. *Journal of Physical Chemistry B* 2005; 109: 14945-53
- (b) Bisquert J. Chemical capacitance of nanostructured semiconductors: its origin and significance for nanocomposite solar cells. *Physical Chemistry Chemical Physics* 2003; 5: 5360-4
- [30] (a) Kern R, Sastrawan R, Ferber L, Stangl R, Luther J. Modeling and interpretation of electrical impedance spectra of dye solar cells operated under open-circuit conditions. *Electrochimica Acta* 2002; 47: 4213-25
- (b) Kuang D, Ito S, Wenger B, Klein C, Moser JE, Humpry-Baker R, Zakeeruddin SM, Grätzel M. High molar extinction coefficient heteroleptic ruthenium complexes for thin film dye-sensitized solar cells. *Journal of the American Chemical Society* 2006; 128: 4146-54
- [31] Kuang D, Uchida S, Humpry-Baker R, Zakeeruddin SM, Grätzel M. Organic dye-sensitized ionic liquid based solar cells: remarkable enhancement in performance through molecular design of indoline sensitizers. *Angewante Chemie International Edition* 2008; 47: 1923-7
- [32] (a) Hsu C-P, Lee K-M, Huang JT-W, Lin C-Y, Lee C-H, Wang L-P, Tsai S-Y, Ho K-C. EIS analysis on low temperature fabrication of TiO<sub>2</sub> porous films

for dye-sensitized solar cells. *Electrochimica Acta* 2008; 53: 7514-22

(b) Wu W, Yang J, Hua J, Tang J, Zhang L, Long Y, Tian H. Efficient and stable dye-sensitized solar cells based on phenothiazine sensitizers with thiophene units. *Journal of Materials Chemistry* 2010; 20: 1772-9

(c) Chen B-S, Chen D-Y, Chen C-L, Hsu C-W, Hsu H-C, Wu K-L, Liu S-H, Chou P-T, Chi Y. Donor–acceptor dyes with fluorine substituted phenylene spacer for dye-sensitized solar cells. *Journal of Materials Chemistry* 2011; 21: 1937-1945

(d) Tian H, Bora I, Jiang X, Gabrielsson E, Kralsson KM, Hagfeldt A, Sun L. Modifying organic phenoxazine dyes for efficient dye-sensitized solar cells. *Journal of Materials Chemistry* 2011; 21: 12462-72

## Summary

Three solubility enhanced phthalocyanine dyes were synthesized, and the dye-based BMs were fabricated with the most soluble dye. The increase in solubility of the prepared dyes was attributed to bulky functional substituents at the peripheral positions of them. Since all dyes had high molar extinction coefficients, dye-based BMs absorbed light in the visible region with the small amounts of the dyes. In addition, the dyes including terminal alkoxy groups showed suitable thermal stability for commercial use due to terminal alkoxy groups are stable at postbaking temperature. The dielectric constants of the BMs containing more than 30wt% of dyes were significantly lower than that of the BM prepared with carbon black only. The dye-based BM films were fabricated with greenish phthalocyanine and reddish perylene dyes. The high thermal stability of the dye-based BM was attributed to the rigid molecular structures of the dyes. In addition, due to the low dielectric characteristics of the dye, the dielectric constants of the dye-based BMs were significantly lower than that of the BM prepared with carbon black only. However, the low solubility of the dyes in industrial solvents and dye aggregations in the baking process limited the input of the dye in the BM resist, resulting in low light absorption of the dye-based BM. By fabricating hybrid-type BM that includes dye and carbon



black together, the light absorption property of the BM would be improved compared to the dye-based BM, satisfying the property requirements of BMs.

The first design and synthesis of three novel phenoxazine-based organic dyes (**WS1**, **WS2** and **WS3**) has been done to study the effects of the various bridge units and an additional donor on the performance of DSSCs. The introduction of the heterocyclic bridge units (furan and thiophene) extended the conjugation and red-shifted the absorption spectra of the dyes, improving  $J_{sc}$ . Consequently, the DSSCs based on **WS1** with the furan unit and **WS2** with the thiophene unit showed higher overall conversion efficiencies in comparison with the reference dye (**POX**) without the bridge unit. The most effective bridge unit was furan, which had a higher recombination resistance and  $V_{oc}$  value. **WS3** with the ethoxy phenyl ring as an additional donor showed more red-shift in the absorption, whereas the planarity of the dye was reduced by the large dihedral angle between the ethoxy phenyl ring and the POZ core. This non-planar structure of the dye led to less adsorption of the dye on the  $TiO_2$  surface, which limited the  $J_{sc}$  enhancement. The DSSC based on **WS1** with the furan bridge unit exhibited the highest overall conversion efficiency of 5.26% ( $J_{sc} = 11.72$  mA/cm<sup>2</sup>,  $V_{oc} = 653$  mV,  $FF = 68.76$ ). In addition, four new organic sensitizers with POZ dyes (**POX**, **WB**, **WH1** and **WH2**) were designed and synthesized to

investigate the effects of an additional anchoring group and the *N*-substituent on the performance of DSSCs. The introduction of the additional anchoring group extended the conjugation of the dyes, leading to the red-shifts of their absorption spectra. The di-anchoring dyes transferred more electrons to the TiO<sub>2</sub> electrode, increasing the  $J_{sc}$  value. The introduction of the methoxyphenyl ring located on the POZ nitrogen atom caused steric hinderance due to the large dihedral angle between the *N*-substituent and the POZ core. As a result, the electron recombination between the injected electron and the electrolyte was retarded, improving the  $V_{oc}$  value. On the other hand, the di-anchoring dyes transferred more protons to the TiO<sub>2</sub> surface compared to the mono-anchoring dyes. This lowered the Fermi level of the TiO<sub>2</sub> and the  $V_{oc}$  of the cells. The adsorption of dyes with the *N*-methoxyphenyl ring was limited by their bulky structures. Therefore, the dyes with the *N*-methoxyphenyl ring showed lower  $J_{sc}$  values compared to the dyes with the butyl chain. Consequently, introduction of the additional anchoring group enhanced  $J_{sc}$ , but decreased  $V_{oc}$ . To improve the lowered  $V_{oc}$  caused by the di-anchoring system, a methoxyphenyl ring was introduced on the POZ core. The introduction of the 4-methoxyphenyl ring increased the  $V_{oc}$ , but decreased the  $J_{sc}$  simultaneously. Thus, with the increases and decreases of  $J_{sc}$  and  $V_{oc}$ , all DSSCs fabricated with the dyes showed similar

overall conversion efficiencies, and the cells based on **WH1** showed the best overall conversion efficiency ( $\eta = 5.09\%$ ,  $J_{sc} = 10.11 \text{ mA/cm}^2$ ,  $V_{oc} = 690 \text{ mV}$ ,  $FF = 72.23\%$ ).

## 초록

액정디스플레이 (LCD) 광차단막으로 가장 빈번하게 쓰이는 물질은 카본 블랙으로, 높은 내열성과 높은 흡광도를 가진다. 반면, 카본블랙은 높은 유전율을 가지기 때문에 광차단막이 박막트랜지스터 바로 위에 형성되는 구조를 가지는 LCD에서는 오작동을 일으킬 가능성이 있다. 이러한 문제를 해결하기 위해서 광차단막 재료로 저유전율을 가지는 유기 안료를 사용할 수 있으나, 유기안료는 물흡광도가 낮기 때문에 상대적으로 낮은 광학 특성을 가진다.

유기염료는 낮은 유전율을 가지는 동시에 높은 물흡광도를 보이기 때문에 위의 두 재료가 가진 단점을 극복할 수 있는 광차단막 물질이 될 수 있다. 반면, 유기염료는 일반적으로 카본블랙이나 유기안료에 비해서 내열성이 낮은 단점이 있으며, 유기염료가 광차단막 제작 공정에 적용되기 위해서는 공정 용매에 높은 용해도를 가져야 한다. 따라서, 높은 내열성을 가지며, 동시에 공정용매에 대해서 높은 용해도를 보이는 유기 염료를 개발이 필요하다.

본 연구에서는 고내열성 및 고용해도를 가지며 녹색을 띠는 금속 없는 프탈로시아닌 염료 3종을 설계하고 합성하였다. 세 염료의 합성은 알킬기 또는 알콕시기를 포함하는 치환체를 프탈로시아닌 염료의 peripheral 위치에

도입을 통해 이루어졌다. 광차단막에 적용 가능성을 알아보기 위해서 합성된 염료의 광학적 특성, 용해도, 내열성을 측정하였으며, 염료로 제작한 광차단막의 광학적, 열적, 유전적 특성을 조사하였다.

금속 없는 프탈로시아닌 염료의 용해도는 염료에 peripheral 위치에 도입된 부피가 큰 치환체로 인해서 상승하였다. 또한 모든 염료는 높은 몰흡광계수를 가지며, 염료를 이용하여 제작한 광차단막도 가시광선 영역에서 넓은 범위의 광 흡수를 보였다. 따라서 상대적으로 적은 양의 염료로도 높은 광 차단 특성을 나타낼 수 있는 가능성을 보여주었다. 염료들 중에서 알콕시기를 포함하는 염료의 경우 염료 광차단막 공정에 적용 가능한 우수한 내열성을 보였다. 또, 제작된 염료기반 광차단막의 유전율은 카본블랙으로 제작된 광차단막에 비해서 상당히 낮은 수치를 보였다. 따라서 카본블랙과 염료를 혼합하여 만든 광차단막 중에서 30wt%이상의 염료를 함유하는 경우 저유전율 광차단막에 적용할 수 있음을 확인 하였다.

한편, 앞서 합성한 금속 없는 프탈로시아닌 염료는 가시광선 영역에서 550nm 근처영역의 빛을 흡수하지 못한다. 그러므로 가시광선 점 범위를 흡수하는 광차단막을 제작하기 위해서, 녹색을 띠는 zinc 프탈로시아닌 염료와 적색을 나타내는 퍼릴렌 염료를 합성하고 두 염료를 혼합하여 광차단막을 제작하였다. 합성한 두 염료 자체의 특성을 조사하였으며, 두 염료를 혼합하

여 제작한 광차단막의 광학적, 열적, 유전적 특성을 측정하였다. 또 제작한 광차단막의 표면 상태를 자세히 보기 위해서 FE-SEM과 AFM을 이용하여 광차단막의 표면을 조사하였다.

Zinc 프탈로시아닌 염료와 퍼틸렌 염료를 혼합하여 만든 광차단막은 높은 내열성을 나타냈으며, 이는 염료 모체 구조의 열적 안정성에 기인하였다. 또, 유전율이 낮은 염료의 특성으로 인해서, 광차단막 역시 카본 블랙 기반 광차단막에 비해서 낮은 유전율을 나타냈다. 반면, 프탈로시아닌 염료의 공정 용매에 대한 낮은 용해도와 열처리 과정에서 형성된 염료 회합 현상으로 인해 광차단막의 흡광 특성이 낮아지게 되었다. 본 연구로부터 유기 염료가 광차단막에 더 성공적으로 적용되기 위해서는 분산제 혹은 계면활성제의 첨가를 통해서 염료의 투입량을 증가시켜야 하며, 더불어서 염료 단독 보다 염료와 카본 블랙을 혼합하여 만드는 것이 필요하다는 것을 확인하였다.

염료감응형 태양전지는 전도유망한 태양전지 중 하나로 그 동안 많은 관심을 받아왔으며, 염료감응형 태양전지의 광감응제로 가장 활발히 연구되었던 루세늄을 포함한 염료를 통해서 11%에 달하는 높은 광전변환효율을 달성하였다. 반면, 높은 생산 단가, 정제의 어려움 같은 단점들이 있어서 상업적인 적용에 어려움이 있었다. 최근에는 이러한 단점을 극복하기 위해서 루세늄을 포함하지 않는 유기 염료에 대해서 많은 관심이 집중되고 있으며,

이러한 유기 염료는 낮은 생산 단가, 구조 변환 및 합성의 용이성, 높은 물 흡광계수, 친환경성 같은 장점을 가지고 있다.

루세늄을 포함하지 않은 여러 유기 염료들 중에서 페녹사진 염료는 비슷한 구조인 트리페닐아민, 페노사이아진 염료에 비해서 상대적으로 높은 광전변환효율을 나타내는 것으로 알려져 있다. 이는 전자가 풍부한 질소, 산소 원자를 포함하고 있는 페녹사진 염료가 더 강한 전자 공여 능력을 가지는데 기인한다. 또한 페녹사진 염료는 염료감응형 태양전지에 도입되기 충분한 전기화학적 특성을 가지고 있다. 이러한 장점에도 불구하고, 염료감응형 태양전지용 광감응체로서 페녹사진 염료에 대한 많은 연구가 이루어지지 않았다.

따라서, 본 연구에서는 페녹사진 염료에 conjugated bridge 도입을 통한 효과를 연구하기 위해서 페녹사진 모체에 conjugated bridge 역할을 하는 five-membered heterocyclic rings 을 도입하였다. 또, 전자 공여 능력과 물 흡광도를 향상시키기 위해서 furan이 달린 페녹사진 염료에 추가적인 전자 주개 그룹인 에톡시 페닐링을 달아주었다. 이러한 전략을 통해서 세 종의 페녹사진 염료를 설계하고 합성하였으며, 도입된 치환체의 효과를 설명하기 위해서 합성한 염료들로 만든 셀의 광학적, 전기화학적 특성 및 광전기적 특성을 측정하였다.

도입된 heterocyclic bridge units 인 퓨란과 싸이오펜은 염료의 흡광 스펙트럼의 장파장화를 시켜서 염료를 이용하여 만든 셀의 광전밀도를 향상시켰다. 추가적인 전자 주개 그룹인 메톡시 페닐링의 도입은 염료의 흡광 스펙트럼을 장파장화시켰으나, 염료 분자 구조를 뒤틀리게 하여 흡착량을 감소시켰다. 따라서 메톡시 페닐링이 도입된 염료의 광전밀도는 크게 향상 되지 못했다. 합성된 염료들 중에서는 퓨란이 달린 염료로 만든 셀이 가장 높은 광전 변환효율을 나타냈으며, 5.26%의 수치를 나타내었다.

더불어, 페녹사진의 염료에 추가적인 전자 받개 그룹을 도입하여 그에 따른 효과를 알아보고자 하였다. 또 전자 받개 그룹이 두 개 달린 염료의 개방전압을 향상시키기 위해서 페녹사진 염료의 질소가 있는 위치에 부피가 큰 메톡시 페닐링을 도입하였다. 이와 같은 계획을 통해서 총 네 종의 염료를 설계하고 합성하였으며, 도입된 치환체의 효과를 설명하기 위해서 염료들을 이용하여 만든 셀의 광학적, 전기화학적 특성 및 광전기적 특성을 측정하였다.

추가적인 전자 주개 그룹을 도입함으로써 흡광 스펙트럼이 장파장화하여 전류밀도가 향상되었으나, 전자재결합 속도가 높아지는 단점이 있었다. 도입된 N-메톡시 페닐링은 전자재결합을 방해하여 개방 전압 값을 향상시켰다. 반면, 부피가 큰 N-메톡시 페닐링으로 인하여 염료의 흡착량이 줄어



들었다. 결과적으로 전류밀도 및 개방 전압값의 증감에 따라서 네 염료 모두 거의 비슷한 효율을 나타내었으며, 합성한 염료 중에서 N-메톡시 페닐링이 달린 염료로 제작한 셀이 가장 높은 광전 변환효율인 (5.09%)을 나타내었다.

## List of Publications

### Original Papers

1. W. Lee, S. B. Yuk, J. Choi, D. H. Jung, S. Choi, J. Park, J. P. Kim “Synthesis and characterization of solubility enhanced metal-free phthalocyanines for liquid crystal display black matrix of low dielectric constant”, *Dyes and Pigments*, 2012, 92, 942 (article)
2. J. Choi, W. Lee, C. Sakong, S. B. Yuk, J. Park, J. P. Kim “Facile synthesis and characterization of novel coronene chromophores and their application to LCD color filters”, *Dyes and Pigments*, 2012, 94, 34 (article)
3. J. Choi, S. H. Kim, W. Lee, C. Yoon, J. P. Kim “Synthesis and characterization of thermally stable dyes with improved optical properties for dye-based LCD color filters”, *New J. Chem*, 2012, 36, 812 (article)
4. J. Choi, W. Lee, J. W. Namgoong, T. Kim, J. P. Kim “Synthesis and characterization of novel triazatetrabenzcorrole dyes for LCD color filter and black matrix”, *Dyes and Pigments*, 2013, 99, 357 (article)
5. J. Lee, S. H. Kim, W. Lee, J. Lee, B. An, S. Y. Oh, J. P. Kim, J. Park “ Electrochemical and optical characterization of cobalt, copper and zinc phthalocyanine complex”, *Journal of Nanoscience and Nanotechnology*, 2013,

13, 4338 (article)

6. W. Lee, J. Choi, S. H. Kim, J. Park, J. P. Kim “Analysis and characterization of dye-based black matrix film of low dielectric constant containing phthalocyanine and perylene dyes”, *Journal of Nanoscience and Nanotechnology*, accepted

7. W. Lee, S. B. Yuk, J. Choi, H. J. Kim, H. W. Kim, S. H. Kim, B. Kim, M. J. Ko, J. P. Kim “The effects of the number of anchoring groups and N-substitution on the performance of phenoxazine dyes in dye-sensitized solar cells”, *Dyes and Pigments*, 2014, 102, 13-21

8. W. Lee, J. Choi, J. W. Namgoong, S. H. Kim, K. C. Sun, S. H. Jung, K. Yoo, M. J. Ko, J. P. Kim “Effects of five-membered heterocyclic bridges and ethoxyphenyl substitution on the performance of phenoxazine-based dye-sensitized solar cells” accepted

9. J. Choi, S. H. Kim, W. Lee, J. B. Chang, C. Sakong, J. W. Namgoong, J. P. Kim

“The Influence of aggregation behavior of novel quinophthalone dyes on optical and thermal property of LCD color filters”, *Dyes and Pigments*, 2014, 101, 186-195

## **List of Presentations**

### **International**

1. 2008 Korea-Japan Forum, W. Lee, J. P. Kim “Synthesis and characterization of novel color compensating dyes for PDP”
2. 2010 International Conference on Porphyrins and Phthalocyanines, W. Lee, S. B. Yuk, J. H. Choi, J. P. Kim “Synthesis and characterization of highly soluble metal-free phthalocyanines for LCD black matrix”
3. 2012 19th International Conference on Photochemical Conversion and Storage of Solar Energy, W. Lee, J. P. Kim “Modification of phenoxazine dyes for efficient sensitizers in dye-sensitized solar cells”
4. 2012 19th International Conference on Photochemical Conversion and Storage of Solar Energy, S. B. Yuk, W. Lee, J. W. Namgoong, J. P. Kim “The effect of additional electron donating group and conjugated linker on the efficiency of DSSCs based on phenoxazine dyes”

## Domestic

1. 2009 춘계 대한화학회, 김현우, 사공천, 이우성, 김재필 “Synthesis and photovoltaic properties of organic dyes containing different hetero atoms in donor group”
2. 2009 추계 대한화학회, 이우성, 육심범, 김재필 “Syntheses and Properties of Novel Metal-free Phthalocyanines derived from sterically hindered Phenols”
3. 2010 추계 대한화학회, 이우성, 김재필 “Synthesis and Photovoltaic properties of efficient oxazine dyes for DSSCs”
4. 2011 춘계 대한화학회, 이우성, 김재필 “Phenoxazine derivatives with heterocyclic five-membered bridge unit for efficient sensitizers in dye-sensitized solar cells”
5. 2011 춘계 대한화학회, 최준, 이우성, 김재필 “Synthesis and characterization of novel coronene chromophores”
6. 2011 춘계 대한화학회, 육심범, 이우성, 김재필 “Synthesis of bay-substituted perylene diimide dyes for black matrix of liquid crystal display”